Optimization of Battery Energy Storage Systems for Microgrids

Optimization of Battery Energy Storage Systems for Microgrids

マイクログリッドのためのバッテリーエネルギー貯蔵システムの最適化

Thongchart Kerdphol

A dissertation presented for the degree of Doctor of Philosophy

Department of Electrical and Electronics Engineering
Graduate School of Engineering
Kyushu Institute of Technology
Japan

September 2016

マイクログリッドのためのバッテリーエネルギー貯蔵システムの最適化

トンチャート　カートポン

(学生番号: 13589504)

指導教員　三谷康範

博士学位論文

九州工業大学　工学府　電気電子工学専攻

平成２８年度

Thongchart Kerdphol
Kyushu Institute of Technology
Department of Electrical and Electronics Engineering
Tobata, Kitakyushu, Fukuoka, Japan
n589504k@mail.kyutech.jp

A record for this book is avalible from the Kyushu Institute of Technology Academic Repository in Publication Data Thesis (http://ds.lib.kyutech.ac.jp/dspace/).

Greatly devoted to His Majesty King Bhumibol Adulyadej

Rama IX of Thailand

Dedicated to my parents

My family, teachers, friends and

Those who take pleasure in my prosperity and

Been there for me during the times of nonlinearities

The doctoral dissertation supervisor and chair of doctoral dissertation approval committee:

Yasunori Mitani, PhD
Professor/President of the Institute of Electrical Engineers of Japan (IEEJ), Power and Energy Society
Department of Electrical and Electronics Engineering
Graduate School of Engineering, Kyushu Institute of Technology
Tobata, Kitakyushu, Fukuoka, Japan

The members of doctoral dissertation approval committee:

Masayuki Hikita, PhD
Professor, Department of Electrical and Electronics Engineering
Graduate School of Engineering, Kyushu Institute of Technology
Tobata, Kitakyushu, Fukuoka, Japan

Mochimitsu Komori, PhD
Professor, Department of Applied Science for Integrated System Engineering
Graduate School of Engineering, Kyushu Institute of Technology
Tobata, Kitakyushu, Fukuoka, Japan

Masayuki Watanabe, PhD
Associate Professor, Department of Electrical and Electronics Engineering
Graduate School of Engineering, Kyushu Institute of Technology
Tobata, Kitakyushu, Fukuoka, Japan

Kazuhiro Toyoda, PhD
Associate Professor, Department of Electrical and Electronics Engineering
Graduate School of Engineering, Kyushu Institute of Technology
Tobata, Kitakyushu, Fukuoka, Japan

The committees have examined the dissertation entitled "Optimization of Battery Energy Storage Systems for Microgrids" presented by Thongchart Kerdphol, a candidate for the degree of Doctor of Philosophy and hereby certify that it is worthy of acceptance.

Acknowledgements

Much of the outcomes, information and insight presented in this dissertation were achieved through a long-term research and study conducted by the author on power system analysis, control and optimization over the last 9 years in Thailand (2007-2012: Kasetsart University) and Japan (Kyushu Institute of Technology: 2013-2016).

This frontier research would not have been possible without the support of so many people in so many ways. First and foremost, the author wish to extend my sincere gratitude to my supervisor, Prof. Dr. Yasunori Mitani who is very patient, helpful and tirelessly offered invaluable assistance, support and guidance. Without his knowledge and assistance, this research would not have been successful. My deep gratitude is also due to Prof. Dr. Masayuki Hikita, Prof. Dr. Mochimitsu Komori, Assoc. Prof. Dr. Masayuki Watanabe and Assoc. Prof. Dr. Kazuhiro Toyoda who served as my supervisory committee members, for their continuous support, guidance and comments, during the period of my study. The author extends many thanks and appreciation to Prof. Dr. Hassan Bevrani (University of Kurdistan, Iran), Asst. Prof. Dr. Komsan Hongesombut (Kasetsart University, Thailand), Dr. Yaser Qudaih (Kyushu Institute of Technology, Japan) and Mr. Thanakorn Penthong (Provincial Electricity Authority of Thailand) for their technical guidance, innovative ideas and supports.

It is pleasure to acknowledge the scholarships, awards and support the author received during Ph.D. program from the various sources: The Japan Student Services Organization (JASSO honors scholarship) established by the MEXT (The Japanese Ministry of Education, Culture, Sports, Science and Technology), Kyushu Institute of Technology (100th anniversary memorial honors scholarship and Meisenkai scholarship) and the Institute of Electrical and Electronics Engineers, Power and Energy Society (Ph.D. student support grant, IEEE PES ISGT Asia 2015).

I would like to express my heartfelt thanks and appreciation to all of my colleagues, students and staffs at Kyushu Institute of Technology as well as the great nation of Japan. Finally, the author offers his deepest personal gratitude to his parents and family for the strength that keeps him standing and believing that this research would be possible, more interest and successful.

Thongchart Kerdphol

July 2016

Preface

During the 2011 Japan great east earthquake, tsunami and nuclear crisis, thousands of people had no access to electricity and facilities. Without electricity, education, health centers and other critical services and facilities declined. Since that time, microgrid development in Japan has been focused on resilience for solving such problems. Together with the emphasizing of Japan's strategic energy plan (SEP 2014), it calls for the enhancing of resilience of domestic energy supply networks, promoting and increasing distributed generations (DGs) and renewable energy resources (RESs), reducing energy demand and promoting decentralized energy by improved batteries and storage systems. For these reasons, Battery Energy Storage Systems (BESS) have become an essential component for microgrids and power systems so as to stabilize, recover and improve microgrids/power systems from instabilities and system collapses. Therefore, BESS can be concluded as a rapid and flexible device for microgrids and power systems.

In the part decades, various optimizations of large interconnected power system including the small size of BESS had been solved. The impact of small size and location of BESS could not cause stability issues and power loss to a large system. Thus, the impact of BESS size and location were negligible. Looking at a small power system currently such as microgrids, BESS size and location cannot be negligible anymore. Without an optimum size and location of BESS, it can cause stability issues, and increase in costs, power loss and larger BESS capacity. Thus, the main challenge in integrating BESS into a microgrid is to evaluate an optimum size and location of BESS in order to secure system stability and performance in both grid-connected and isolated operations as well as guarantee the full use of a microgrid with efficiency.

To evaluate an optimum size and location of BESS, a conventional method known as the analytic method in Chapter 3 is introduced to solve the mentioned problems. However, the results based on the analytic method are not acceptable with frequency and voltage conditions of the microgrid. Hence, artificial intelligent (AI) techniques are introduced to solve the mentioned optimization problems. First, this research proposes a novel optimization method using particle swarm optimization (PSO) based on frequency control of the microgrid to determine an optimum size of BESS in Chapter 4. Based on the PSO results, the optimization-based PSO method can achieve the optimum size of BESS and system performance-based PSO is acceptable with frequency and voltage conditions of the microgrid. However, the optimization-based PSO method is not flexible to evaluate an optimum location of BESS once its output change. Then, this research proposes a new optimization method using artificial neural networks (ANN) based on frequency control and loss minimization of the microgrid to evaluate both an optimum size and location of BESS in Chapter 5. Based on the ANN results, the optimization-based ANN can determine an optimum size and location of BESS with a high accuracy and low prediction errors. Nevertheless, the optimization-based ANN provides the very fast calculation time and almost the same BESS size and system performance with the optimization-based PSO. However, the best optimum size of BESS is still achieved by the optimization-based PSO method. Afterwards, a brand new optimization idea combining the strengths of both PSO and ANN methods is promoted to evaluate online optimum powers of BESS for microgrids in Chapter 6. Based on the online optimization of BESS, the results show that the online optimization of BESS can accurately determine online optimum powers of BESS based on frequency control of the microgrid under the environments of a sunny and rainy day as well as the changes of typical loads/generations without the necessity of performing the new optimization process.

Contents

Acknowledgements VI

Preface VII

Contents VIII

List of Figures XIII

List of Tables XVII

List of Acronyms XVIII

Chapter 1: Introduction 1

1.1 Significance of Power System Optimization 1

1.2 Artificial Intelligent Applications in Power System Optimizations 2

1.3 Background and Motivation 4

1.4 Research Objective and Contribution 6

1.5 Dissertation Outline 7

1.6 Summary 9

1.7 References 9

Chapter 2: Microgrid Concept and Design 11

2.1 Microgrids Introduction and Concept 11

2.1.1 What are Microgrids ? 13

2.1.2 What are not Microgrids ? 13

2.2 Microgrids Control and Operation 15

2.2.1 Microgrid Local Controls 18

2.2.2 Microgrid Secondary Controls 19

2.2.3 Microgrid Global Controls 19

2.2.4 Microgrid Emergency/Centralized Controls 20

2.3 Study Microgrid Design and Construction 21

2.3.1 Background of Study Microgrid 21

2.3.2 Hydro Generation Power System 24

2.3.2.1 Introduction 24

2.3.2.2 Control of Hydro Generation Power System 24

2.3.2.3 Hydro Generation Model in PowerFactory 25

2.3.3 Solar Photovoltaic Power System 28

2.3.3.1 Introduction 28

2.3.3.2 Control of Solar Photovoltaic Power System 28

2.3.3.3 Solar Photovoltaic Model in PowerFactory 30

2.3.4 Battery Energy Storage System (BESS) 32

2.3.4.1 Introduction 32

2.3.4.2 Control of Battery Energy Storage System 34

2.3.4.3 BESS Model in PowerFactory 36

2.4 Summary 38

2.5 References 39

Chapter 3: Analytic Method-based BESS Size Optimization 42

3.1 Introduction of Analytic Method 42

3.2 Analytic Method Structure 42

3.2.1 Main DPL Script for Analytic Method 47

3.3 Results and Discussion 51

3.4 Summary 53

3.5 References 54

Chapter 4: PSO-based BESS Size Optimization 56

4.1 Introduction of PSO Method 56

4.2 PSO Method Structure for BESS sizing 58

4.2.1 Main DPL Script for BESS Sizing based PSO 63

4.2.1.1 PSO Script 63

4.2.1.2 Objective Function Script 69

4.3 Results and Discussion 71

4.4 Summary 75

4.5 References 77

Chapter 5: ANN-based BESS Size and Location Optimization 78

5.1 Introduction of ANN Method 78

5.2 ANN method structure for Determining Size and Location of BESS 82

5.2.1 RBFNN Structure for Determining Size of BESS 84

5.2.2 RBFNN Structure for Determining Location of BESS 87

5.3 Results and Discussion 91

5.4 Summary 99

5.5 References 100

Chapter 6: Online Optimization of BESS 102

6.1 Introduction of Online Optimization Method 102

6.2 Structure of Online Optimization of BESS 104

6.2.1 PSO Optimization 107

6.2.2 RBFNN Optimization Method 109

6.2.3 MLPNN Optimization Method 111

6.3 Results and Discussion 114

6.4 Summary 123

6.5 References 124

Chapter 7: Conclusions 126

Appendix A: Microgrid System Parameters 129

Appendix B: Control Parameters for Solar PV Model 132

Appendix C: Control Parameters for BESS Model 136

List of Publications by the Author 137

Biography of the Author 139

List of Figures

Figure 2.1 A basic microgrid system 12

Figure 2.2 A model of a micro-generation connected to a microgrid 15

Figure 2.3 The ω-P droop control characteristic 17

Figure 2.4 The V-Q droop control characteristic 18

Figure 2.5 The typical microgrid structure 22

Figure 2.6 The simulated study microgrid in PowerFactory 23

Figure 2.7 The hill chart for a hydro generation turbine 25

Figure 2.8 A hydro generation module in PowerFactory 26

Figure 2.9 Load flow setting page of the hydro generation module (ElmSym) in PowerFactory 26

Figure 2.10 Load flow setting page of the mini-hydro generation module (ElmSym) in PowerFactory 27

Figure 2.11 A solar PV structure 29

Figure 2.12 The typical power-voltage and current-voltage characteristics of a solar PV module for irradiance of 1000 W/m^2 and 500 W/m^2 29

Figure 2.13 A solar PV module in PowerFactory 30

Figure 2.14 Load flow setting page of the solar PV module (ElmGenstat) in PowerFactory 31

Figure 2.15 Structure of control components in the solar PV module in PowerFactory 31

Figure 2.16 The structure of BESS 34

Figure 2.17 The equivalent circuit of BESS 35

Figure 2.18 A BESS model in PowerFactory 37

Figure 2.19 Load flow setting page of the BESS module (ElmVscmono) in PowerFactory 37
Figure 2.20 The structure of control components in the BESS module in PowerFactory 38
Figure 3.1 The analytic method structure for BESS sizing 43
Figure 3.2 The flow chart of the optimal sizing of BESS by using analytic method-based frequency control 47
Figure 3.3 Frequency deviation of the microgrid after the severe disturbance 51
Figure 3.4 Voltage deviation of the microgrid after the severe disturbance 52
Figure 3.5 PV power output measured from the system during the severe disturbance 52
Figure 4.1 The PSO structure for BESS sizing 58
Figure 4.2 The flow chart of the optimal sizing of BESS by using PSO-based frequency control 62
Figure 4.3 The DPL command basic options for the PSO script 63
Figure 4.4 The DPL command basic options for the objective function script 69
Figure 4.5 The DPL command advanced options for the objective function script 70
Figure 4.6 The convergence rate for BESS size 72
Figure 4.7 The convergence rate for the total cost of VR BESS 72
Figure 4.8 The convergence rate for the total cost of PB BESS 73
Figure 4.9 Frequency deviation of the microgrid after the severe disturbance 74
Figure 4.10 Voltage deviation of the microgrid after the severe disturbance 74
Figure 5.1 ANN structure of a nonlinear model 79
Figure 5.2 Activation transfer functions of ANN 80
Figure 5.3 The RBFNN method structure for BESS sizing and locating 83

Figure 5.4 The detail inside of the RBFNN block 84
Figure 5.5 The RBFNN structure for determining an optimum size of BESS (Stage 1) 86
Figure 5.6 The RBFNN structure for determining an optimum location of BESS (Stage 2) 88
Figure 5.7 The proposed RBFNN method flowchart 90
Figure 5.8 A regression analysis between the RBFNN output and target for Stage 1 91
Figure 5.9 A comparison between measured BESS size and estimated BESS size for evaluating an optimum size of BESS 92
Figure 5.10 A regression analysis between the RBFNN output and target for Stage 2 93
Figure 5.11 A comparison between measured and estimated power loss for determining an optimum location of BESS 94
Figure 5.12 The considered buses for determining an optimum location of BESS in the study microgrid 95
Figure 5.13 The optimum size of BESS for the study microgrid 95
Figure 5.14 The optimum location of BESS for the study microgrid 96
Figure 5.15 Frequency deviation of the microgrid after the severe disturbance 98
Figure 5.16 Voltage deviation of the microgrid after the severe disturbance 98
Figure 6.1 The structure of the online optimization of BESS 104
Figure 6.2 Inside of the proposed online optimization of BESS 105
Figure 6.3 The online process structure 106
Figure 6.4 PV generation profiles for a sunny and a rainy day 106
Figure 6.5 Load demand profiles 107
Figure 6.6 The RBFNN structure for determining optimum powers of BESS 110

Figure 6.7 The MLPNN structure for determining optimum powers of BESS 112
Figure 6.8 A regression analysis between the network outputs and the optimization targets based on MLPNN 115
Figure 6.9 A regression analysis between the network outputs and the optimization targets based on RBFNN 116
Figure 6.10 The active power of BESS under the environment of a sunny day 118
Figure 6.11 The reactive power of BESS under the environment of a sunny day 119
Figure 6.12 The active power of BESS under the environment of a rainy day 119
Figure 6.13 The reactive power of BESS under the environment of a rainy day 120
Figure 6.14 Frequency deviations of the microgrid under the environment of a sunny day 121
Figure 6.15 Voltage deviations of the microgrid under the environment of a sunny day 121
Figure 6.16 Frequency deviations of the microgrid under the environment of a rainy day 122
Figure 6.17 Voltage deviations of the microgrid under the environment of a rainy day 123

List of Tables

Table 2.1	Specific types of hydro generation units	27
Table 3.1	Redox-flow BESS technical and economical data	44
Table 3.2	Comparison parameters of two methods	53
Table 4.1	Comparison parameters of different methods	75
Table 5.1	The proposed RBFNN parameters for Stage 1	86
Table 5.2	The proposed RBFNN parameters for Stage 2	88
Table 5.3	Error indexes for the proposed RBFNN method	97
Table 5.4	Comparison parameters of different methods	99
Table 6.1	RBFNN parameters for determining optimum powers of BESS	111
Table 6.2	MLPNN parameters for determining optimum powers of BESS	114
Table 6.3	Error indexes for the online optimization of BESS	117

List of Acronyms

AC	Alternative Current
ACO	Ant Colony Optimization
AI	Artificial Intelligent
ANN	Artificial Neural Networks
BESS	Battery Energy Storage System
BPNN	Back-Propagation Neural Networks
EGAT	Electricity Generating Authority of Thailand
EMS	Energy Management System
EV	Electric Vehicle
FPC	Full Power Converter
DC	Direct Current
DFIG	Doubly Fed Induction Generator
DG	Distributed Generation
DPL	DIgSILENT PowerFactory Programming Language
DSI	Demand Side Integration
FACTS	Flexible Alternative Current Transmission System
GA	Genetic Algorithm
GEF	Global Environment Facility
GHG	Greenhouse Gas
IEEE	Institute of Electrical and Electronics Engineers
JPY	Japanese Yen Currency
MAE	Mean Absolute Error
MLPNN	Multilayer Perceptron Neural Networks
MNN	Modular Neural Networks
MPPT	Maximum Power Point Tracking

MRE	Mean Relative Error
MSE	Mean Square Error
NEDO	New Energy and Industrial Technology Development Organization
NHK	Nippon Hoso Kyokai Broadcast
PB	Polysulfide-Bromine
PLL	Phase Locked Loop
PSO	Particle Swarm Optimization
PV	Photovoltaic
PWM	Pulse Width Modulation
RES	Renewable Energy Resource
RBFNN	Radial Basis Function Neural Networks
RMSE	Root Mean Square Error
RNN	Recurrent Neural Networks
SA	Simulated Annealing
SCADA	Supervisory Control and Data Acquisition
SOC	Stage of Charge
SOFM	Self-Organization Feature Maps
THB	Thai Bath Currency
VR	Vanadium Redox
V2G	Vehicle to Grid
UNDP	United Nation Development Programme
USD	United States Dollar Currency
YN	Wye to Neutral Connection

Chapter 1

Introduction

1.1 Significance of Power System Optimizations

From the past up to present, optimization techniques have been implemented to power system analysis, operations and controls worldwide served as an important role. The main contributions of optimization are involved in terms of cost, improved operational reliability, stability, flexibility and system security. Currently, power systems are growing larger and more complicated due to the rising of load demand, fossil fuel demand of thermal power plants, resulting in an increase in costs and emission such as greenhouse gas (GHG) into Earth's atmosphere. Hence, optimization has become important for the power system utilities and operations [1], [2].

Since the 2011 Fukushima nuclear crisis in Japan, there are many concerns about the effects of uranium mining near tribal lands and unstable levels of environmental emissions worldwide. Together with a reduction of fossil fuel resources and the limitations of large scale renewable energy development. Thus, optimization has become even more essential in power systems [3].

Several optimization approaches including conventional and AI techniques have been applied to solve problems in power systems. These approaches are continuously developed and improved to coup with large and complex sizes of power systems. Optimization problems are complex because of a large number of constraints. Thus, the ability for achieving better solutions and shorter calculation times is the essential goal of these optimization methods. Various optimization problems have been concerned and solved in power system operations such as optimal power flow, maintenance, unit commitment, hydrothermal scheduling, economic dispatch and etc. [4].

1.2 Artificial Intelligent Applications in Power System Optimizations

Nowadays, artificial intelligent (AI) techniques have been applied for solving optimization problems worldwide. The main advantages of AI techniques are the ability to deal with complex problems that conventional methods cannot solve, and the simplicity of AI methods due to the simple mathematical structures. AI methods are also easy to combine with other methods for the hybrid ability, combining the strengths of each single method. A brief survey on the numerous AI methods for power system optimizations is presented as follows:

Fuzzy logic systems are forms of mathematical means of describing vagueness in linguistic terms where the truth values of variables between 0 and 1, known as "Fuzzy". They are suitable to deal with uncertainties and approximate reasoning. The fuzzy logic systems were introduced in 1965 with the fuzzy set theory by Lotfi Zadeh [5], [6].

Artificial neural networks (ANN) are information processing models inspired by the biological neural networks known as the brain. ANN consist of layers linked by weight connections which can be tuned based on experience, making neural networks adaptive to inputs and creating learning capability. There are many types of ANN defined by their structures and abilities such as backpropagation, feed forward, radial basis function, recurrent networks and etc. The main benefit of ANN is the ability to learn algorithms, the online adaptation of dynamic systems, fast parallel computation, and intelligent management of data. ANN was introduced in 1943 by Warren McCulloch and Walter Pitts [7], [8].

Simulated annealing (SA) method is a meta-heuristic method for solving unconstrained and bound-constrained optimization problems. The SA method simulates the physical process of heating and controls cooling a material and then slowly decreases the temperature to reduce defects, minimizing the system energy. The SA method was developed in 1983 by Scott Kirkpatrick, Daniel Gelatt and Mario Vecchi [9], [10].

Ant colony optimization (ACO) algorithm is a probabilistic method for solving computational problems which can be reduced to determine the optimum paths via graphs based on the behavior of ants in finding food for their colony by marking their trails with pheromones. The optimum path is the trail with the most pheromone marks which ants will follow to bring their food back to a colony. The ACO method was developed in 1992 by Marco Dorigo in his PhD dissertation [11].

Genetic algorithm (GA) is a search method for solving both constrained and unconstrained optimization problems based on a natural selection process. The GA method belongs to the evolutionary computation inspired by evolutionary biology such as inheritance, mutation, selection and crossover. The GA method may take long calculation times to find the optimum solution. The GA method was developed step by step from 1950 by Alan Turing and 1954 by Nils Aall Barricell [2], [12].

Particle swarm optimization (PSO) is a newest and popular computational method that optimizes a problem by iteratively trying to improve a candidate solution considering a given measure of quality from particles. PSO solves a problem by a population of candidate solutions and moves these particles around in the search space. Each particle searches for the optimum solution and has the ability for remembering the previous position. At each an iteration, each particle improves its position and velocity. The main advantages of PSO are ease of use, high convergence rates, minimum storage requirements and less depend on the set of initial values, implying the robustness compared with others AI methods. The PSO was developed step by step from 1995 by James Kennedy, and Russell Eberhart [13], [14].

From the past up to now, AI methods have been proved and solved various major problems for power systems in terms of power system expansion and planning such as AC and DC transmission systems, a distribution system, load, FACTS devices and so on, in terms of power system operation such as economic dispatch, optimum power flow, unit commitment, voltage control, load frequency control, static and dynamic security assessment, maintenance scheduling, fuel scheduling, energy management system (EMS) in SCADA, load forecasting, fault analysis and so on, in terms of power system modeling and analysis such as power flow analysis, transient stability, harmonics, dynamic stability, control design, simulation, protection and so on.

Moreover, the hybrid methods mixing the strengths of each method are designed and introduced by many researches due to several benefits of the single mentioned methods. However, the AI methods are continuously developed ahead in order to deal with large complex power systems including the rising number of constraints and to manage with new applications in modern power systems.

1.3 Background and Motivation

During the 2011 Japan great east earthquake, tsunami and nuclear disaster, a major impact was direct damage to the megagrid's generations. The disaster had shut down electricity to factories and households in Miyagi prefecture for two weeks. It caused difficulties to rescue teams for providing assistance. Based on NHK public broadcaster, around 380,000 people were evacuated to emergency shelters, many of them could not access to electric power [3]. Without electricity, education, health centers and other critical services and facilities declined. To solve such a problem, facilities are needed to provide electricity at the time of a blackout or disaster. Since that time, microgrid development in Japan has been focused on resilience for solving such problems. Microgrids are interconnection groups of low-voltage distributed energy sources, such as micro-turbines, wind turbines, photovoltaics and storage devices for supplying domestic loads. The microgrids can operate in either a grid-connected mode or an islanding mode. In the grid-connected mode, the microgrid loads receive power from both a utility grid and local generations. In the islanding mode (e.g., disaster or blackout), the microgrids can be separated from a utility grid and works independently; hence, they must have enough local distributed generations to supply loads at least to meet the critical/sensitive loads [15], [16]. When the microgrid is islanded, the frequency/voltage might go beyond the power quality limits. Sometime, it causes large mismatches between generations and loads, causing a critical frequency and voltage control problem. To solve such circumstances, energy storage systems can deal with the mentioned problems and offer excellence solutions to microgrids.

Together with the emphasizing of Japan's strategic energy plan (SEP 2014), it calls for enhancing of resilience of domestic energy supply networks, promoting and increasing distributed generations (DGs) and renewable energy resources (RESs), reducing energy demand and promoting decentralized energy by improved batteries, fuel cells, and other technologies [3]. Looking at modern power systems, RESs and DGs are the indispensable part of the systems due to their environmental friendly and sustainability, reducing global carbon emissions. However, the power outputs of RESs/DGs cannot predict and depend on weather conditions. The fluctuations of RES/DG power output can result in stability issues to power systems. Thus, microgrids or power systems should be capable of handling unexpected fluctuations and maintaining system stability. For these reasons, energy storage systems have become the essential component for microgrids and power systems.

Battery Energy Storage Systems (BESS) can offer good solutions to microgrids in terms of an improvement of stability issues, control of active and reactive powers, reduction in power loss, suppressing RES/DG power outputs, and preventing microgrids from instability and collapse [17]. For small disturbances, BESS is discharging when the system frequency is lower than the nominal frequency of 50 or 60 Hz. On the other hand, BESS is charging when the system frequency is higher than the nominal frequency of 50 or 60 Hz. For large disturbances, BESS can enhance the performance of the system frequency control by integrating BESS with an under-frequency load shedding scheme, or frequency generation trip. With these different functions, BESS can be concluded as a rapid and flexible device for microgrids and power systems [18].

During the past decades, various optimizations of large interconnected power system including the small size of BESS had been solved. The impact of small size and location of BESS could not cause stability issues and power loss to a large system. Thus, the impact of BESS size and location were negligible [19]. Looking at a small power system such as microgrids, BESS size and location cannot be negligible anymore. Without an optimum size and location of BESS, it can cause stability issues, increase in cost, system loss and larger BESS capacity. Thus, an optimum size and location of BESS is the main challenge for integrating BESS into microgrid systems. The study microgrid is typical to a real system available at the promoting renewable energy in Mae Hong Son province which is initiated and funded by United Nation Development Programme (UNDP), Global Environment Facility (GEF), and Ministry of Energy of Thailand aimed for promoting DGs/RESs, learning, sharing knowledge and supporting the environmental agreements in Thailand [20]. [21]. The remote location and limited resource availability at this location make the microgrid an ideal platform to test new proposed intelligent techniques and technologies for the next generation of microgrids.

To determine an optimum size and location of BESS, a conventional method known as the analytic method is introduced to solve the mentioned problem. However, the results based on the analytic method are not acceptable with frequency and voltage conditions of the microgrid. Hence, AI techniques are introduced to solve the mentioned optimization problems. Firstly, this research proposes a novel optimization method using particle swarm optimization (PSO) based on frequency control to determine an optimum size of BESS for microgrids. Based on the PSO results, the optimization-based PSO method can achieve the optimum size of BESS and system performance-based PSO is acceptable but this method is not flexible to determine an optimum location of BESS once its output change. Then, this research proposes a new optimization method using artificial neural networks (ANN) based on frequency control and loss minimization to evaluate both an optimum size and

location of BESS for microgrids. Based on the ANN results, the optimization-based ANN can determine an optimum size and location of BESS with a high accuracy and low prediction errors. Nevertheless, the optimization-based ANN gives the very fast calculation time and almost the same BESS size and system performance with the optimization-based PSO. However, the best optimum size of BESS is still achieved by the optimization-based PSO. Afterwards, the brand new optimization idea combining the strengths of both PSO and ANN methods is promoted to determine online optimum powers of BESS for microgrids. Based on the online optimization of BESS, the results show that the online optimization of BESS can precisely determine online optimum powers of BESS based on frequency control of the microgrid under the environments of a sunny and rainy day as well as the changes of typical loads/generations without the necessity of performing the new optimization process.

This book is written in form of papers, which were presented at conference proceedings and published in numerous technical journals and transactions.

1.4 Research Objective and Contribution

This book designs the novel optimization methods by using AI techniques to determine an optimum size and location of BESS for microgrids. The novel optimization methods are trained and tested based on the typical microgrid system and parameters. The main work is divided into three parts based on different objectives, AI techniques and constraints as follows:

Firstly, a novel optimization method of BESS by using PSO based on frequency control of the microgrid is proposed to determine an optimum size of BESS at minimum total BESS cost for microgrids. The objective of this method is to evaluate an optimum size of BESS to prevent the microgrid from instability and collapse in presences of DG/load changes or the outage of generations or utility grid. Looking at the contribution, the proposed PSO method-based frequency control will be useful to help the operators to guarantee a lowest size and total cost of BESS with constraints of frequency control and the full use of the microgrid.

Secondly, a new method evaluating both optimum size and location of BESS is designed and presented by using ANN based on frequency control and power loss minimization for microgrids. The objective of this method is to determine both optimum size and location of BESS so as to avoid the microgrid from instability and

collapse in presences of DG/load changes or the outage of a generation or utility grid. As regard to the contribution of this method, the proposed ANN method-based frequency control and power loss minimization will be beneficial to help the operators to determine both optimum size and location of BESS with constrains of frequency control and power loss minimization, responding the full use of the microgrid.

Thirdly, this book designs and promotes a brand new intelligent optimization method by combining the strengths of both PSO and ANN to determine online optimum powers of BESS, and use it as an online effective controller of BESS for microgrids. The objective of this online method is to evaluate online optimum active and reactive powers of BESS based on frequency control of the microgrid. Any change in loads or generations will be compensated by the online optimization of BESS in a short period of time. The contribution of this method is a fast and accurate ability to determine online optimum powers of BESS under any change in loads or generations including the loss of the generation or utility grid without the necessity of performing the new optimization process.

Finally, the proposed novel methods are implemented and verified through the simulated microgrid system which is a real microgrid available at promoting renewable energy in Mae Hong Son province, Thailand. It is obvious that the proposed novel optimization methods are more effective for enhancement of system stability, flexibility and reliability as compared to the conventional methods.

1.5 Dissertation Outline

This book is separated into seven chapters and three appendices. Chapter 1 provides an introduction on the significant of power system optimizations. Fundamental concepts of artificial intelligent applications in power system optimizations, and background and motivation are emphasized. The research objectives are described and the contributions are explained.

Chapter 2 introduces the general aspects of microgrids including the concept, design and structure as basic elements of future smart grid, which have an important role to increase the grid efficiency, reliability, and to satisfy the environmental issues. The design and construction of the study microgrid are explained including the general aspects and physical descriptions of the DGs (i.e., Hydro power generation, Photovoltaic system) and Battery Energy Storage System (BESS). The modellings of the DGs and BESS in the study microgrid are designed by using PowerFactory-

DIgSILENT which is the power system analysis software for application in generation, transmission and distribution systems (License Key ID: 0008261).

Chapter 3 presents an analytic method to determine an optimum size of BESS for microgrids, known as a conventional method. The background of the analytic method is briefly reviewed. Later, the optimum sizing of BESS using analytic method is designed based on frequency control of the microgrid. Multi-objective functions are considered in this method; that is, the minimization of BESS size and cost with different storage technologies. The modelling of the proposed analytic method is designed and demonstrated using PowerFactory-DIgSILENT/DPL Script. The simulation results of the analytic method are shown and discussed. Afterwards, the result evaluation of the analytic method is provided.

Chapter 4 proposes a new optimization method to evaluate an optimum size of BESS by using particle swarm optimization (PSO). The PSO method is developed through simulation of simplified social models is one of the most modern heuristic algorithms. The BESS size optimization using PSO is designed based on frequency control of the microgrid with the multi-objective functions; that is, the minimization of BESS size and cost. The modern and conventional BESS cost with different technologies are also covered. Afterwards, the simulation results of the PSO are shown and discussed. The modelling of the proposed PSO are designed and demonstrated by using PowerFactory-DIgSILENT/DPL Script. The results of the PSO method are validated and compared with the results of the conventional method. Then, the result evaluation of the PSO method is demonstrated.

Chapter 5 designs a novel optimization method to determine both optimum size and location of BESS by using artificial neural networks (ANN) for microgrids. The optimization of BESS size and location using ANN is designed based on frequency control of the microgrid and power loss minimization. The modelling of the proposed ANN are designed and demonstrated by using Matlab/Toolboxes (License Key ID: 1065261). Afterwards, the simulation results of the ANN for determining an optimum size and location of BESS are revealed and discussed. Later, the result evaluation of the ANN method is emphasized.

Chapter 6 presents a combination of both the PSO and ANN methods to determine online optimum powers of BESS, and use it as an online effective controller of BESS for microgrids. By combining the advantages of the PSO and ANN methods, the novel online optimization of BESS is designed and presented. This chapter explains both offline model (i.e., PSO) and online model (i.e., radial basis function and multilayer perceptron known as the most popular/conventional model) for evaluating optimum active and reactive powers of BESS for microgrids. The

modelling of the online optimization of BESS are designed and demonstrated by using the interface data between PowerFactory-DIgSILENT/DPL Script (i.e, the PSO process modelling) and Matlab/Toolboxes (i.e., the ANN process modelling). Later, the simulation results of the offline and the online optimization methods for determining optimum active and reactive powers of BESS in the microgrid are compared and discussed.

Chapter 7 concludes the whole results from the proposed optimization methods. Finally, appendices including simulation data and control parameters in this research are revealed.

1.6 Summary

This chapter provides an introduction on the significant of power system optimizations. Fundamental concepts of artificial intelligent applications in power system optimizations, as well as background and motivation are emphasized. The research objectives and contributions are described and the outline of this book is explained.

1.7 References

1. A.J. Wood and B.F. Wollenberg, *Power generation, operation and control*. 2nd edn., Wiley and Sons, New York, 1996.
2. J.A. Momoh, *Electrical power system applications of optimization*, Marcel Dekker, Inc., New York, 2001.
3. C. Marnay, H. Aki, K. Hirose, A. Kwasinski, S. Ogura and T. Shinji, How two microgrid fared after the 2011 earthquake, *IEEE Power Energy Magazine*, 13(3):44-57, 2015.
4. W. Ongsakul, D.N. Vo, *Artificial intelligent in power system optimization*, Taylor & Francis Group, New York, 2013.
5. M. E. El-Hawary, *Electric power applications of fuzzy systems*, IEEE Press, New York, 1998.
6. R. C. Bansal, Bibliography on the fuzzy set theory applications in power, *IEEE Trans. Power Systems*, vol. 18, no. 4, 2003, pp. 1291–1299. 2001.

7. G. Li, J. Na, D. Stoten, and X. Ren, Adaptive neural network feedforward control for dynamically substructured systems, *IEEE Trans., Control System Technology*, 22(3):944–954, 2014.
8. M. Bianchini, P. Frasconi, and M. Gori, Learning without local minima in radial basis function networks, *IEEE Trans. Neural Networks*, 6(1):749–756, 1995.
9. F. Rodriguez, C. Garcia-martinez, M. Lozano, Hybrid metaheuristics based on evolutionary algorithm and simulated annealing: Taxonomy comparison, and synergy test. *IEEE Trans Evol. Comput*.,16(6):787–800, 2012.
10. T. Kerdphol, Y. Qudaih, Y. Mitani, Optimum battery energy storage system using PSO considering dynamic demand response for microgrids. *International Journal of Electrical Power and Energy Systems*, 83(1):58–66,2016.
11. M. Dorigo and T. Stutzle, *Ant colony optimization*, The MIT Press, Massachusetts, 2004.
12. D. P. Kothari and J. S. Dhillon, *Power system optimization*, Prentice-Hall of India Private Limited, New Delhi, 2006.
13. J. Zhu, *Optimization of power system operation*, John Wiley & Sons Inc., New Jesey, 2010.
14. J. Kennedy, R. Eberhart, Particle swarm optimization. *In Proceeding of IEEE Int. Conf. neural networks*, vol. 4. p. 1942–1948, 1995.
15. C. Cecati, G. Mokryani, A. Piccolo, and P. Siano, An overview on the smart grid concept, *In Proceeding of Conf. on 36th annual IEEE Industrial Electronics Society*, pp.3322-3327, 2010.
16. R. Lasseter, A. Akhil, C. Marnay *et al*., White paper on Integration of Distributed Energy Resources – The CERTS MicroGrid Concept. *s.l.: Office of Power Technologies of the US Department of Energy*, Contract DE-AC03-76SF00098. 2012.
17. I. Serban, C. Marinescu, Battery energy storage system for frequency support in microgrids and with enhanced control features for uninterruptible supply of local loads. *Int J Electr Power Energy Syst,* 54:432–41, 2014.
18. S.K. Aditya, D. Das, Application of battery energy storage system to load frequency control of an islanded power system. *Int J Energy Res*, 23:247–58, 1999.
19. F. Katiraei, M. Iravani, P. Lehn, Micro-grid autonomous operation during and subsequent to islanding process. *IEEE Trans Power Delivery,* 20 (1):248–57, 2005.
20. W. Ithiam, S. Asadamonkol, T. Sumranwanich, Smart grid national pilot project in Mae Hong Son Province, Thailand. *J Energy Environ,* 26(1):23–34, 2015.
21. United Nations Development Programme (UNDP) in Thailand, [Online], <http://www.th.undp.org/content/thailand/en/home/operations/projects/environment_and_energy/REinMHS.html>.

Chapter 2

Microgrids Concept and Design

2.1 Microgrids Introduction and Concept

Recently, modern communities are growing concerns on a secure supply of energy and environmental issues as one of the main challenges for economical harvesting of electricity. Future electricity grids have to deal with changes in community, technology, environment and economy. According to the Japanese technology platform of smart-grids funded by the new energy and industrial technology development organization (NEDO), an electricity network, that can intelligently integrate the actions of all users incorporating generations or loads in a manner suitable for providing an economically sustainable and secure power system, is called the smart-grids. Microgrids are also considered as the building block of smart girds [1]. As the solution of micro/smart-grids is capable of facilitating wide penetration of renewable energy sources (RESs), distributed generations (DGs) and energy storage systems into power systems, reducing power loss and greenhouse gas (GHG) emissions in power systems, increasing the security and reliability of energy supply to users, for these reasons, micro/smart grids have been gaining more and more attention recently.

Microgrids are the interconnected groups of RESs/DGs including micro-generations such as micro-turbines, solar photovoltaic (PV), together with energy storage devices (e.g., energy capacitors, flywheels and batteries) and domestic loads at distribution level as shown in Fig. 2.1. A microgrid is based on the control abilities over the network operations. These control abilities allow microgrids connect to the

upstream distribution network in order to operate when isolated from the utility grid in case of faults or severe disturbances or disasters, thus increasing the quality of supply. The microgrid control is the key point that examines microgrids from the distribution networks with RESs/DGs. In the grid-connected operation, microgrids obtain electrical power from both utility grid and local micro-generations, relying on the user's circumstance. Looking at the isolated operation (e.g., faults, blackouts, voltage drops, frequency drops), microgrids can disconnect from the utility grid through a static switch in about a cycle. The intentional isolated operation of microgrids can be operated for specific reasons such as maintenance purposes or economical condition.

One of the most requirements in microgrid management and control, in both grid-connected and isolated operations, is the power balance between micro-generation and domestic load. For the grid-connected operation, microgrids trade electrical power between itself and an interconnected grid to match the balance. For the isolated operation, microgrids should match the balance between micro-generations and domestic loads by increasing/decreasing micro-generations or performing load shedding/dynamic demand response. All such actions are clarified in the IEEE 1547 standard [2].

Two important control modes which involve in microgrid control: current-control and voltage-control. In the grid-connected mode, the micro-generations operate in current-control mode where they can maintain power exchanges between the microgrid and the utility grid. In the isolated operation, micro-generations operate in voltage-control mode where they should regulate the microgrid voltage and share with domestic loads. For the isolated operation, microgrds need to have enough micro-generation to supply load demand at least to meet the requirement of the critical/sensitive loads [3].

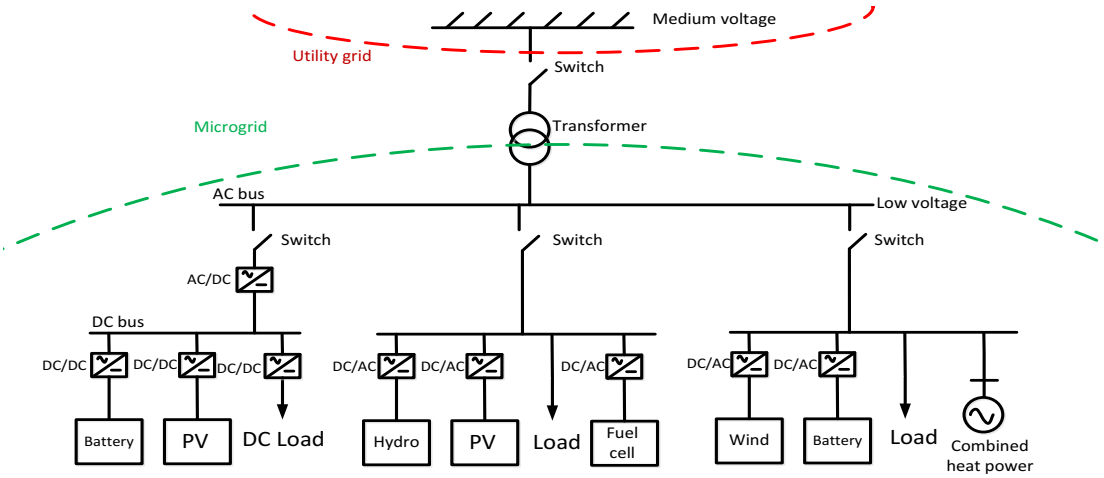

Figure 2.1 A basic microgrid system [3]

2.1.1 What are Microgrids ?

The major definitions of microgrids are briefly described as follows [34]:

1. A microgrid is an interconnected group of RESs/DGs (i.e., micro-generation), with energy storage units and domestic loads (i.e., controllable load) located at local distribution grid. According to the microgrid concept, it focuses on local supply of electrical power to nearby loads. Hence, the combined groups that disregard locations of generations and loads (e.g., virtual power plants) are not considered as the microgrids. Microgrids are generally located at low-distribution level with total installed micro-generation capacity under a MW range.

2. A microgrid should be operated in both grid-connected and isolated operations. The majority of microgrids will be operated in the grid-connected operation; hence the advantages of microgrid will improve from the grid-connected operation. Looking at the isolated operation, if the microgrid needs to achieve long-term isolated operation, it must satisfy the requirements on energy storage size, rated capacity of RESs/DGs or it must activate load shedding/dynamic demand response in order to continue to supply domestic loads.

3. The difference between a microgrid and a grid operated by micro-generations is the management and collaboration of accessible generations. Microgrids can handle with conflicting interests of various stakeholders in order to achieve optimum operated decision for all stakeholders.

2.1.2 What are not Microgrids ?

Some misconceptions and misunderstandings of microgrids, which are collected from various technical sources, are briefly explained as follows [34]:

1. Microgrids are isolated/stand-alone systems.

    - Microgrids can be operated in the isolated operation for emergency purposes but they are mainly operated in the grid-connected operation

for a normal situation. Thus, microgrids can be operated in both the isolated and grid-connected systems.

2. Microgrids consist of RESs, thus they must be unreliable, causing easily failures and blackouts.

    - A microgrid can smooth out the fluctuation of RES outputs by its own energy storage units during the isolated operation and by a utility grid during the grid-connected operation. With these options, microgrids can be considered as a reliable system.

3. The investment of a microgrid is too expensive, so the microgrid concept will be limited only in the study systems and remote areas.

    - The installation of RESs/DGs is growing and increasing worldwide and their financial support schemes have already proved that the installation of RESs/DGs and storage devices gives better profitability than conventional generations in terms of future cost reductions of micro-generation. Thus, microgrid concept can be implemented not only in the study and remoted systems but also in modern power systems.

4. The microgrid controllers will force users to shift their demand following the availability of RESs/DGs. For example, to charge an electric vehicle during the strong wind or sunshine.

    - According to the demand side integration (DSI)concept for commercial and household, it should perform the scheme called "load follow generation" only to long-term stand-by appliances (e.g., air-conditioners, refrigerators, freezers) and time-intensive devices (e.g., electric kettle). Apart from that, users can use the loads following their patterns.

5. Shareholders who own micro-generations create a microgrid.

    - The penetration of micro-generations (e.g., shareholder) is a part of the microgrid structure but a microgrid needs more than the penetration of micro-generations and requires active supervision, control and management as well as optimization schemes.

2.2 Microgrids Control and Operation

Nowadays, as the high penetration of RESs/DGs in microgrds is growing worldwide due to their reliable, sustainable and environmental friendly, it increases the complexity of control, protection and communication of RESs/DGs in microgrids. Thus, the microgrid control and operation is one of the indispensable issues for microgrid development [3].

The micro-generations and energy storage elements connect to the microgrid by interfacing power electronic circuits. The interfaces of power electronic circuits characterize by a type of generation and separated feeders (i.e., AC/AC, AC/DC and DC/AC inverters/converters). Due to the elements of RESs/DGs in microgrids, the microgrid control and operation relies on the inverter/converter control. The inverters/converters consist of two action modes, operating as a current source or voltage source. The simplify model of a micro-generation incorporating an inverter is displayed in Fig. 2.2. The micro-generation consists of power source or prime mover, DC system interface and inverter, connecting to the microgrid via a feeder. The frequency output, voltage output, active power and reactive power of a micro-generation can be controlled by the inverter equipped local feedback. The micro-generation can control the magnitude and phase of its voltage output (V) and from the feeder reactance (X). Then, the exchanging of active power (P) and reactive power (Q) flows from the micro-generation to the microgrid [4].

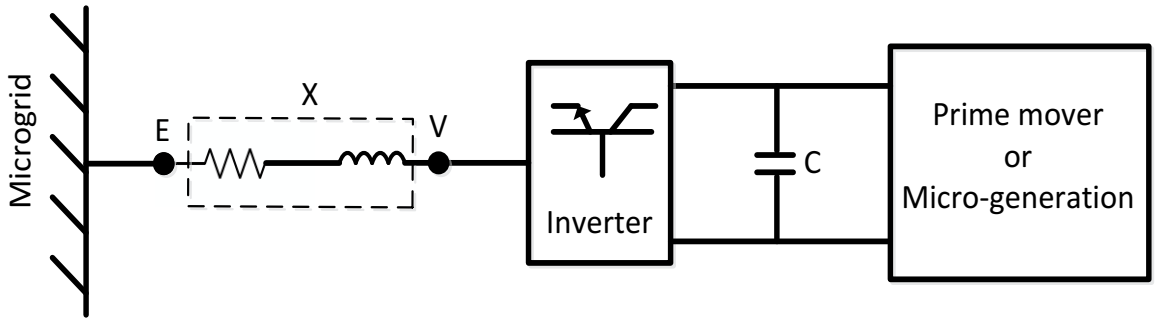

Figure 2.2 A model of a micro-generation connected to a microgrid [3]

The active and reactive powers of a micro-generation can be determined as follows:

$$P = \frac{3}{2}\frac{E \cdot V}{X}\sin\delta \tag{2.1}$$

$$Q = \frac{3}{2}\frac{V}{X}(V - E\cos\delta) \tag{2.2}$$

where

$$\delta = \delta_V - \delta_E \tag{2.3}$$

The E is the voltage at a microgrid side of the connecting feeder; δ_V and δ_E are the angles of V and E, respectively. In case of small angle (δ), active and reactive powers rely on δ and V.

$$P \approx \frac{3}{2}\frac{E \cdot V}{X}\delta \tag{2.4}$$

$$Q \approx \frac{3}{2}\frac{V}{X}(V - E) \tag{2.5}$$

According to equations (2.1) to (2.5), the feedback loops can be created in order to control output power and voltage of microgrids for the isolated operation. It is obvious that if the active power in a microgrid produced by micro-generations increases, the local frequency will decrease, and vice versa, forming the equation (2.6). There is the similar behavior for voltage versus reactive power, forming the equation (2.7).

$$\omega - \omega_0 = -R_P(P - P_0) \tag{2.6}$$

$$V - V_0 = -R_Q(Q - Q_0) \tag{2.7}$$

where R_P and R_Q are the frequency and voltage droop coefficients, respectively. ω_0, Q_0, P_0, V_0 are the nominal values of frequency, voltage, active power and reactive power, respectively.

Based on the equations (2.6) and (2.7), the feedback loops are formed so as to control active power, reactive power, frequency and voltage of a microgrid. Hence, the interconnected RESs/DGs with different droop characteristics can follow and correct the load demand changes in order to restore the nominal frequency and voltage of a microgrid as shown in the equations (2.8), (2.9) and Figs. 2.3 and 2.4.

$$\Delta P_{DGi} = \frac{\Delta\omega}{R_{Pi}} \tag{2.8}$$

$$\Delta Q_{DGi} = \frac{\Delta V}{R_{Qi}} \tag{2.9}$$

Thus,

$$\frac{\Delta P_{DG1}}{\Delta P_{DG2}} = \frac{R_{P2}}{R_{P1}} \tag{2.10}$$

$$\frac{\Delta Q_{DG1}}{\Delta Q_{DG2}} = \frac{R_{Q2}}{R_{Q1}} \tag{2.11}$$

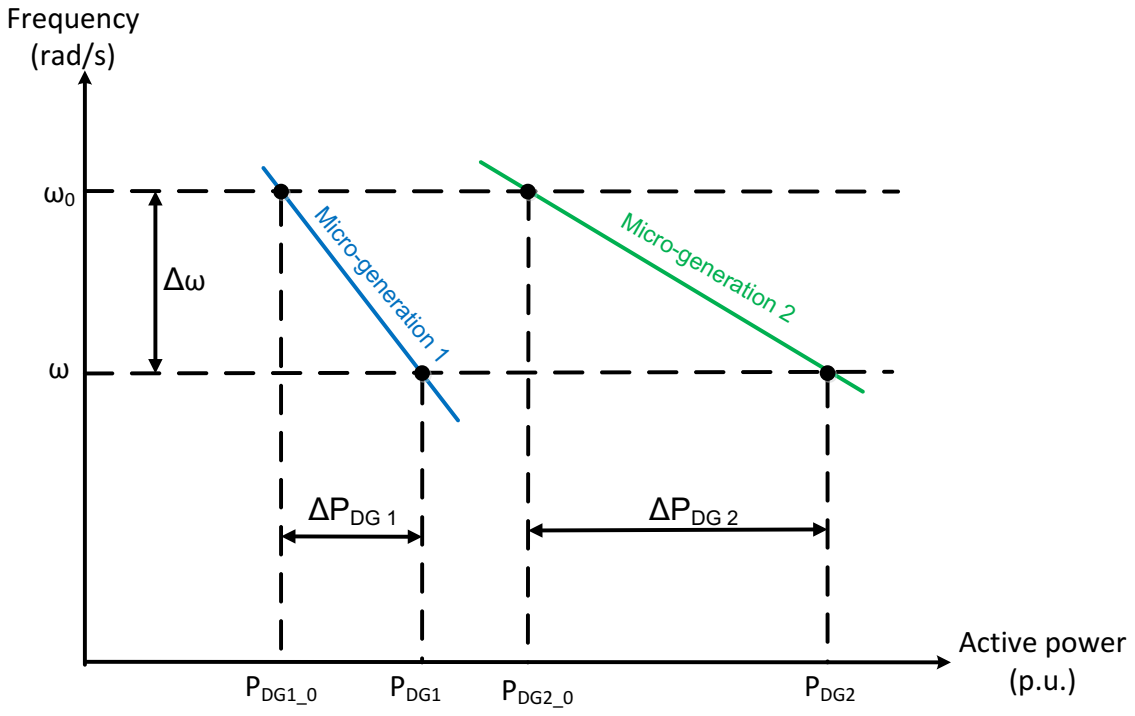

Figure 2.3 The *ω-P* droop control characteristic [3]

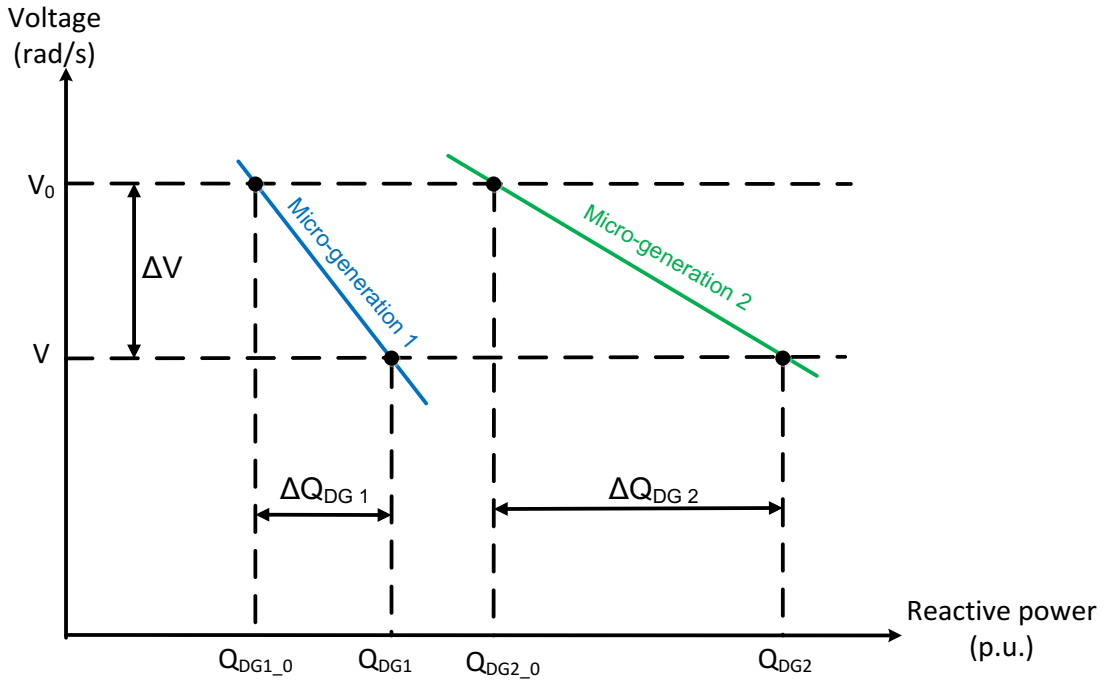

Figure 2.4 The *V-Q* droop control characteristic [3]

According to a general scheme for microgrid controls, microgrids can be controlled based on many types of control loops which can be mainly divided into four groups: local control, secondary control, emergency/centralized control and global control [3]. The four types of microgrid controls are briefly discussed in the following part.

2.2.1 Microgrid Local Controls

Microgrid local controls have different patterns relying on the type of micro-generations which are characterized based on their technologies (e.g., synchronous machines, induction machines, power invertors/convertors). The microgrid local controls operate with the inner control of the RESs/DGs which do not require the communication links, making simple circuits and reduction in costs. The main objective of microgrid local controls is the regulation and control of micro-generations in order to operate in a normal operation [3]. The scope of the controls focus on the operating point controls of micro-generations including power electronic interfaces. Due to a large penetration of RESs/DGs, local controllers become the

essential parts of a microgrid so as to suppress the fluctuated outputs of RESs/DGs in a microgrid. Examples of local controller designs are given in [5-7].

2.2.2 Microgrid Secondary Controls

The aim of microgrid secondary controls is to improve the power quality and system performance of a microgrid as the second layer controls after the local controls. Generally, the microgrid secondary controls can operate using two methods as follows [3]:

Single master operation is a method that a master micro-generation/inverter fixes frequency and voltage for other units in a microgrid. The connected micro-generations are operating using the reference from the master micro-generation.

Multi-master operation is a method that various micro-generations/inverters are controlled by methods of the central controller. The central controller will select and provide the set point to all micro-generations in a microgrid [8].

In the grid-connected operation, all micro-generations including inverters refer the reference frequency and voltage from a utility grid. Looking at the isolated operation, micro-generations lose the reference signals referred from a utility grid. In this case, micro-generations in a microgrid will coordinate to manage the operation using one of the mentioned methods for microgrid secondary controls.

The secondary control can be applied to synchronize a microgrid before connecting to a utility grid, to assist the transition from the isolated to grid-connected operation. Numerous examples of microgrid secondary controls are explained in [9-11].

2.2.3 Microgrid Global Controls

Microgrid global controls handle with all responsibilities of a microgrid including an interchange power with the utility grid or other microgrids. The central controller will control these responsibilities for an economic based on energy management level between a microgrid and the others. To achieve the goal of microgrid global controls,

estimation and wide-area motoring is required for numerous indices and parameters such as load pattern, predicted weather, generator reliability, system frequency, equipment status, system constraint and etc. For example, in Hachinohe microgrid project in Japan [12], economic dispatch and weekly operational planning are optimized and performed centrally by central controller incorporating global controls.

The global controls of a microgrid are responsible for determining the optimum generation plan to minimize production costs and balancing the generation and load demand, online capabilities of microgrid security and reliability, supervising the microgrid's market activities, and performing an energy management system (EMS). The microgrid global controls will be applied via the service of many controllers located in all levels. Examples of global controls are described in [13-15].

2.2.4 Microgrid Emergency/Centralized Controls

According to standards of an effective microgrid, the connected RESs/DGs in a microgrid should satisfy some interconnection standards (e.g., IEEE Standard 100-2000 for the operation controls of DGs outputs) and they should have the ability of intentional disconnection during a deviation from the specified frequency, voltage and phase angle (i.e., synchronization) [16]. In the emergency situation, a microgrid will transfer the operation from a dispatched power mode to a frequency control mode or voltage control mode of the islanding microgrid, hence a sudden change in the output power control of a microgrid is needed. After a microgrid survives from the islanding, the microgrid emergency/centralized control will perform technical and economical optimization processes of the isolated microgrid [3].

Thus, the plan for islanding operation can be considered as the most essential emergency control scheme for microgrids. During islanding, the frequency and voltage of a microgrid may operate outside the power quality conditions. Sometimes the islanding results in large mismatches between micro-generations and domestic loads, causing severe frequency and voltage control issues. Hence, the islanding plan is requested an aware scheduling of the available level of generation and load. To provide a secure system after islanding, it is importance to exploit energy storage systems, micro-generations, local loads, dynamic demand response and load shedding plans in a cooperative way [17]. Thus, dynamic demand response or load shedding can be included as an effective emergency/centralized control plan in order to handle with instability and collapse due to the generation or load changes for isolated microgrids [18].

2.3 Study Microgrid Design and Construction

2.3.1 Background of Study Microgrid

The study microgrid including equipment, load, feeder, generator parameters and constraints in this book is simulated from a real microgrid system available at the promoting renewable energy project in Mae Hong Son province, Thailand. According to Thailand's alternative energy development plan (2012-2021), it expects utilizations of renewable energy for 25 % of total energy consumption by 2021. Hence, the promoting renewable energy project in Mae Hong Son province is initiated and funded by United Nation Development Programme (UNDP) as well as Global Environment Facility (GEF) with Mae Hong Son governor office and provincial energy office ministry of energy as local partners. It aims to provide the national policy in promoting renewable energy by overcoming the obstacles that currently block widespread and sustainable utilization of renewable technologies for the facility of energy services in rural areas of Thailand [19-21].

Mae Hong Son province is situated in the north-west of Thailand, sharing a border with Myanmar. It has highest numbers of mountains. 90 % of its area is the thick forest and 3% is proper for agriculture. Mae Hong Son is the poorest province in Thailand. Looking the minimum basic need of income, Thailand expresses that the minimum income per person per year should be 20,000 THB (i.e., 60,000 JPY). In 2004, 62% of household in Mae Hong Son remained under this threshold [22].

Power supply in Mae Hong Son receives from the local generations (i.e., hydro, solar, and diesel) owned by the government, and from the neighboring utility grid (i.e., Chiang Mai province). In the wet season, excess electricity production in Mae Hong Son will be exported through the utility grid to Chiang Mai province, while this same grid line serves as back-up in the dry season. 97 % of Mae Hong Son population can access to electric power. 55 % of its population (i.e., 228 villages) can access to the utility grid. 10 % of its population (i.e., 173 villages) is provided by the off-grid systems (i.e., diesel generation sets, micro-hydro and PV). Looking at energy demand in Mae Hong Son, electricity consumption reaches the peak demand in May. Daily peak demand occurs from 7 p.m. to 8 p.m. according to the report from electricity generating authority of Thailand (EGAT) and households are the main electricity consumer (i.e., 55% of the share). The business and industrial has only 28 % of the share [22].

The study microgrid in this book considers three major generation units: the hydro generation unit with a power rating of 2 MVA (i.e., Hydro-Mae Pai), the mini-hydro

generation unit with a power rating of 1.2 MVA (i.e., Hydro-Mae Sarieng) and the solar photovoltaic (PV) generation unit (i.e., Solar PV farm) with a power rating of 3 MVA, and Battery Energy Storage Systems (BESS) with a power rating of 4 MVA as shown in Fig. 2.5. Each generation unit has its own local controller to handle with the relevant electrical variables. This microgrid is connected with groups of feeders which can be parts of distribution design. Each unit's feeder has a circuit breaker for disconnecting the corresponding feeder in order to avoid the impacts of severe disturbances. As seen in the demand side, the domestic load can be separated to sensitive/critical loads and non-sensitive/non-critical loads through separated feeders. The loads 1 and 4 are the sensitive loads with a peak power of 1.85 MW and 1.9 MW, respectively. The loads 2, 3 and 5 are the non-sensitive loads with a peak power of 1.7 MW, 1.75 MW and 2.4 MW, respectively. The microgrid is connected to the distribution system or other microgrids by a point of common coupling (PCC). The PCC is able to island the microgrid for maintenance purposes or when a fault or contingency occurs.

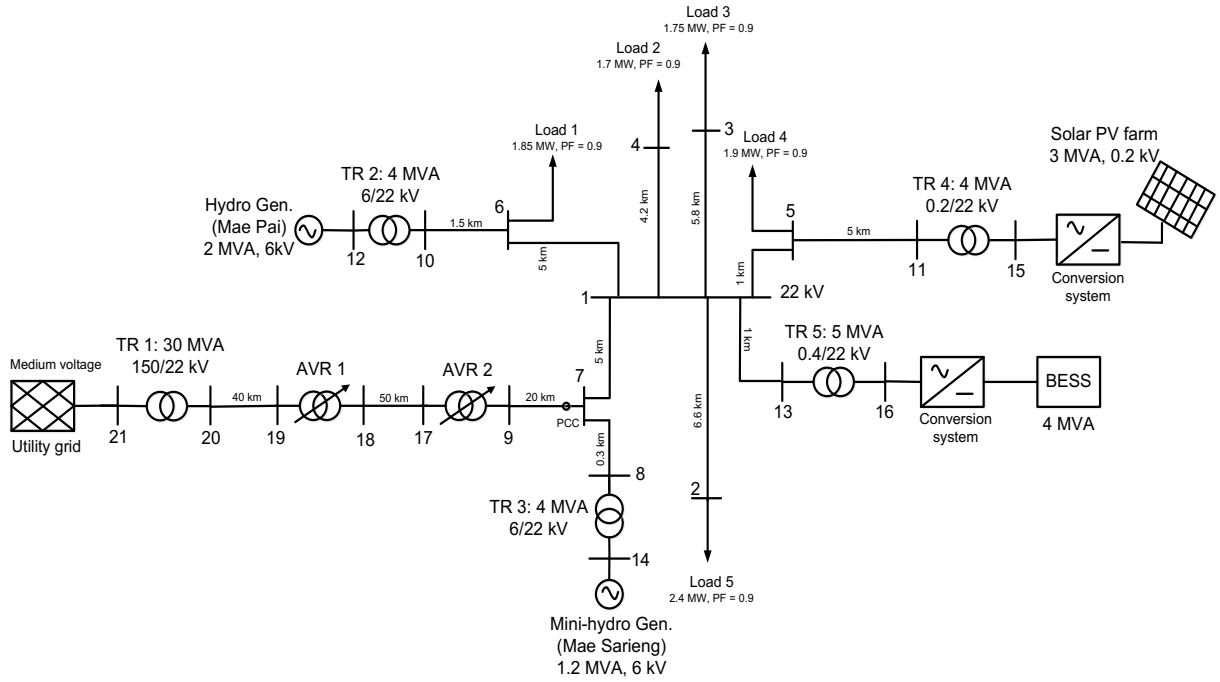

Figure 2.5 The typical microgrid structure

The structures and controls of micro-generation units in the study microgrid are explained based on their physical structures and power electronic interfaces. The simulated modelling of the study microgrid including the micro-generation units and domestic loads is designed and demonstrated by using PowerFactory-DIgSILENT (License Key ID: 0008261) which is the power system analysis software for application in generation, transmission and distribution systems as shown in Fig. 2.6. All system parameters of the typical microgird are provided in Appendix A.

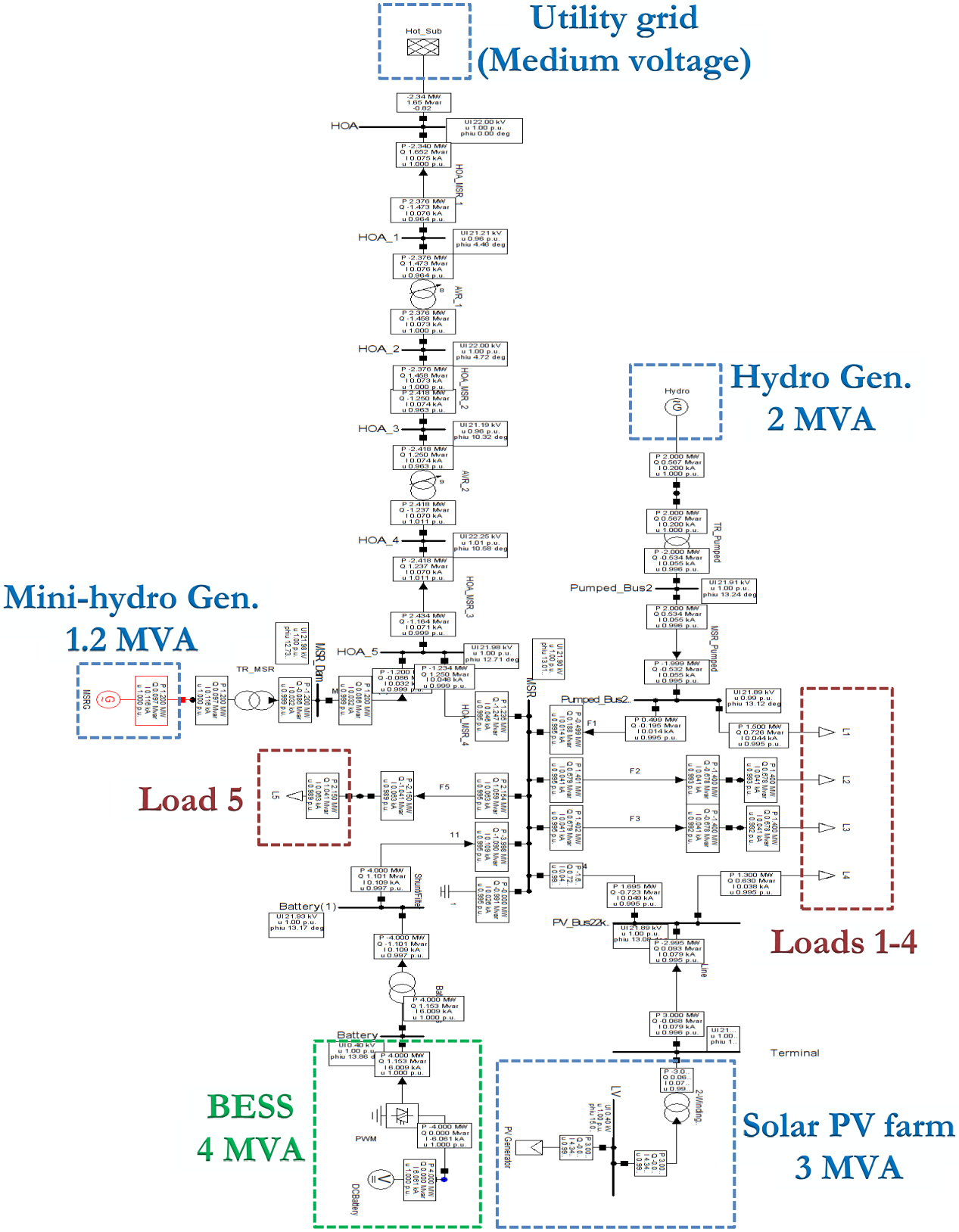

Figure 2.6 The simulated study microgrid in PowerFactory

2.3.2 Hydro Generation Power System

2.3.2.1 Introduction

Hydro generation power system is a clean, renewable and reliable energy resource which converts the kinetic energy from falling/moving water into electrical energy. Hydro generation power system is a nature technology with unit sizes from a few kW to hundreds of MW. In order to generate electrical power from the kinetic energy in water, the water must be moving with sufficient speed and volume to enable a generator. The economically attractive sites have been exploited for large hydro generation plants. Looking at the development of small/micro-hydro generation, their efficiency across a wide range of water flows can be enhanced using a variable speed generator with a power electronic interface. To improve the efficiency of micro-hydro generation, the doubly fed induction generators (DFIG) or full power converter (FPC) technologies based generators can be applied for variable speed operation [23].

2.3.2.2 Control of Hydro Turbines

A hydro turbine is designed and optimized for a defined rotational speed, hydraulic head and discharge. The conversion efficiency of the turbine changes due to the hydraulic conditions. To maximize the efficiency of variable speed operation over a range of different hydraulic conditions, the turbine speed can be varied or adjusted.
The turbine performance is demonstrated by the hill chart as shown in Fig. 2.7. The hill chart describes the efficiency curve of the turbine for different flow rates due to the rotor speed changes. As seen from the hill chart, it is obvious that the maximum efficiency of a turbine (i.e. optimum rotor speed) can be achieved through the solid dot line [23, 24].

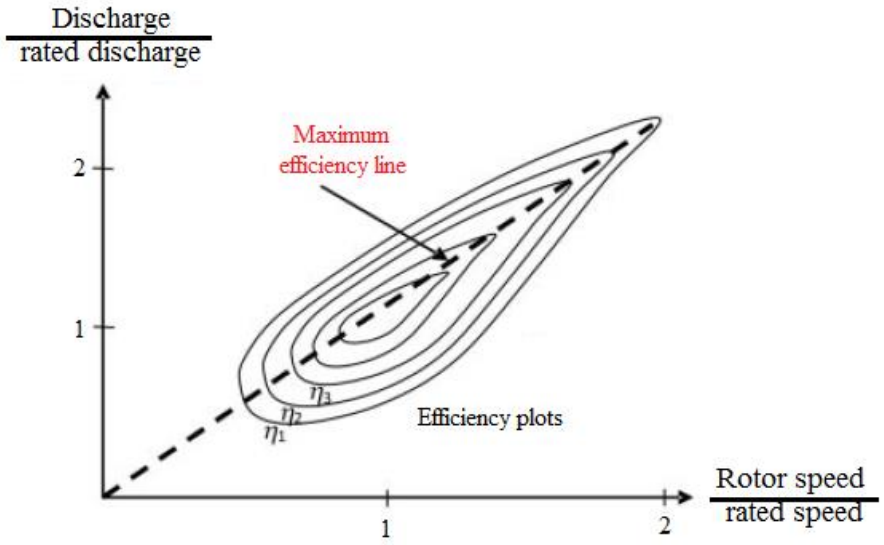

Figure 2.7 The hill chart for a hydro generation turbine [25]

The generated power output of hydro generation can be calculated as follows:

$$P_{Hydro} = \gamma \cdot Q \cdot H \cdot \eta \tag{2.12}$$

where P_{Hydro} is the generated power of a hydro plant (W),
Q is the water flow through a turbine (m^3/sec),
η is the efficiency of a turbine,
γ is the specific weight of water (N/m^3),
H is the net head of water/the different level of water between upstream and downstream of a turbine (m).

2.3.2.3 Hydro Generation Model in PowerFactory

The simulated modellings of the hydro generation and mini-hydro generation units are applied using a model of synchronous machine (i.e., ElmSym) connected with the busbar (i.e., ElmTerm) in DIgSILENT PowerFactory as shown in Fig. 2.8.

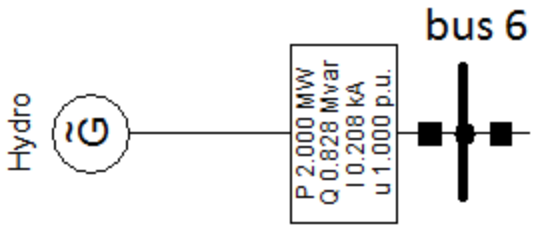

Figure 2.8 A hydro generation module connected the bus 6 in PowerFactory

Load flow setting parameters of hydro and mini-hydro generation units in PowerFactory is displayed in Figs. 2.9 and 2.10, respectively.

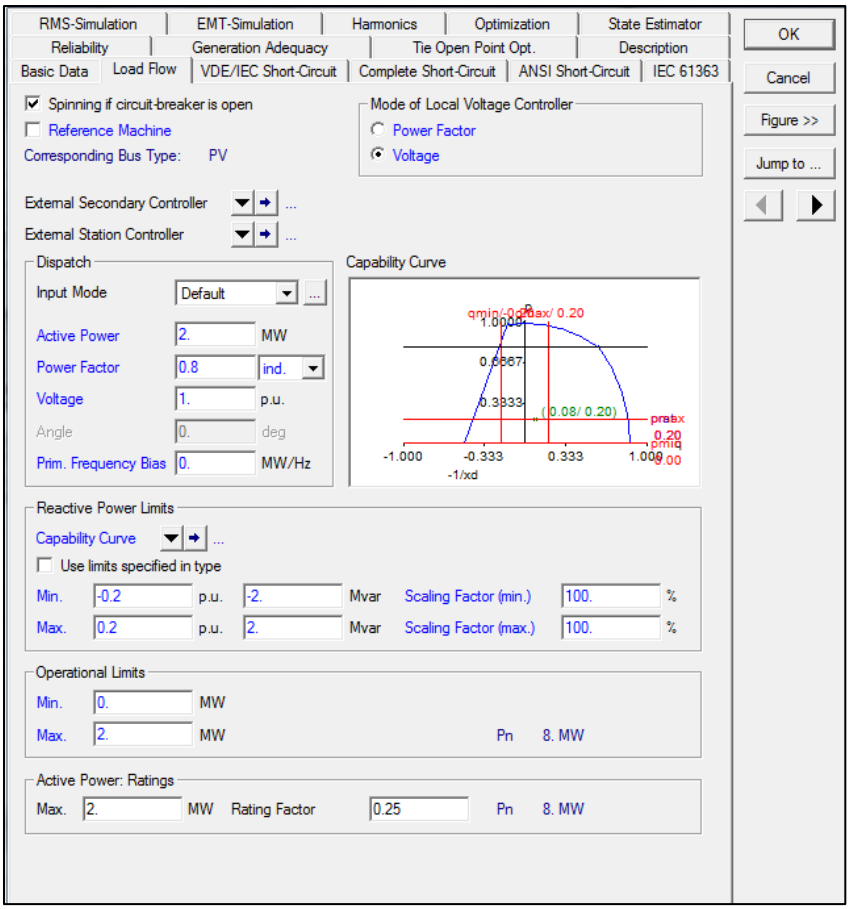

Figure 2.9 Load flow setting page of the hydro generation module (ElmSym) in PowerFactory

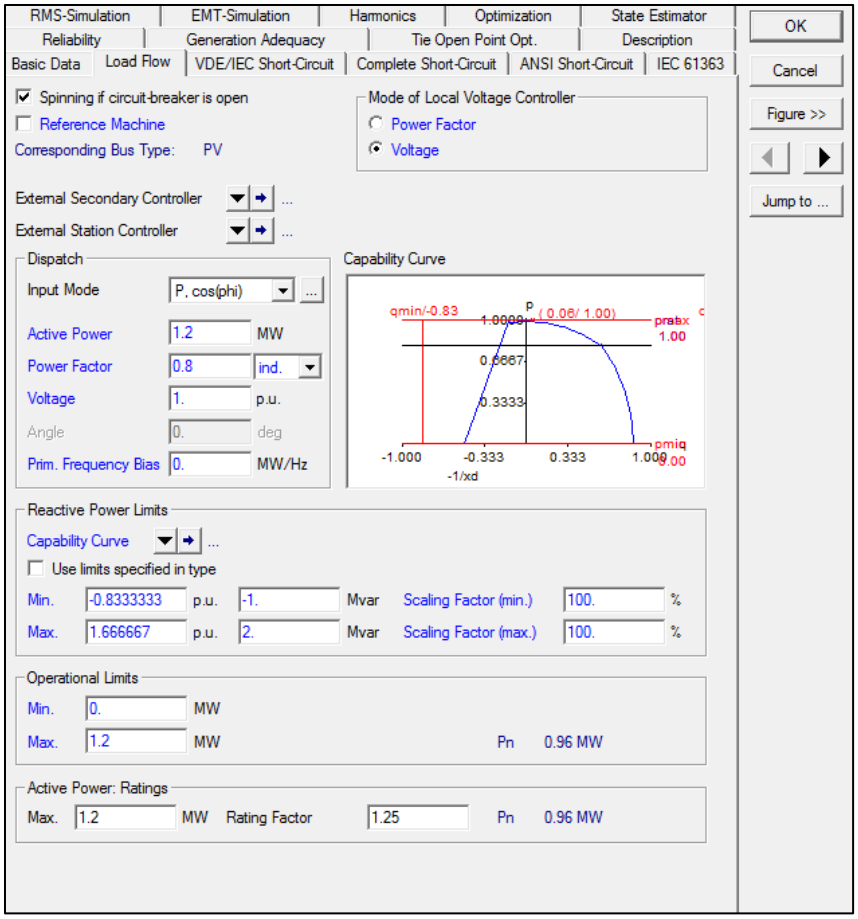

Figure 2.10 Load flow setting page of the mini-hydro generation module (ElmSym) in PowerFactory

The specific types of hydro generation and mini-hydro generation units are provided in Table. 2.1.

Table 2.1 Specific types of hydro generation units

Generation	Nominal apparent power (MVA)	Nominal voltage (kV)	Power factor	Connection
Hydro	2	6	0.8	YN
Mini-hydro	1.2	6	0.8	YN

2.3.3 Solar Photovoltaic Power Generation

2.3.3.1 Introduction

A solar photovoltaic (PV) generation system is an electric power system aimed to exploit usable power from the sun by means of photovoltaics. The sunlight is consisted of photons, or particles of solar energy. These photons collect numerous amount of energy with the different wavelengths. When the photons impact PV cells, they may be reflected, pass through, or be absorbed. Only the absorbed photons can produce energy to generate electric power. The environmental benefit of a solar PV system is minimal requiring no water for system cooling and generating. Generally, the PV cells generate direct current (DC) which can be used for small loads (e.g., electronic equipment). For commercial appliances or electric utilities, the generated power from PV cells must be converted to alternating current (AC) using inverters before fed into such a system. Nowadays, the numbers of PV installations are increasing worldwide due to their sustainable, clean and environmental friendly. For attractive PV installations, the feed-in-tariffs are the essential issue to demonstrate and guarantee payment per unit of electricity (p/kWh) for renewable energy generation.

2.3.3.2 Control of Solar Photovoltaic Power Generation

The control of a solar PV system consists of four major parts: a DC/DC converter (e.g., boost, push-pull, full bridge, flyback converters) for determining maximum power point tracking (MPPT) and increasing voltage, a single phase DC/AC inverter, an interface system, and a control system (e.g., MPPT, PWM, voltage control) as shown in Fig. 2.11.

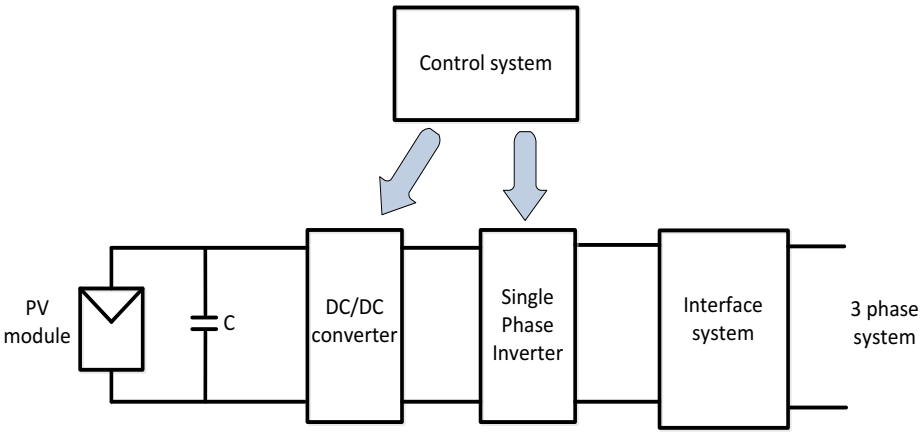

Figure 2.11 A solar PV structure

Inside of the PV module, it consists of a number of PV cells connected in series and in parallel. These cells operate based on the current versus voltage and the power versus voltage characteristics as shown in Fig. 2.12.

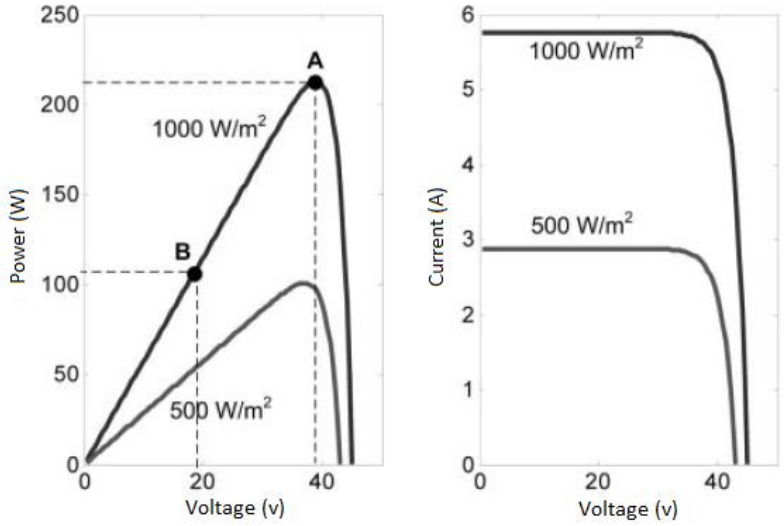

Figure 2.12 The typical power-voltage and current-voltage characteristics of a solar PV module for irradiance of 1000 W/m^2 and 500 W/m^2 [25]

The output power of PV is uncertain as it is mostly affected by the environmental factors, particularly the environmental random changes will inevitably lead to constantly changing of output power of PV [26, 27]. In order to illustrate PV characteristics in the operating condition, the influence of solar radiation and atmosphere temperature are designed. The temperature effect is denoted by a

temperature coefficient of T_{co} (1/c°) [28]. The efficiency of the inverter is multiplied by the DC output converting DC to AC power output of a PV system as shown in (2.13).

$$P_{PV} = n_{PV} P_{rate\ PV} (G / G_0)\left(1 - T_{co}\left(T_A - 25^{\circ}\right)\right) \eta_{inv}\eta_{rel} \tag{2.13}$$

where n_{PV} is PV module number,
$P_{rate\ PV}$ is PV array rated power (W),
G is the global insolation on PV array (W/m^2),
G_0 is the standard amount of insolation capacity of PV modules (W/m^2),
T_A is the ambient temperature,
T_{CO} is the temperature coefficient of the maximum power of PV,
η_{rel} is the relative efficiency of the PV modules,
η_{inv} is the efficiency of the inverter.

2.3.3.3 Solar Photovoltaic Model in PowerFactory

The solar PV generation model is represented in PowerFactory by the model of static generator in a built-in module when it is applied in the mode of current source. Thus, the simulated modelling of the solar PV unit is applied using a model of photovoltaic (i.e., ElmGenstat) connected with the bus 15 (i.e., ElmTerm) in PowerFactory as shown in Fig. 2.13.

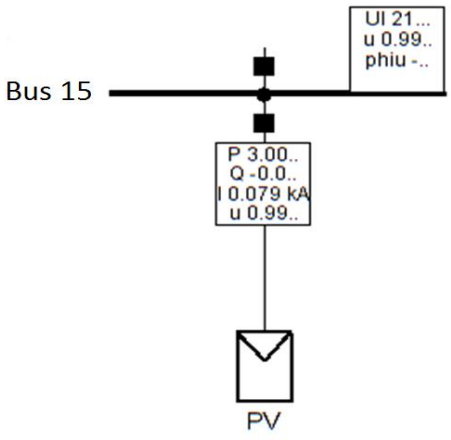

Figure 2.13 A solar PV module connected the bus 15 in PowerFactory

Load flow setting parameters of the solar PV unit in PowerFactory is displayed in Figs. 2.14.

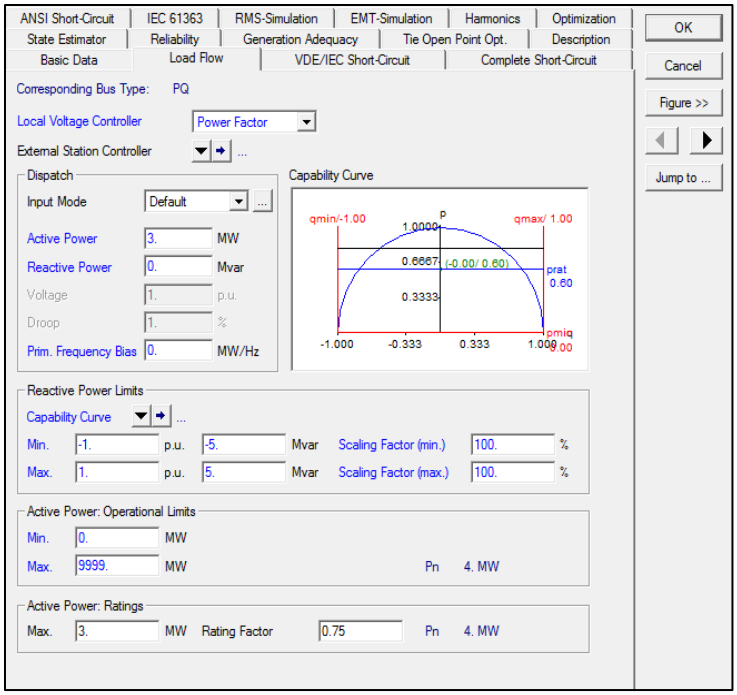

Figure 2.14 Load flow setting page of the solar PV module (ElmGenstat) in PowerFactory

Looking inside the solar PV module in Fig 2.15, it consists of ten major composite frames of control components: Solar radiation, Temperature, Photovoltaic model, Power measurement, Slow-frequency measurement, DC busbar and capacitor model, AC voltage, Active power reduction, Controller and Phase measurement [33]. These composite frames make the PV module more realistic. All control parameters are provided in Appendix B.

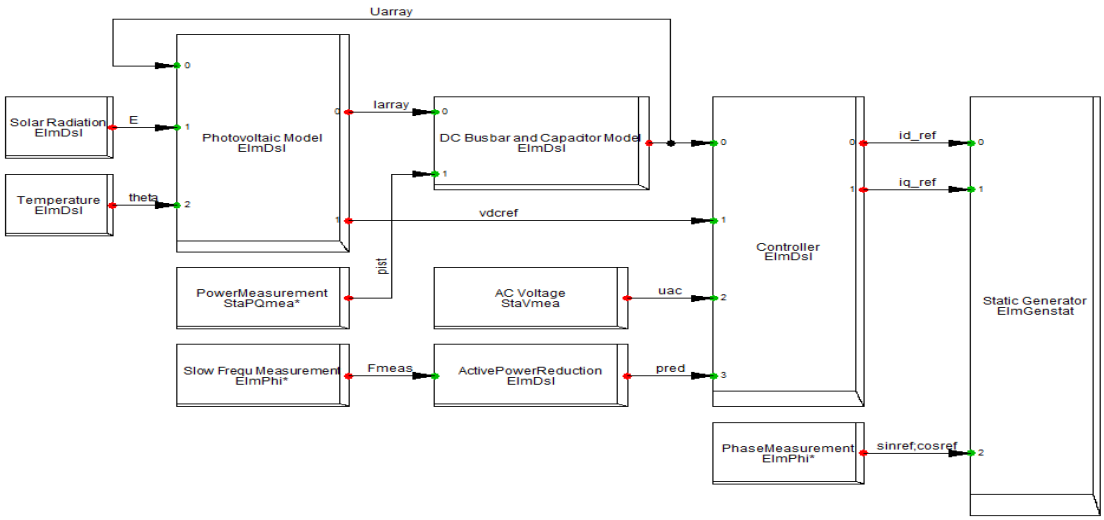

Figure 2.15 The structure of control components in the solar PV module in PowerFactory [33]

2.3.4 Battery Energy Storage System (BESS)

2.3.4.1 Introduction

Large amounts of electrical power can be stored in energy storage systems such as batteries, flywheels and superconducting magnetic energy storage (SMES) devices. Applications of battery energy storage systems (BESS) can be divided as an important function that can deliver short-term power (kW) or primarily supply energy (kWh) over a longer duration to power systems. BESS can also provide power quality, voltage and frequency supports to a system. Moreover, BESS can deliver a large amount of energy and discharge duration from several minutes to hours for supporting renewable energy and electrical energy shifting [1, 2].

Focusing on a small power system such as microgrids, it is considered by fast changes in the rotating speed of generators after any abrupt imbalance between generation and load demand. Conventional technologies applied for power generation cannot always response suddenly enough to avoid unacceptable frequency and voltage in such situations. To solve such problems, BESS can support a microgrid to reduce the frequency and voltage excursions caused by the changes of generation/load or the loss of generation or utility grid. The major benefits of BESS can be briefly explained as follows:

1. **Power quality**: BESS is used as un-interruptible power supplies (UPSs) or back-up system to improve, recover and stabilize the system during the loss of generation or utility grid. BESS can enhance system stability including frequency, voltage and power fluctuations as well as harmonics.

2. **Load following**: As BESS response is fast and high power output, thus BESS can be applied to track load change situations for load following services.

3. **Reserve power**: This application exploits BESS and aims to ensure system stability under unexpected conditions or the loss of load/generation. BESS is applied to replace the spinning reserve of large generators.

4. **Time shifting of electrical power**: The goal of this application is to store the power by BESS during durations of low demand or low price of electricity. Then, the stored power is discharged during high demand or high price.

5. **Renewable energy support**: Renewable energy resources (RESs) are intermittent supply and depend on weather conditions. BESS could support both RESs and the power system by smoothing their output and shifting the generated power in durations.

From the past up to present, BESS have been introduced in many types based on their capacities and BESS technologies [31, 32]. The brief review of BESS types and technologies are explained as follow:

Lead acid BESS have been applied for decades in stationary utility applications as back-up systems. Lead acid BESS are cheap but they require highly maintenance. Their lifetime is short compared with other BESS technologies. The utilizations of lead acid BESS are focused on large utility applications in comparable number.

Sodium sulfur (NaS) BESS have a large energy capacity and applied for electrical energy time shifting as well as smoothing RESs outputs. The utilizations of NaS BESS are focused on large utility applications like lead acid BESS.

Lithium ion (Li-ion) BESS are mostly considered as a distributed energy storage system (e.g., electric vehicles). Currently, Li-ion BESS is the fastest growing and most promising battery chemistry. They are a low maintenance BESS and their lifetime are quite long compared with other BESS technologies.

Nickel cadmium (NiCd) BESS were applied for cellphones, laptops and power tools. They have been replaced by other BESS from markets over past decades. NiCd BESS are made for wide range of sizes and capacities. They offer good lifetime and performance at low temperatures compared with other BESS. However, their materials are more expensive than lead acid BESS.

Redox flow BESS are introduced and suitable for renewable energy applications or stand-alone operations as they have a higher speed response and can withstand a large number of charge or discharge cycles. A redox flow BESS uses two electrolytes (i.e., positive and negative). The electrolytes are separately stored and pumped through a cell for recharged ability. The energy capacity depends on the electrolyte volume (i.e., amount of liquid electrolyte) in the tank. Their power outputs depend on the speed of ion transfer across the membrane.

In this research, the surplus power is stored by BESS for future uses, when the generation is higher than load demand for a grid-connected operation in the typical microgrid. The stored power is used to supply the load or stabilized the system when

there is any shortage/loss of generation or the utility grid during the isolated operation. For the isolated operation, BESS is used to stabilize the typical microgrid from instability and collapse in the presence of violent changes of generations/loads or the outage of generation/utility grid.

2.3.4.2 Control of Battery Energy Storage System

The control structure of the BESS consists of power conversion systems, battery cells and control parts which are shown in Fig. 2.16. The BESS uses power electronic circuits to connect to the microgrid via the power conversion systems. Thus, the voltage and frequency, as well as active and reactive powers of the BESS can be controlled by the power conversion system.

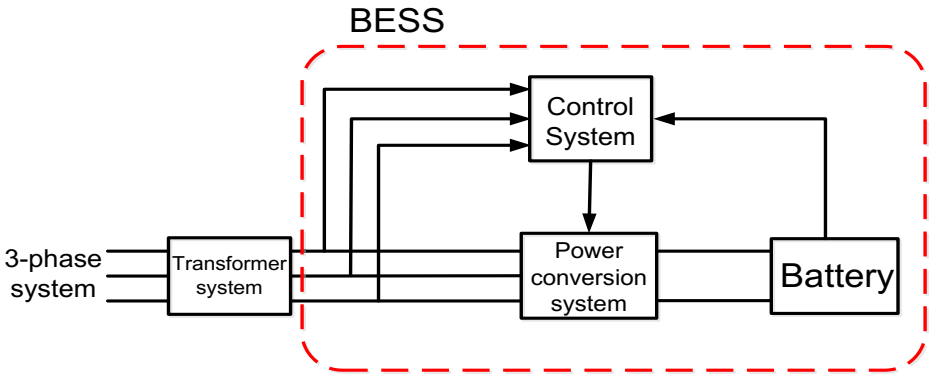

Figure 2.16 The structure of BESS

From the structure of BESS, the output of the DC voltage is presented as:

$$\Delta E_{do} = \frac{6\sqrt{6}}{\pi} E_t \tag{2.14}$$

where E_t is the AC voltage among a line and neutral.

The equivalent circuit analysis of BESS consists of a power conversion system connected to an equivalent battery, as shown in Fig. 2.17.

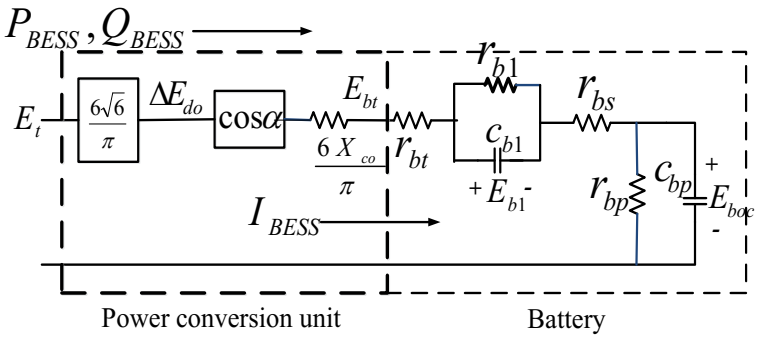

Figure 2.17 The equivalent circuit of BESS [18]

The terminal voltage of the equivalent battery is calculated from:

$$E_{bt} = \Delta E_{do}\cos\alpha - \frac{6}{\pi}X_{co}I_{BESS} \tag{2.15}$$

$$E_{bt} = \frac{3\sqrt{6}}{\pi}E_t\left(\cos\alpha_1 - \cos\alpha_2\right) - \frac{6}{\pi}X_{co}I_{BESS} \tag{2.16}$$

According to the equivalent circuit of the BESS, the expression of the DC current flowing into the battery is expressed as:

$$I_{BESS} = \frac{E_{bt} - E_{boc} - E_{b1}}{r_{bt} + r_{bs}} \tag{2.17}$$

where

$$E_{boc} = \frac{r_{bp}}{1 + ST_{bp}}I_{BESS} \tag{2.18}$$

$$E_{b1} = \frac{r_{b1}}{1 + ST_{b1}}I_{BESS} \tag{2.19}$$

where

$$T_{bp} = r_{bp}C_{bp} \tag{2.20}$$

$$T_{b1} = r_{b1}C_{b1} \tag{2.21}$$

According to the power conversion circuit analysis, the active and reactive powers of BESS are calculated as:

$$P_{BESS} = \frac{3\sqrt{6}}{\pi} E_t I_{BESS} \left(\cos\alpha_1 + \cos\alpha_2\right) \tag{2.22}$$

$$Q_{BESS} = \frac{3\sqrt{6}}{\pi} E_t I_{BESS} \left(\sin\alpha_1 + \sin\alpha_2\right) \tag{2.23}$$

where a_i is the firing delay angle of the power conversion system *i,*
E_{d0} is the maximum DC voltage of the converter,
E_{b1} is the battery overvoltage,
E_{bt} is the terminal voltage of the battery side,
E_{boc} is the battery open circuit voltage,
I_{BESS} is the DC current through the battery,
P_{BESS} is the active power provided by BESS,
Q_{BESS} is the reactive power provided by BESS,
r_{bt} is the connecting resistance,
r_{bs} is the battery internal resistance,
r_{bp} is the self-discharge resistance,
c_{bp} is the battery capacitance,
c_{b1} is the overvoltage capacitance,
X_{co} is the commuting reactance,
r_{b1} is the overvoltage resistance.

2.3.4.3 BESS Model in PowerFactory

In this book, the BESS is modeled as the voltage source (i.e., ElmDcu) connected with the pulse width modulation (PWM) converter (i.e., ElmVscmono) as shown in Fig. 2.18. The model of BESS is described by the terminal voltage and the internal resistance, which indicate functions of different characteristics and variables of BESS

such as the state of charge (SOC), the BESS lifetime and BESS temperature. The BESS is fully charged if the SOC is equal to one and it is zero if the BESS is empty.

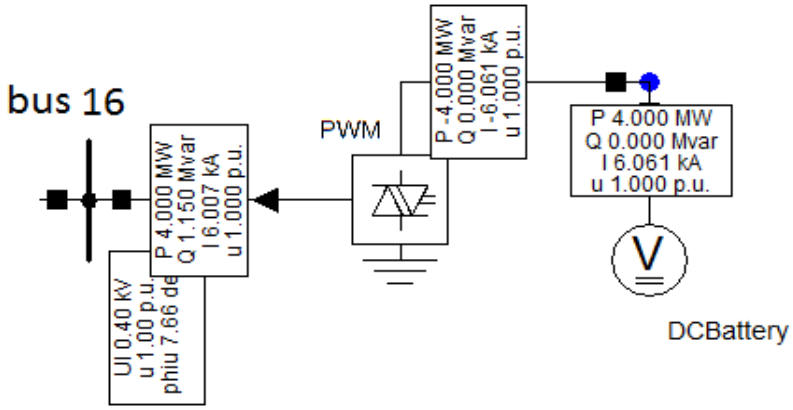

Figure 2.18 A BESS model connected the bus 16 in PowerFactory

Load flow setting parameters of the BESS in PowerFactory is displayed in Figs. 2.19.

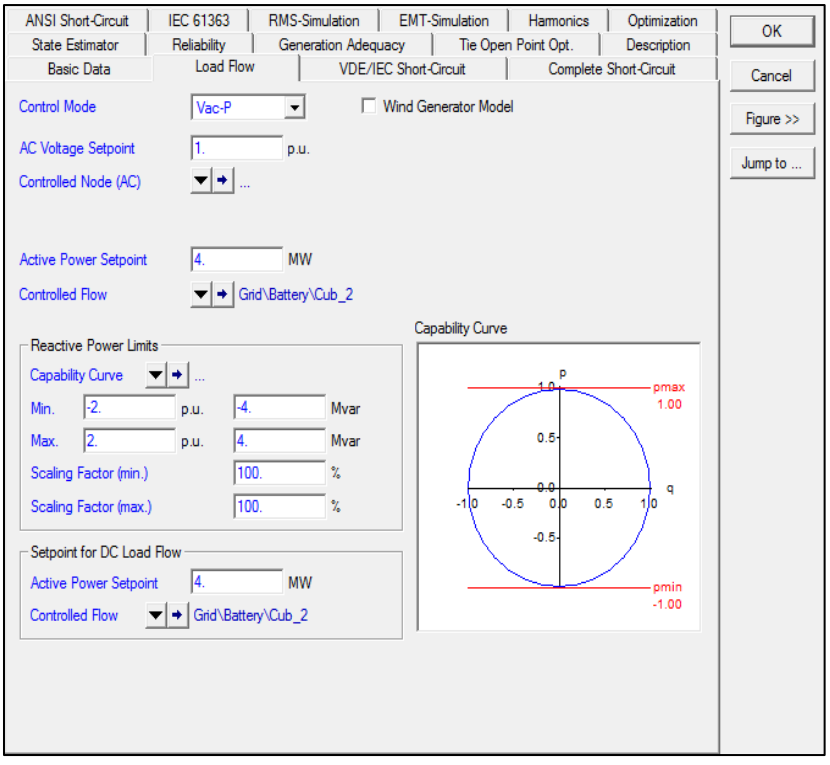

Figure 2.19 Load flow setting page of the BESS module (ElmVscmono) in PowerFactory

It is assumed that the SOC battery does not reach less than 20 %. Thus, voltage is assumed as linearly dependent on the SOC. The internal resistance is assumed to be a constant as it must be very small due to the high current applications [33]. Afterwards, the BESS model (i.e., ElmDSL) is designed by using DIgSILENT simulation language (DSL) model according to:

$$E_{bt} = E_{b1} \cdot SOC + E_{boc}(1 - SOC) - I_{BESS} \cdot r_{bs} \tag{2.24}$$

The BESS model requires DC current as input signal and the outputs of BESS model are DC voltage, SOC and DC cell voltage and current for the charge controller as seen in Fig. 2.20 [33]. All control parameters are given in Appendix C.

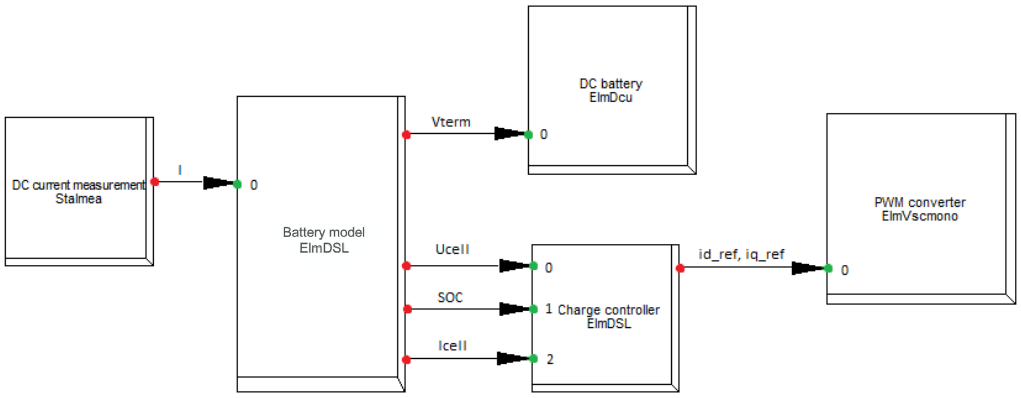

Figure 2.20 The structure of control components in BESS module in PowerFactory

2.4 Summary

In this chapter, the subject of microgrids providing definitions and basic concepts is addressed and described. The microgrid operation, control and its application are presented. Afterwards, the typical microgrid background is described and then extended to the modellings and controls of generation units and BESS. Finally, the

constructions of generation units and BESS in the typical microgrid are designed and explained using DIgSILENT PowerFactory.

2.5 References

1. C. Marnay, H. Aki, K. Hirose, A. Kwasinski, S. Ogura and T. Shinji, How two microgrid fared after the 2011 earthquake, *IEEE Power Energy Magazine*, 13(3), 44-57, 2015.
2. H. Beverani, Y. Mitani, and Y. Watanabe, Microgrid controls. In: H. Wayne Beaty, editor, *Standard Handbook for Electrical Enineers,* 16th edn, McGraw-Hill, New York, Section 16.9, 159-176, 2013.
3. H. Beverani, Y. Mitani, and Y. Watanabe, *Power System Monitoring and Control*. John Wiley & Sons, New York, Chapter 9, 187-206, 2014.
4. H. Beverani, and T. Hiyama, Automatic generation control (AGC): fundamentals and concepts. *Intelligent Automatic Generation Control*, CRC Press, New York, Chapter 2, 11-36, 2011.
5. H. Karimi, E. J. Davison, and R. Iravani, Multivariable servomechanism controller forautonomous operation of a distributed generation unit: design and performance evaluation, *IEEE Trans. Power Syst.*, 25(1), 2010.
6. F. Habibi, A. H. Naghshbandy, and H. Bevrani, Robust voltage controller design for an isolated microgrid using Kharitonov's theorem and D-stability concept, *Int. J. Electr. Power*, 44, 656–665, 2013.
7. F. Habibi, On robust and intelligent frequency control synthesis in the microgrids, M.Sc. thesis, University of Kurdistan, Sanandaj, Iran, 2012.
8. J. A. Peças Lopes, C. L. Moreira, and A. G. Madureira, Defining control strategies for analyzing microgrids islanded operation, *IEEE Trans. Power Syst.*, 21(2), 916–924, 2006.
9. H. Bevrani and S. Shokoohi, An intelligent droop control for simultaneous voltage and frequency regulation in islanded microgrids, *IEEE Trans. Smart Grid*, 4(3), 1505–1513, 2013.
10. H. Bevrani, F. Habibi, P. Babahajyani, M. Watanabe, and Y. Mitani, Intelligent frequency control in an AC microgrid: on-line PSO-based fuzzy tuning approach, *IEEE Trans. Smart Grid*, 3(4), 1935–1944, 2012.
11. H. Bevrani and T. Hiyama, Neural network based AGC design. In: *Intelligent Automatic Generation Control*, CRC Press, New York, 2011, Chapter 5, pp. 95–122.
12. Y. Fujioka, H. Maejima, et al., Regional power grid with renewable energy resources: a demonstrative project in Hachinohe. In: *CIGRE Session, Paris*, 2006.
13. F. Katiraei, R. Iravani, N. Hatziargyriou, and A. Dimeas, Microgrids management, *IEEE Power Energy Mag.*, 6(3), 54–65, 2008.

14. A. Vaccaro, M. Popov, D. Villacci, and V. Terzija, An integrated framework for smart microgrids modeling, monitoring, control, communication, and verification, *Proc. IEEE*, 99(1), 119–132, 2011.
15. 30. A. G. Tsikalakis and N. D. Hatziargyriou, Centralized control for optimizing microgrids operation, *IEEE Trans. Energy Convers.*, 23(1), 241–248, 2008.
16. IEEE Standard 100-2000, IEEE Standard Dictionary of Electrical and Electronic Terms, 2000.
17. C. C. L. Moreira, Identification and development of microgrids emergency control procedures, Ph.D. thesis, University of Porto, 2008.
18. T. Kerdphol, Y. Qudaih, Y. Mitani, Optimum battery energy storage system using PSO considering dynamic demand response for microgrids. *International Journal of Electrical Power and Energy Systems*, 83(1), 58–66, 2016.
19. CIGRE Thailand [Online]. Available: <http://www.cigre-thailand.org/tncf/events/seminar2014/mae_hong_son.pdf>.
20. W. Ithiam, S. Asadamonkol, T. Sumranwanich, Smart grid national pilot project in Mae Hong Son Province, Thailand. *J Energy Environ*., 26(1), 23–34, 2015.
21. United Nations Development Programme (UNDP) in Thailand [Online].Available: <http://www.th.undp.org/content/thailand/en/home/operations/projects/environment_and_energy/REinMHS.html>.
22. United Nations Development Programme (UNDP) project document, *Promoting Renewable Energy in Mae Hong Son Province*, GEF project ID:3359, UNDP PIMS ID: 3908; 2013.
23. Fraile-Ardanuy, J., Wilhelmi, J.R., Fraile-Mora, J.J. and Perez, J.I., Variable speed hydro generation: operation and control. *IEEE Transaction Energy Conversion*, 21(2), 569–574, 2006.
24. EU project ENERGIE, *Status Report on Variable Speed Operation in Small Hydropower*, 2000, <http://ec.europa.eu/energy/res/sectors/doc/small_hydro/statusreport_vspinshp_colour2.pdf>.
25. J. Ekanayake, K. Liyanage, J. Wu, A. Yokoyama, and N. Jenkins, *Smart Grid Technology and Applications*, John Wiley & Sons, New York, Chapter 10, 204-232, 2012.
26. N. Jenkins, J.B. Ekanayake, and G. Strbac, *Distributed Generation*, Institution of Engineering and Technology, Stevenage, 2010.
27. N. Mohan, T.M. Undeland, and W.P. Robbins, *Power Electronics: Converters, Applications and Design*, John Wiley & Sons, Inc., New York, 1995.
28. S.B. Kjaer, J.K. Pedersen, and F. Blaabjerg, A review of single-phase gridconnected inverters for photovoltaic modules. *IEEE Transactions on Industry Applications*, 41(5), 1292–1306, 2005.

29. R. Sarrias, L.M. Fern´andez, C.A. Garc´ıa, and F. Jurado, Energy storage systems for wind power application. *International Conference on Renewable Energies and Power Quality* (ICREPQ'10), 23–25, 2010.
30. Public Interest Energy Research Program, *An Assessment of Battery and Hydrogen Energy Storage Systems Integrated with Wind Energy Resources in California*, California Energy Commission, 2005.
31. A. Ter-Gazarian, *Energy Storage for Power Systems*, IEE Energy Series 6. 1994.
32. J. Ekanayake, K. Liyanage, J. Wu, A. Yokoyama, and N. Jenkins, *Smart Grid Technology and Applications*, John Wiley & Sons, New York, Chapter 12, 259-277, 2012.
33. DIgSILENT GmbH, *PowerFactory user's manual version 14.1*, Gomaringen, Germany, 2012.
34. N. Hatziargyriou, *Microgrids: Architectures and Control*, John Wiley & Sons, New York, Chapter 1, 1-24, 2014.

Chapter 3

Analytic Method-based BESS Size Optimization

3.1 Introduction of Analytic Method

From the past up to present, generation and demand balancing strategies have been designed and applied in numerous researches and studies in order to control and balance the system in response to load/generation change situations or the outage of distributed generation/utility grid [1-4]. These strategies are implemented by exploiting energy storage systems to store excess power during low demand periods for release as demand rises such as in a vehicle-to-grid (V2G) system in Japan to use the energy storage from electric vehicles (EVs) during peak times and then charge it during the off peak times. These strategies can also be done by increasing/decreasing generation, applying load shedding or dynamic demand response to the system so as to balance power between generation and load, reducing frequency and voltage excursions. Focusing on smart grid technology incorporating generation and demand balancing, users, industrial and appliances can communicate with the grid using digital means and can be switched on and off by the grid operator in order to operate at off-peak times [5].

3.2 Analytic Method Structure for BESS sizing

In this chapter, generation and demand balancing in the microgrid is achieved by an optimum size of BESS. The optimum size of BESS is determined by using the proposed analytic method with the objective of frequency control of the microgrid.

The goal of the optimum sizing of BESS-based analytic method is to determine an optimum size of BESS at minimal total BESS cost in order to balance generation and load demand after the loss of the utility grid, and to prevent the microgrid from instability and system collapse. The input of the proposed analytic method is frequency of the microgrid and then the output are an optimum size and total cost of BESS as shown in Fig. 3.1.

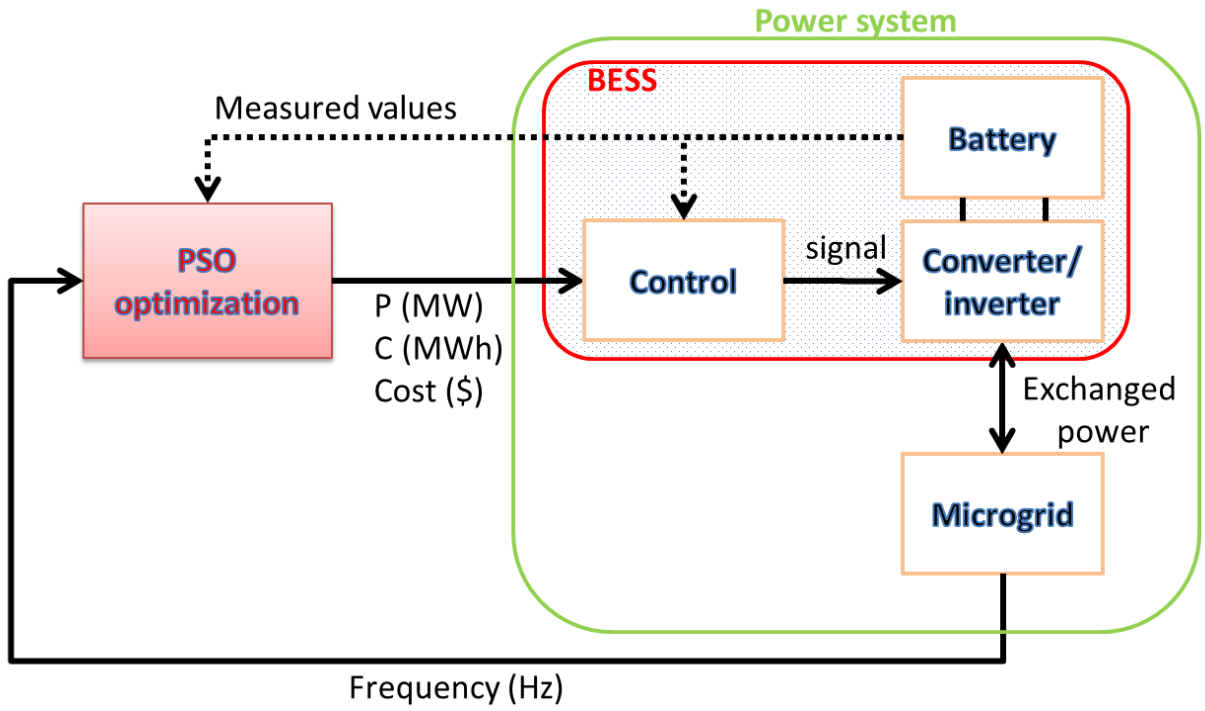

Figure 3.1 The analytic method structure for BESS sizing

Recently, modern BESS technologies such as redox-flow battery are introduced to markets and they are better suited for renewable energy applications or stand-alone operations as they have a higher speed response and can withstand a larger number of charge or discharge cycles. The utilizations of redox-flow BESS are gaining more attention lately. However, there is no clear suggestion and comparison of these BESS technologies for integrating into microgrids. Hence, this chapter investigates and determines the economical performance of redox-flow BESS in different technologies for integrating into a microgrid [6-8].

The capital, operating and maintenance costs are considered for integrating BESS into the microgrid which are included the cost of required inverter. The studies of BESS retail prices have confirmed that BESS cost is a function of power and capacity rating [9].

The Capital Cost of BESS

The capital cost of BESS ($C_{Capital}$) is characterized as a function of two major parts; that is, BESS capacity and BESS power. Thus, the capital cost of BESS can be calculated as follows:

$$C_{Capital} = C_P P_{BESS} + C_W C_{BESS} \tag{3.1}$$

where P_{BESS} is the BESS power (MW),
C_{BESS} is the BESS capacity (MWh),
C_P is the specific power cost of BESS ($/MWh),
C_W is the specific capacity cost of BESS ($/MWh).

The Operating and Maintenance Cost of BESS

The operating and maintenance cost of BESS ($C_{O\&M}$) is consisted of two main parts; that is, the fixed part depending on the BESS power and the variable part related to its annual discharged energy. The operating and maintenance cost of BESS can be calculated as follows:

$$C_{O\&M} = C_{Mf} P_{BESS} + W_{annual} C_{MV} \tag{3.2}$$

where C_{Mf} is the fixed cost of BESS ($/MW/year),
C_{MV} is the variable operating and maintenance cost of BESS ($/MWh/year),
W_{annual} is the BESS annual discharge energy (MWh/year) [10].

In this chapter, the total cost of installed BESS (C_T) is calculated in two cases depending on BESS technologies. This paper uses the following technologies: Polysulfide-Bromine (PB) and Vanadium Redox (VR) BESS technologies which are the most popular redox-flow battery as shown in Table 3.1.

Table 3.1 Redox-flow BESS technical and economical data [10]

Technologies	VR BESS	PB BESS
C_P ($/kW)	426	150
C_W ($/kWh)	100	65
C_{Mf} ($/kW/year)	9	9
C_{MV} ($/kWh/year)	0	0
Life time (years)	15	15
Efficiency (%)	70	65

The Objective Functions of Analytic Method

The first objective of the proposed analytic method for BESS sizing is to determine an optimum size of BESS in order to prevent the microgrid from instability and system collapse after the loss of the utility grid (e.g., blackouts or disasters) and the second objective is to minimize a total cost of BESS for 15 years installation in the microgrid due to the BESS life time in Table 3.1. The objective functions are expressed as follows:

(1) BESS size minimization

$$\text{Minimize } f_1 = \min (P_{BESS}) \tag{3.3}$$

(2) Total BESS cost minimization

$$\text{Minimize } f_2 = \min (C_T) = \min (C_{Capital} + C_{O\&M}) \tag{3.4}$$

Subject to:

BESS constraints are imposed on the optimization as follows:

$$P_{BESS}^{\min} \le P_{BESS} \le P_{BESS}^{\max} \tag{3.5}$$

where P_{BESS} is the rated power capacity of BESS (MW) ,
P^{BESS}_{min} is the allowed minimum rated power capacity of BESS,
P^{BESS}_{max} is the allowed maximum rated power capacity of BESS.

$$C_{BESS}^{\min} \le C_{BESS} \le C_{BESS}^{\max} \tag{3.6}$$

where C_{BESS} is the rated energy capacity of BESS (MWh),
C^{BESS}_{min} is the allowed minimum rated energy capacity of BESS,
C^{BESS}_{max} is the allowed maximum rated energy capacity of BESS.

Microgrid frequency constraint is imposed on the optimization as follows:

$$F_{\min} \le F \le F_{\max} \tag{3.7}$$

where F is the nominal frequency of the isolated microgrid (Hz.),
F_{min} is the allowed minimum nominal frequency of the isolated microgrid,
F_{max} is the allowed maximum nominal frequency of the isolated microgrid.

Description of the Optimum Sizing of BESS based on Analytic Method

The overall flow chart of the optimal sizing of BESS-based analytic method is shown in Fig. 3.2. The solution algorithm of this method is shown as follows [11, 12]:

Step 1: Initialize generation data from photovoltaic (P_{PV}), hydro generation (P_{HV}), mini hydro generation (P_{Mini}).

Step 2: Set the total load demand in the microgrid (P_{Load}).

Step 3: Calculate differential power (P_D) between generation and load.

Step 4: Set differential power (P_D) equal to BESS power (P_{BESS}).

Step 5: Check the condition if $P_{BESS} > 0$, execute the objective functions. If $P_{BESS} \leq 0$, the process ends and there is no BESS installation in the system

Step 6: After executing the objective functions, check the condition if the microgrid frequency is within the frequency acceptable range. If the microgrid frequency does not satisfy the condition, the program will increase P_{BESS} by 0.1 MW and go to Step 5 again. This step will continue until it meets the condition.

Step 7: If the microgrid frequency satisfies the frequency condition, the process ends and then an optimal size and cost of BESS are obtained.

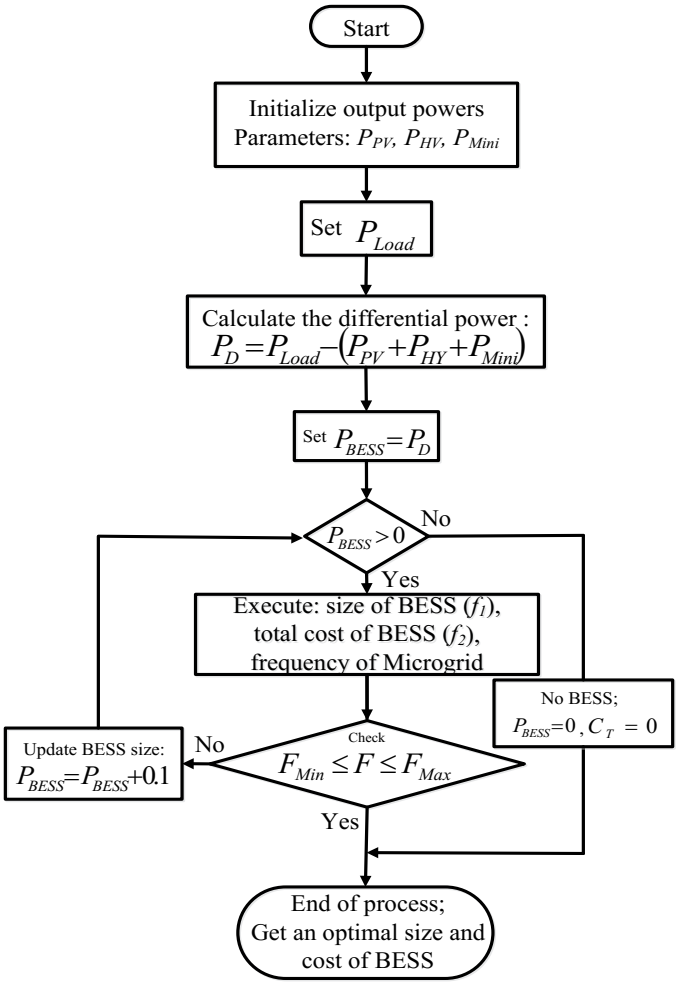

Figure 3.2 The flow chart of the optimal sizing of BESS by using analytic method-based frequency control

3.2.1 Main DPL Script for Analytic Method

In this section, an implementation of the optimum sizing of BESS based on analytic method using DIgSILENT PowerFactory programming language (DPL) is discussed and shown below [13]. In this code, several comments are included to describe step-by-step the proposed analytic method. First of all, all of the internal variables have to be declared in this program. The function "GetCaseObject" is used to extract active project current functions. In this case, the command "ComLdf" is applied in object "ldf". Then, power flow algorithm is calculated using the "Execute"

command. In the first step, the micro-generations and domestic loads in the microgrid must be scaled. The command "AllRelevant" is a DPL internal method that returns a set with calculation relevant objects. Thus, a set must be created that should contain all the system's generations and loads. The associated DPL object class for hydro generations is "*.ElmSym". The associated DPL object class for the solar PV farm is "*.ElmGenstat". Afterwards, each element of the generations is accessed and obtained with the active power values by using the commands "FirstFilt" and "GetVal", respectively. As shown in the following piece of code, the parameters "pgini" of each micro-generation (i.e., Hydro, Mini-hydro and Solar PV) are obtained for the active power.

```
!=========================================================================
!      Optimal Sizing of BESS-based analytic method for Microgrids
!      Developer: Thongchart KERDPHOL
!      Kyushu Institute of Technology, Mitani Laboratory, Japan
!=========================================================================:
! Variable declaration
set A,A1;
object O,ldf,sim,O1,HY,HM,PV,L1,L2,L3,L4,L5;
double PB,F,i,G1,G2,PV1,L11,L21,L31,L41,L51,sum, Cvr, Cpb,cap;

ClearOutput();
ldf = GetCaseObject('ComLdf');     ! Run power flow calculation
ldf.Execute();


A=AllRelevant();                   ! All components are saved in A

HY=A.FirstFilt('Hydro*.ElmSym');   ! Access Hydro generation
HY.GetVal(G1,'pgini');             ! Obtain power data from Hydro
printf('Hydro Gen :%f MW',G1);     ! Show data to command window

HM=A.FirstFilt('MSRG*.ElmSym');    ! Access Mini-hydro generation
HM.GetVal(G2,'pgini');             ! Obtain power data from Mino-hydro
printf('Mini-Hydro Gen :%f MW',G2);! Show data to command window

PV=A.FirstFilt('PV*.ElmGenstat');  ! Access PV farm
PV.GetVal(PV1,'pgini');            ! Obtain power data from PV farm
printf('PV gen :%.2f MW',PV1);     ! Show data to command window
```

In the second step, domestic load powers in the microgrid must be scaled. The associated DPL object class for domestic loads is "*.ElmLod". Later, each element of the loads is accessed and obtained with the active power values by using the commands "FirstFilt" and "GetVal", respectively. As shown in the following piece of the code, the parameters "plini" of each domestic load are obtained for the active power.

```
L1=A.FirstFilt('L1*.ElmLod');          ! Access Load 1
L1.GetVal(L11,'plini');                ! Obtain power data from Load 1
printf('Critical Load1 :%f MW',L11);   ! Show data to command window

L2=A.FirstFilt('L2*.ElmLod');          ! Access Load 2
L2.GetVal(L21,'plini');                ! Obtain power data from Load 2
printf('Non-Critical Load2 :%f MW',L21);! Show data to command window

L3=A.FirstFilt('L3*.ElmLod');          ! Access Load 3
L3.GetVal(L31,'plini');                ! Obtain power data from Load 3
printf('Non-Critical Load3 :%f MW',L31); ! Show data to command window

L4=A.FirstFilt('L4*.ElmLod');          ! Access Load 4
L4.GetVal(L41,'plini');                ! Obtain power data from Load 4
printf('Critical Load4 :%f MW',L41);   ! Show data to command window

L5=A.FirstFilt('L5*.ElmLod');          ! Access Load 5
L5.GetVal(L51,'plini');                ! Obtain power data from Load 5
printf('Non-Critical Load5 :%f MW',L51); ! Show data to command window
```

Next step, the differential power between generation and load is calculated and saved in the variable "sum".

```
sum=(L11+L21+L31+L41+L51)-(PV1+G1+G2);   ! Determine different power
```

Afterwards, the associated DPL object class for the PWM converter in the BESS is "*.ElmVscmono". The element of PWM converter in the BESS is accessed by using the command "FirstFilt". Later, the differential power is set equal to the BESS power by using the command "SetVal".

```
O=A.FirstFilt('PWM*.ElmVscmono');  ! Access to BESS
O.SetVal(sum,'psetp',0);    ! Setting BESS power equal to different power
printf('Set the intitial size of BESS :%.2f MW',sum); ! Show data
```

According to the checking condition of BESS size as regard to Step 5, an "if…else" statement is used to define whether a BESS size is higher than zero.

After that, power flow calculation is calculated using the "Execute" command again. The simulation case of the microgrid is executed using the command "ComSim". A set with calculation relevant objects from the simulation case is collected in the set "A" by using the command "AllRelevant". The system frequency of the microgrid is accessed and obtained by using the commands "FirstFilt" and "GetVal", respectively. Later, check the condition if the system frequency is within the frequency acceptable range. If the system frequency does not satisfy the condition,

the program will increase/decrease the BESS power from the variable "sum" by 0.1 MW. This process will continue until it meets the condition.

```
if (sum>0) { ! Check BESS power > 0 ? If yes, do the for-loop, else, end
for(i=1;i<100;i=i+1) {
ldf = GetCaseObject('ComLdf');  ! Run power flow calculation
ldf.Execute();
sim = GetCaseObject('ComSim');  ! Run the simulation case
sim.Execute();

A=AllRelevant();
O1=A.FirstFilt('MSR*.ElmTerm');  ! Access system frequency of MG
O1.GetVal(F,'m:fehz');           ! Check system frequency of MG
printf('Frequency of Microgrid :%f Hz',F);!Show frequency to command win
          if(F<49.95){     ! in case of frequency < 49.45
                sum=sum+0.1; ! increase BESS power by 0.1
                O.SetVal(sum,'psetp',0); ! Set the power to BESS
                printf('Size of BESS at iteration %d :%f MW',i,sum);
                cap=5*sum;   ! determine BESS capacity
                ! determine total cost of VR BESS
                 Cvr=(426*1000*sum)+(100*1000*cap)+(15*9*1000*sum);
                ! determine total cost of PB BESS
                 Cpb=(150*1000*sum)+(65*1000*cap)+(15*9*1000*sum);
                }
                else if (F>50.05){ ! in case of frequency > 50.05
                sum=sum-0.1;   ! decrease BESS power by 0.1
                O.SetVal(sum,'psetp',0); ! Set the power to BESS
                printf('Size of BESS at iteration %d :%f MW',i,sum);
                 cap=5*sum;    ! determine BESS capacity
                 ! determine total cost of VR BESS
                 Cvr=(426*1000*sum)+(100*1000*cap)+(15*9*1000*sum);
                 ! determine total cost of PB BESS
                 Cpb=(150*1000*sum)+(65*1000*cap)+(15*9*1000*sum);
                 }
     else{
        break;} ! if frequency is within the acceptable range,
                ! then program breaks the for-loop and gets optimum BESS
  }
 }
```

As shown in the following piece of the code, when the system frequency of the microgrid satisfies the condition, the program breaks the "for loop" statement and the optimal size and cost of BESS are automatically obtained and deployed.

```
!Show optimum BESS size in MW
printf('The optimal size of BESS :%f MW',sum);
!Show optimum BESS capacity in MWh
printf('The optimal capacity of BESS :%f MWh',cap);
!Show optimum total cost of VB for 15 years installation
printf('The total cost of VR BESS:%f $/15 years',Cvr);
!Show optimum total cost of VB for 15 years installation
printf('The total cost of PB BESS :%f $/15 years',Cpb);
```

3.3 Results and Discussion

In the performed simulation, the study microgrid performance is tested by implementing the most severe disturbance (i.e., disconnecting of the microgrid from the utility grid) at 10.0 s. The microgrid operation is transited from the grid connected to isolated operation, resulting in the shortage of power supply in the microgrid at that time. It is assumed that the nominal system frequency is 50 Hz and system frequency declines below 49.95 Hz is required the implementation of the optimum size of BESS based on analytic method.

As regard to Fig. 3.3, the magnitude of the frequency deviation with the BESS-based conventional size reaches 51 Hz and takes more time to stabilize than the optimum sizing of BESS-based analytic method. In case of no BESS, the system frequency drops drastically because the power supply cannot meet the load demand, resulting in system collapse. It is confirmed that the performance of system frequency is much better when the optimum sizing of BESS-based analytic method is applied as shown in Table. 3.2.

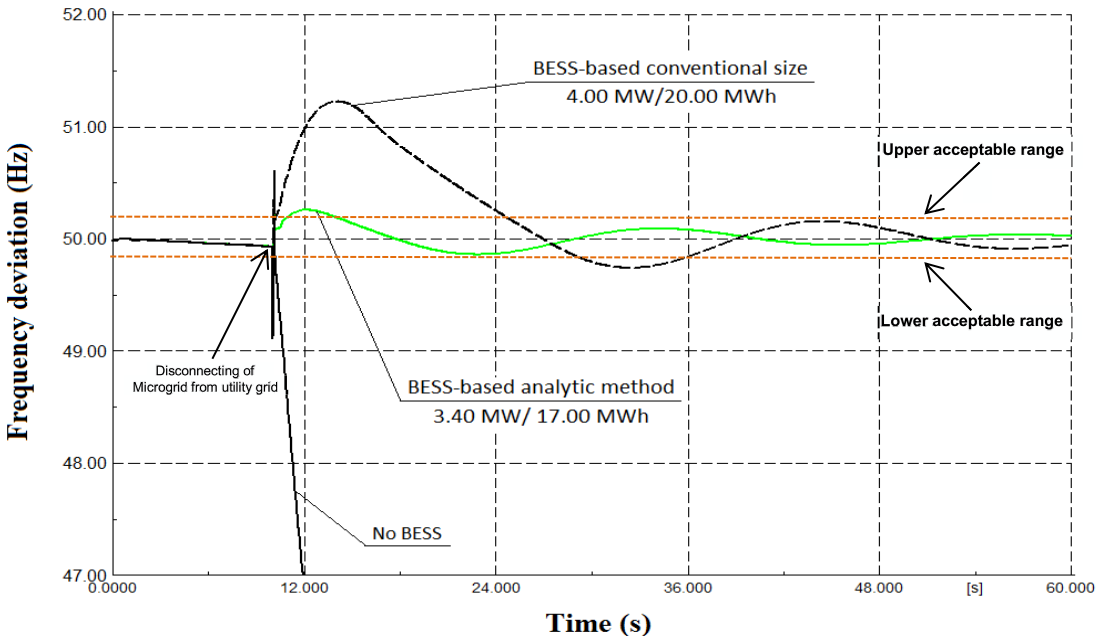

Figure 3.3 Frequency deviation of the microgrid after the severe disturbance

Looking at the system voltage in Fig. 3.4, it is obvious that the optimum sizing of BESS-based analytic method can remain almost the same voltage deviation as the conventional size of BESS. As seen in the case of no BESS, the system voltage

decreases drastically because the power supply cannot meet the load demand, resulting in system collapse.

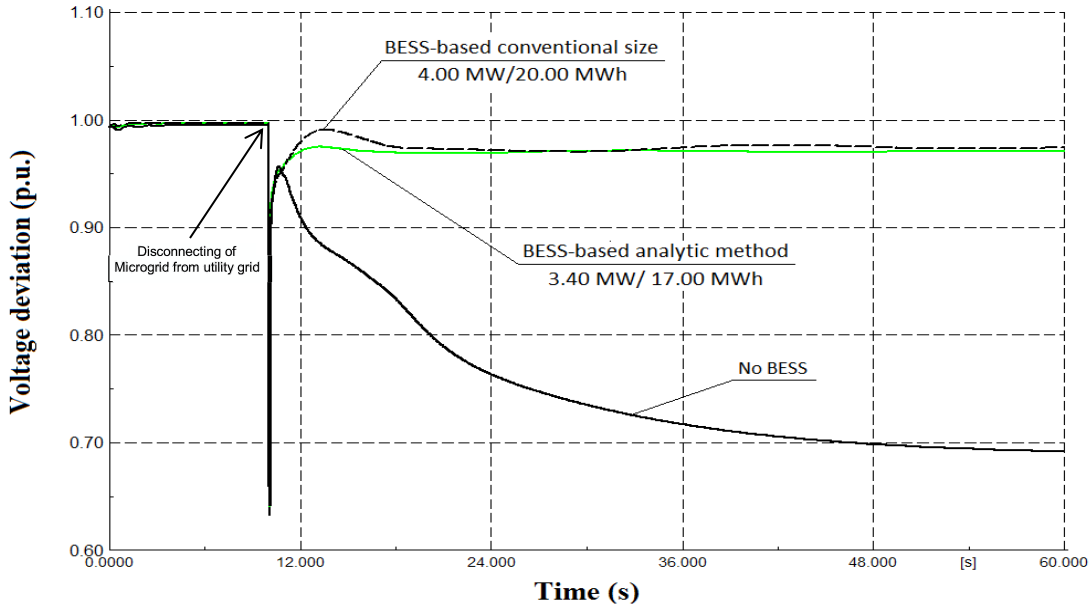

Figure 3.4 Voltage deviation of the microgrid after the severe disturbance

As seen in Fig. 3.5, the PV output power measured from the system is shown during the severe disturbance. It is obvious that the severe disturbance is capable of causing the interruption about 2.95 s to the solar PV power output measured from the system.

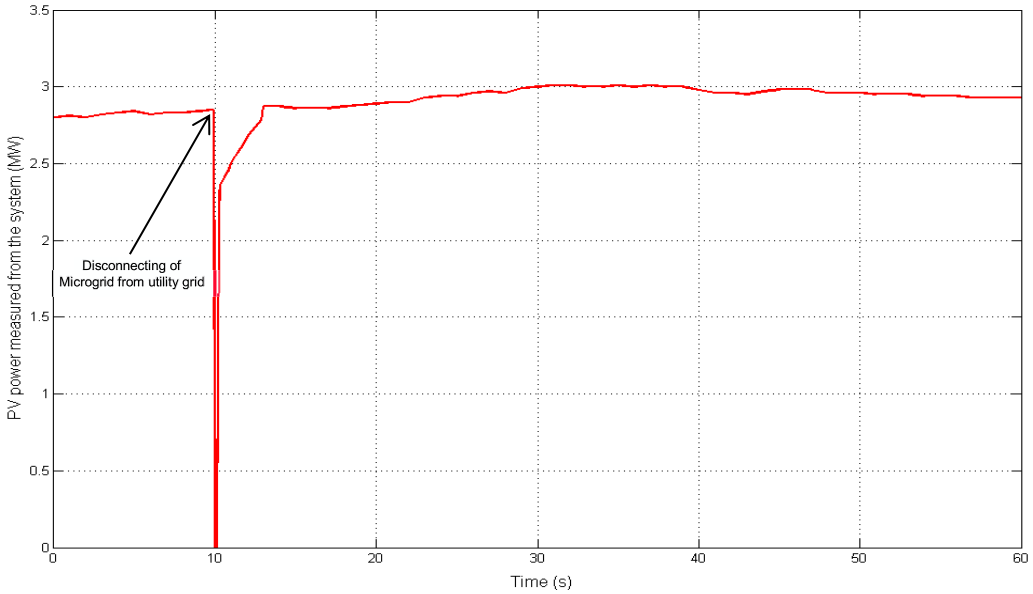

Figure 3.5 PV power output measured from the system during the severe disturbance

In terms of BESS economical performance, it is obvious that the microgrid incorporating the polysulfide-bromine (PB) BESS provides lower the total cost of BESS than the microgrid incorporating vanadium redox (VR) BESS for 15 years installation as shown in Table. 3.2. Thus, it can be summarized that the installation of polysulfide-bromine BESS is likely to be more cost-effective than the installation of vanadium redox BESS for 15 years installation in a microgrid.

Table 3.2 Comparison parameters of two methods

Parameters	BESS-based conventional size	BESS-based analytic method
Power capacity (MW)	4.000	3.400
Energy capacity (MWh)	20.000	17.000
Frequency magnitude (Hz) Reference: 50.00	51.223	50.310
Voltage (p.u.) Reference: 0.990	0.974	0.971
Total cost of VR BESS ($/15 years)	4,244,000	3,607,400
Total cost of PB BESS ($/15 years)	2,440,000	2,074,000

3.4 Summary

This chapter presents an analytic method to determine an optimum size of BESS for microgrids, known as a conventional method. The background of the analytic method is briefly reviewed. Later, the optimum sizing of BESS using analytic method is designed based on frequency control of the microgrid. Multi-objective functions are considered in this method; that is, the minimization of BESS size and cost with different storage technologies. The modelling of the proposed analytic method is designed and demonstrated using DIgSILENT PowerFactory/DPL Script. Based on the results, it is obvious that the optimal sizing of BESS-based analytic method can improve and recover dynamic stability of the microgrid from the emergency situation

to the normal equilibrium state. Compared with the conventional size of BESS, the optimum sizing of BESS-based analytic method gives better performance of the microgrid in terms of peak deviation and settling time. The conventional size of BESS is reduced to the optimum size of BESS, resulting in the reductions in the total cost and capacity of BESS. In terms of BESS economical performance, it is demonstrated that the installation of polysulfide-bromine BESS is likely to be more cost-effective than the installation of vanadium redox BESS for 15 years installation in a microgrid.

Result Evaluation of Analytic Method

According to the optimum sizing of BESS-based analytic method, it shows that the analytic method is still not smooth and not stable enough to recover the system dynamic and performance from the emergency situation to the normal equilibrium state. Hence, a fast, smooth and secure optimization method is required to determine an optimum size of BESS for microgrids.

3.5 References

1. J.P. Chaves-Avila, K. Wurzburg, T. Gomez, P. Linares, How renewable sources are changing EU electricity prices. *IEEE PES Power Energy Mag*, 13(4):29–40, 2015.
2. Y. Ono, N. Uchiyama, T. Nakamura, Y. Fujita, Short-term balanced supply and demand control system for microgrids. *Hitachi Rev.*, 54(3):141–144, 2005.
3. N. Uchiyama, and et al., Supply and demand control method in local distribution system including distributed generators. *In: Annual meeting record of IEEJ*, 1(6-085) in Japanese.2004.
4. V. Zdraveski, M. Todorovski, L. Kocarev, Dynamic intelligent load balancing in power distribution networks. *Int J Electr Power Energy Syst*, 73 (1):157–162, 2015.
5. T. Kerdphol, K. Fuji, Y. Mitani, M. Watanabe, and Y. Qudaih, Optimization of a battery energy storage system using particle swarm optimization for stand-alone microgrids. *International Journal of Electrical Power and Energy Systems*, 81(1), 32–39, 2016.
6. H. Ibrahim, A. Ilinca, J. Perron, Energy storage systems-characteristics and comparisons. *Renew Sustain Energy Rev*, 12(5):1221–50, 2008.

7. S. Chakraborty, T. Senjyu, H. Toyama, A. Saber, T. Funabashi, Determination methodology for optimizing the energy storage size for power system. *IET Gen Trans Distr*, 3(11):987–99, 2009.
8. B. Turker, S. Klein, E. Hammer, B. Lenz, and L. Komsiyska, Modeling a vanadium redox battery system for large scale applications. *Int J Electr Power Energy Syst*, 66:26–32. 2013.
9. C. Lo, and K. Kwan, Economic dispatch and optimal sizing of battery energy storage systems in utility load-leveling operations. *IEEE Trans Energy Convers*, 14 (3):824–9. 1999.
10. F. Chacra, P. Bastard, G. Fleury, R. Clavreul, Impact of energy storage costs on economical performance in a distribution substation. *IEEE Trans Power Syst*. 20(2):684–91. 2005.
11. T. Kerdphol, Y. Qudaih, P. Garasi, and Y. Mitani, Optimal Sizing of Battery Energy Storage System in Microgrid Considering Load Shedding Scheme, *International Journal of Smart Grid and Clean Energy,* 4(1): 22-29, 2015.
12. T. Kerdphol, Y. Qudaih, and Y. Mitani, Optimal Battery Energy Storage Size using Particle Swarm Optimization for Microgrid System, *International Review of Electrical Engineering,*10(2): 125-130, 2015.
13. DIgSILENT GmbH, *PowerFactory user's manual version 14.1*, Gomaringen, Germany, 2012.

Chapter 4

PSO-based BESS Size Optimization

4.1 Introduction of PSO Method

Particle swarm optimization (PSO) method is one of the famous and modern intelligent techniques inspired by social behavior of bird flocking or fish schooling. It was invented by Kennedy and Eberhart in 1995 [1]. PSO optimizes a problem by trying to improve a candidate solution considering a given measure of quality from particles. PSO is initiated with a group of random particles to determine optimum solutions by updating generations. These particles move around in the search space according to the particle's position and velocity. Each particle remembers its own best position found in the search space [2]. This position is called the personal best (Pbest). Among these Pbest, only one particle, that has the best fitness, called the global best (Gbest). Thus, each particle's movement is influenced by its local personal best and global best [3, 4]. The velocity and position update equations of PSO are expressed as follows:

$$x_j^{i+1} = x_j^i + v_j^{i+1} \tag{4.1}$$

$$v_j^{i+1} = v_j^i + c_1 r_1 \left(P_{best}^i - x_i^i \right) + c_2 r_2 \left(G_{best}^i - x_j^i \right) \tag{4.2}$$

where

x	is particle's position,
v	is particle's velocity (path direction),
c_1	is weight of local information,
c_2	is weight of global information,
P_{best}	is best position of the particle,
G_{best}	is best position of the iteration,
r_1,r_2	are random variable,
N_I	is iteration number,
N_P	is particle number,
i	is iteration; i = 1,2...,N_I,
j	is particle; j = 1,2,...,N_P.

Compared with other conventional AI techniques, the main benefits of PSO are briefly described as follows [5]:

1. PSO is less dependent on the set of the initial values, implying the robustness of the method.
2. PSO needs only a fitness function to measure the quality of a solution instead of complex mathematic operations such as Hessian, gradient or matrix inversion. Thus, it can reduce the computational complexity and relieve some of the limitations that are usually imposed on the objective function such as differentiability, continuity or convexity.
3. PSO is easy to combine with other optimization tools so as to perform hybrid capabilities.
4. PSO is less sensitive to a good initial solution as it is a population-based method.
5. PSO has the capability to avoid local minima as it follows probabilistic transition rules.
6. PSO requires less parameter tuning compared with other AI methods.

4.2 PSO Method Structure for BESS sizing

In this chapter, an optimum size of BESS is determined by using the proposed PSO with the objective of frequency control of the microgrid [6]. The goal of the optimum sizing of BESS-based PSO is to evaluate an optimum size of BESS at minimal total BESS cost in order to balance generation and load after the loss of the utility grid, and to prevent the microgrid from instability and system collapse [7]. The input of the proposed PSO is frequency of the microgrid and then the output are an optimum size and total cost of BESS as shown in Fig. 4.1.

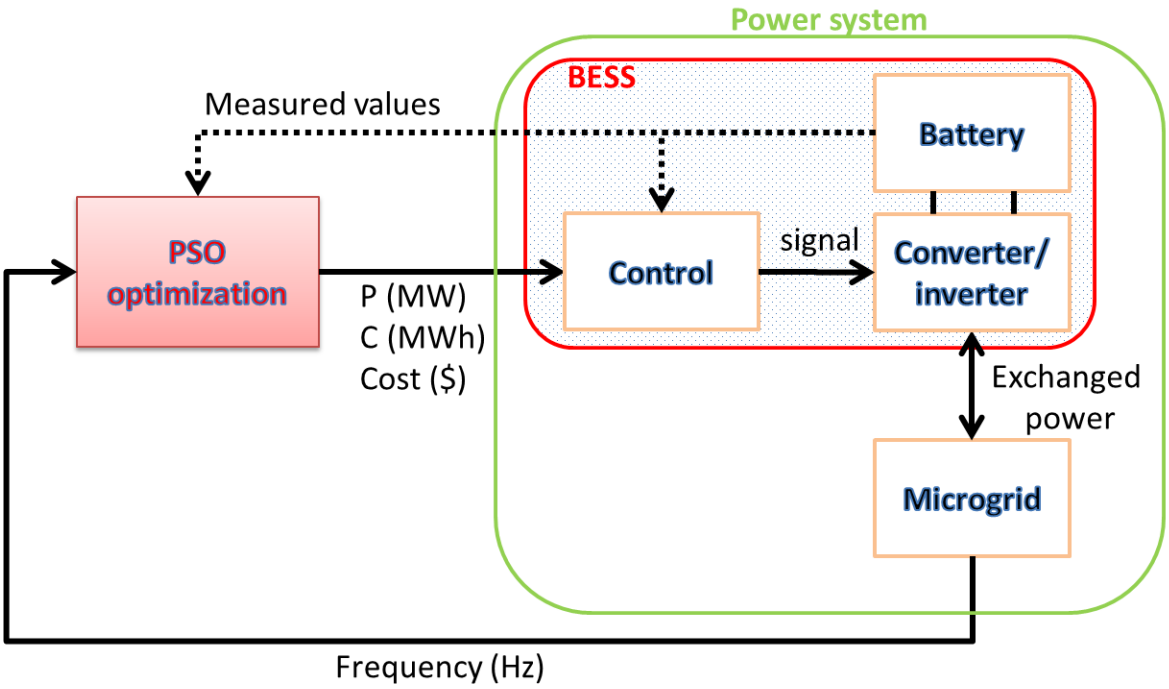

Figure 4.1 The PSO structure for BESS sizing

Currently, new BESS technologies such as redox-flow battery are introduced to markets and they are better suited for renewable energy applications or stand-alone operations as they have a higher speed response and can withstand a larger number of charge or discharge cycles. The utilizations of redox-flow BESS are gaining more attention lately. In order to compare with the analytic method, this chapter also investigates and evaluates the economical performance of redox-flow BESS in different technologies for integrating into a microgrid [8-10].

The capital, operating and maintenance costs are considered for integrating BESS into the microgrid which are included the cost of required inverter. The studies of

BESS retail prices have confirmed that BESS cost is a function of power and capacity rating [11].

The Capital Cost of BESS

The capital cost of BESS ($C_{Capital}$) is characterized as a function of two major parts; that is, BESS capacity and BESS power. Thus, the capital cost of BESS can be calculated as follows:

$$C_{Capital} = C_P P_{BESS} + C_W C_{BESS} \tag{4.3}$$

where P_{BESS} is the BESS power (MW),
C_{BESS} is the BESS capacity (MWh),
C_P is the specific power cost of BESS ($/MWh),
C_W is the specific capacity cost of BESS ($/MWh).

The Operating and Maintenance Cost of BESS

The operating and maintenance cost of BESS ($C_{O\&M}$) is consisted of two main parts; that is, the fixed part depending on the BESS power and the variable part related to its annual discharged energy. The operating and maintenance cost of BESS can be calculated as follows:

$$C_{O\&M} = C_{Mf} P_{BESS} + W_{annual} C_{MV} \tag{4.4}$$

where C_{Mf} is the fixed cost of BESS ($/MW/year),
C_{MV} is the variable operating and maintenance cost of BESS ($/MWh/year),
W_{annual} is the BESS annual discharge energy (MWh/year) [12].

In this section, the total cost of installed BESS (C_T) is calculated in two cases depending on BESS technologies. This paper uses the following technologies: Polysulfide-Bromine (PB) and Vanadium Redox (VR) BESS technologies which are the most popular redox-flow battery as shown in Table 3.1.

The Objective Functions of PSO

The first objective of the proposed PSO method is to evaluate an optimum size of BESS in order to avoid the microgrid from instability and system collapse after the loss of the utility grid (e.g., blackouts or disasters) and the second objective is to minimize a total cost of BESS for 15 years installation into the microgrid due to the BESS life time in Table 3.1. The objective functions are represented as follows:

(1) BESS size minimization

$$\text{Minimize } f_1 = \min (P_{BESS}) \tag{4.5}$$

(2) Total BESS cost minimization

$$\text{Minimize } f_2 = \min (C_T) = \min (C_{Capital} + C_{O\&M}) \tag{4.6}$$

Subject to:

BESS constraints are imposed on the optimization as follows:

$$P_{BESS}^{\min} \le P_{BESS} \le P_{BESS}^{\max} \tag{4.7}$$

where P_{BESS} is the rated power capacity of BESS (MW),
P^{BESS}_{min} is the allowed minimum rated power capacity,
P^{BESS}_{max} is the allowed maximum rated power capacity of BESS.

$$C_{BESS}^{\min} \le C_{BESS} \le C_{BESS}^{\max} \tag{4.8}$$

where C_{BESS} is the rated energy capacity of BESS (MWh),
C^{BESS}_{min} is the allowed minimum rated energy capacity,
C^{BESS}_{max} is the allowed maximum rated energy capacity of BESS.

Microgrid frequency constraint is imposed on the optimization as follows:

$$F_{\min} \le F \le F_{\max} \tag{4.9}$$

where F is the nominal frequency of the isolated microgrid (Hz.),
F_{min} is the allowed minimum nominal frequency of the isolated microgrid,
F_{max} is the allowed maximum nominal frequency of the isolated microgrid.

Description of the Optimum Sizing of BESS based on PSO

In this work, the number of iteration (N_I) is 30. The number of particle (N_P) is 20. The learning factors are c_1 and c_2 which are equal to 1.4950. The inertia weight (w) is 0.7930. The learning factors have significant effects on the algorithm convergence rate. Further information for PSO can be found in [1-4]. Afterwards, the optimum sizing of BESS is achieved by using the PSO based on frequency control. As regard to Fig. 4.2, the process of the proposed optimum BESS-based PSO is demonstrated as follows:

Step 1: Define the constraints of the objective functions and initialize the parameters and iteration $i = 1$ with random position (x_i) and velocity (v_i).

Step 2: Start the particle $j = 1$ in the swarm.

Step 3: Execute the objective function for particle j^{th} of iteration i^{th}.

Step 4: Find P_{best} and G_{best} for particle j^{th} of iteration i^{th}. If the fitness value of $j^{th} \leq$ the best global fitness value, the program sets $P_{best} = f_1(x_j)$ and saves the best capital cost $(P_{best\_Capital}) = f_2(x_j)$, the best operating and maintenance cost $(P_{best\_O\&M}) = f_3(x_j)$.

Step 5: Increase particle j^{th} by 1. Then, check the condition If particle $j^{th} + 1 \leq N_P$, go back to Step 3.

Step 6: Adjust G_{best} of i^{th} = the best values of P_{best} at i^{th}.

Step 7: Increase iteration i^{th} by 1. Then, check the condition if iteration $i^{th} + 1 \leq N_I$, go back to Step 2 and update the new position (x_{i+1}) and new velocity (v_{i+1}) for the next iteration.

Step 8: If iteration i^{th} +1> N_I, the process ends and then an optimum size and costs of BESS are achieved.

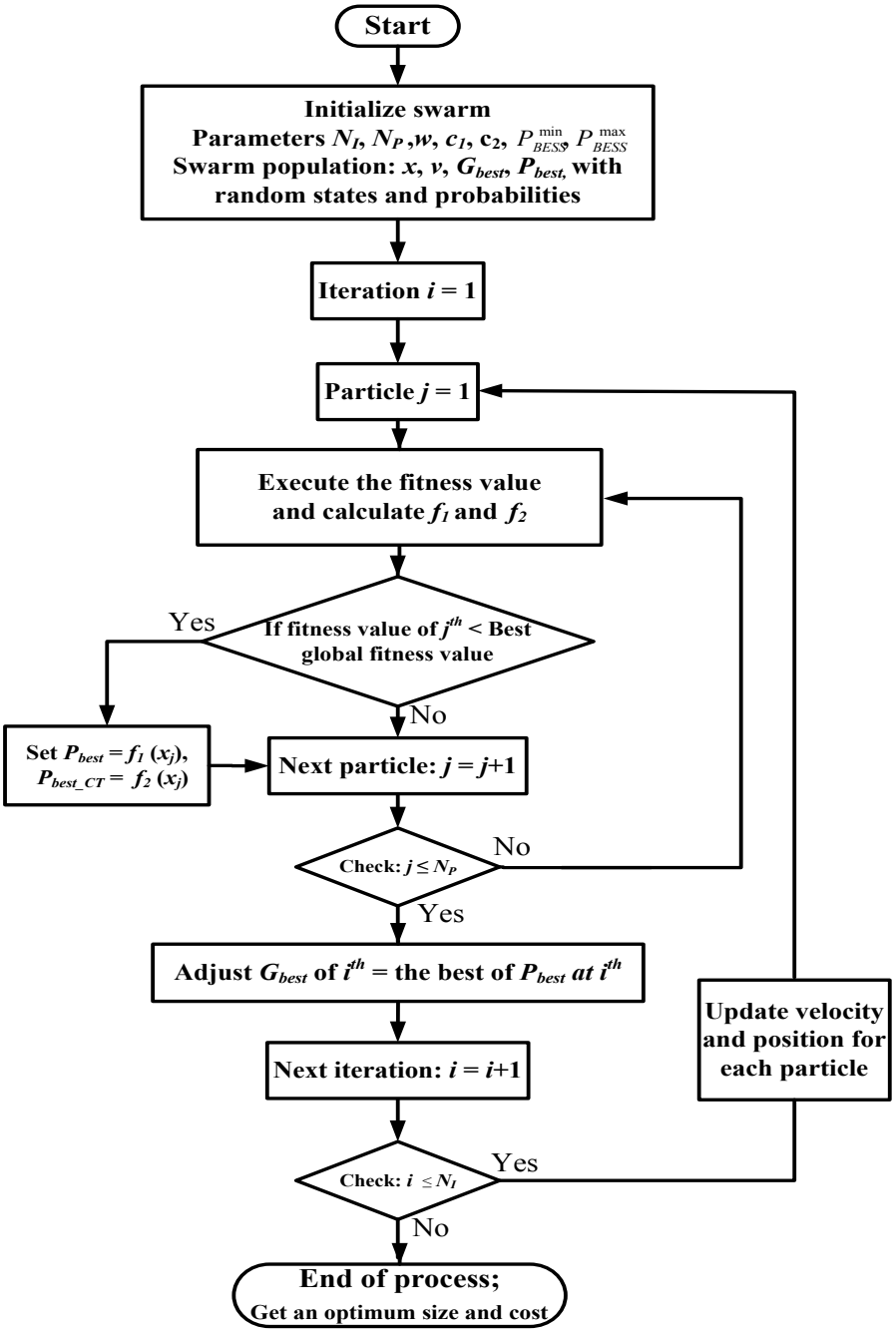

Figure 4.2 The flow chart of the optimal sizing of BESS by using PSO-based frequency control

4.2.1 Main DPL Script for BESS Sizing based on PSO

After executing the DPL script "PSO_BESS size.ComDpl", the DPL script is mainly divided into two script sections (i.e., PSO script and objective function script). Various comments are included to describe step-by-step PSO script and objective function script in the following part [13].

4.2.2.1 PSO Script

The main parameters of the PSO script are set via the dialogue window by the user to control the optimization parameters. As seen in Fig. 4.3, the basic options dialogue of the PSO script, where "input parameters" section consists of the number of particles, the number of iterations, the dimension of the problem, lower and upper bound constraints of BESS, cognitive weight, social/global weight, cognitive and social randomization weight and the objective function script. The programming variables are included in the DPL programming code (i.e., script section), whereas numerous internal objects (e.g., vectors/IntVec, matrices/IntMat, results/ElmRes) are contained within the content section in the following piece of code.

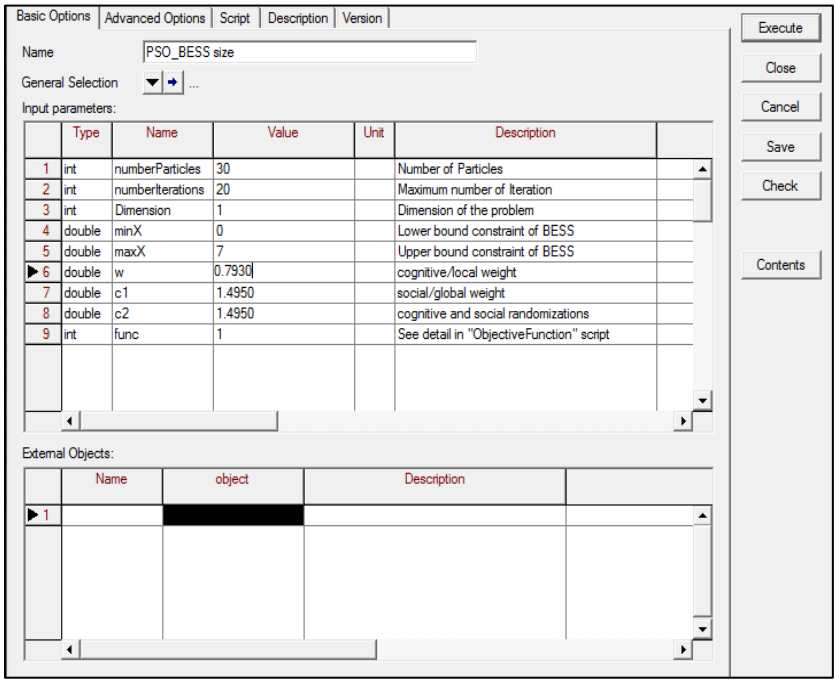

Figure 4.3 The DPL command basic options for the PSO script

At first, all internal variables must be declared in the PSO script as follows:

```
!=========================================================================
!     Particle Swarm Optimization (PSO) for BESS sizing in Microgrids.
!     Developer: Mr. Thongchart KERDPHOL.
!     Kyushu Institute of Technology, Mitani Laboratory, Japan
!=========================================================================
! PSO internal varible declaration
int iteration;
int i,j,dim,s;
double bestGlobalFitness,nomFreq;
double minV,maxV;
double hi,lo;
double fitness,newFitness;
double randomPosition,randomVelocity,cost,newcost;
double newPosition,newVelocity;
double temp,temp1,temp2,temp3,C1, temp8, temp9, temp88;
double r1,r2;
set M,V;
object pPosition,pBestPosition,pVelocity,pBestGBF,pCos,bestGlobalCos;
object bestGlobalPosition,pBestFitness,pFitness,pBestCos;
```

Stage 1: Parameter and space definition

The definitions of internal parameters of PSO are stated such as the best global fitness, iteration and nominal frequency of the micrigrid as shown below.

```
! Set initial parameters of the swarm
iteration = 1;
minV = -1.0*maxX;
maxV = maxX;
bestGlobalFitness = 1000; ! Set initial reference best global fitness
nomFreq=50.00;            ! Set nominal reference frequency
```

The matrices and vectors of BESS size and total cost in terms of PSO variables are created in order to accomplish all the required space definition. All vectors and matrix will be adequately resized as space definition requirements as shown below.

```
! Creating new matrices and vectors for BESS size
pPosition = this.CreateObject('IntMat','sPosition');
pBestPosition = this.CreateObject('IntMat','sBestPosition');
pVelocity = this.CreateObject('IntMat','sVelocity');
bestGlobalPosition = this.CreateObject('IntVec','sbestGlobalPosition');
pBestFitness = this.CreateObject('IntVec','sBestFitness');
pFitness = this.CreateObject('IntVec','sFitness');
pBestGBF = this.CreateObject('IntVec','sBestGBF');

! Creating matrices and vectors for BESS cost
pBestCos = this.CreateObject('IntVec','sBestCostVRB');
pCos = this.CreateObject('IntVec','sCostVRB');
bestGlobalCos = this.CreateObject('IntVec','sBestGlobalCostVRB');

! Initialize the swarm size
pBestFitness.Resize(numberParticles);
pBestPosition.Resize(numberParticles,Dimension);
pFitness.Resize(numberParticles);
pPosition.Resize(numberParticles,Dimension);
pVelocity.Resize(numberParticles,Dimension);
pBestGBF.Resize(numberIterations);
bestGlobalPosition.Resize(Dimension);
bestGlobalCos.Resize(Dimension);
pBestCos.Resize(numberParticles);
pCos.Resize(numberParticles);

! Output parameter settings
ClearOutput();
printf('\ceBegin Particle Swarm Optimization');
printf('\cfObjective function to minimize has %d dimensions',Dimension);
printf('\nNumber iterations = %d',numberIterations);
printf('Number particles in swarm = %d',numberParticles);
printf('Lower constraint = %.2f',minX);
printf('Upper constraint = %.2f',maxX);
printf('Initializing swarm with random positions/solutions');
```

Stage 2: Initialization of PSO parameters

The initial candidate solution of PSO (e.g., P_{best}, G_{best}) is generated by randomly determining the position and velocity of each particle within their boundaries and constraints. At first, the initial position and velocity for each particle in the swarm is randomly generated. Next, the objective function script is used by the command "Execute" so as to determine the system frequency and total cost of BESS incorporating the BESS size/particle position from the PSO script. Then, frequency condition is used to define whether the obtained solutions are within the requirement. The following command code involved in this stage is shown as follows:

```
! Initialize each Particle of the swarm
SetRandSeed(2);
for (i=1;i<=numberParticles;i+=1){ ! for each particle of the swarm
! Calculate random initial position
  for (j=1;j<=Dimension;j+=1){
      lo = minX;       ! Set lower bound of the search space
      hi = maxX;       ! Set upper bound of the search space
      temp = fRand(0); ! Random number in [0,1] at the uniform
      randomPosition =(hi - lo)* temp + lo;  ! Calculate random initial position
      printf('random position = %f',randomPosition);
      pPosition.Set(i,j,randomPosition);     ! Set initial position as a current position
      pBestPosition.Set(i,j,randomPosition); ! Set initial position as a best particle position
  }
! Calculate objective functions for each particle
  ObjectiveFunction.Execute(pPosition,i,func,fitness,cost);
  pFitness.Set(i,fitness);      ! Set initial fitness 1 as current fitness 1
  pBestFitness.Set(i,fitness);  ! Set initial fitness 1 as best particle fitness 1
  pCos.Set(i,cost);             ! Set initial fitness 2 as current fitness 2
  pBestCos.Set(i,cost);         ! Set initial fitness 2 as best particle fitness 2
  for (j=1;j<=Dimension;j+=1) {

! Calculate initial velocity
     lo = -1.0 * abs(maxX - minX-minX);  ! Set lower constraint of velocity
     hi = abs(maxX + minX);              ! Set upper constraint of velocity
     temp1 = fRand(0);                   ! Random at uniform in [0,1]
     randomVelocity = (hi - lo) * temp1 + lo; ! Calculate velocity
     printf('Initial velocity = %f',randomVelocity);
     pVelocity.Set(i,j,randomVelocity);  ! Set velocity as current velocity
```

```
! Check: Does current particle/BESS size has best global system frequency?
  temp = pFitness.Get(i);      ! Get current system frequency
  temp8=abs(nomFreq-temp);     ! Find different value between norminal frequency and current system frequency
  temp9=abs(nomFreq-bestGlobalFitness);  ! Find different value between norminal frequency and best global system frequency
  if (temp8 < temp9) { ! Check frequency condition
      bestGlobalFitness = temp; ! if true, set current frequency as a new best system frequency
      for (j=1;j<=Dimension;j+=1){
          temp1 = pPosition.Get(i,j);
          bestGlobalPosition.Set(j,temp1);!save best global position/size of BESS
          bestGlobalCos.Set(j,cost);      !save best global cost of BESS
      }
  }
}
printf('\nInitialization complete');
printf('Best initial position/solution:');
printf('Initial best global fitness = %.5f',bestGlobalFitness);
```

Stage 3: PSO main loop

The main PSO loop is initiated from calculating updated velocity and position for each particle. Then, the objective function script is used by the command "Execute" so as to determine the system frequency and total cost of BESS incorporating the BESS size/particle position from the PSO script. Afterwards, frequency condition is used to define whether the obtained solutions are within the requirement. The command code involved in this stage is displayed as follows:

```
! Starting PSO algorithm
printf('\nEntering main PSO processing loop');
while (iteration <= numberIterations) {  ! Repeat this loop until last iteration is reached

! Each Particle
    printf(' ');
    printf('Begin iteration No.%d', iteration);
    for (i=1;i<=numberParticles;i+=1) {         ! for every particle
! Calculate velocity update for each particle
        printf('Loop No.%d',iteration);
        printf('\nUpdate velocity and position');
        for (j=1;j<=Dimension;j+=1) {     ! update each dimension
            r1 = fRand(0);                ! ramdom at uniform in [0,1]
            r2 = fRand(0);                ! ramdom at uniform in [0,1]
            temp = pVelocity.Get(i,j);
            temp1 = pBestPosition.Get(i,j);
            temp2 = pPosition.Get(i,j);
            temp3 = bestGlobalPosition.Get(j);
            ! Calculate new velocity
            newVelocity = (w*temp)+(c1*r1*(temp1-temp2))+(c2*r2*(temp3 - temp2));
            ! Check if new velocity is within boundaries and save
            if (newVelocity < minV) {
               newVelocity = minV;
            }
            else if (newVelocity > maxV) {
               newVelocity = maxV;
            }
            pVelocity.Set(i,j,newVelocity);




    }
    for (j=1;j<=Dimension;j+=1) {
        ! Calculate new position for each particle
        temp = pPosition.Get(i,j);
        temp1 = pVelocity.Get(i,j);
        newPosition = temp + temp1; ! Calculate new position
        ! Check if new position is within boundaries and save
        if (newPosition < minX) {
           newPosition = minX;
        }
        else if (newPosition > maxX) {
           newPosition = maxX;
        }
        pPosition.Set(i,j,newPosition);
    }

! Calculate opjective functions for each updated particle
    ObjectiveFunction.Execute(pPosition,i,func,newFitness,newcost);
    pFitness.Set(i,newFitness); ! save new fitness
    pCos.Set(i,newcost);        ! save new total cost of BESS
```

```
! Check: Is MG frequency of new particle position better than MG frequency of former particle position ?
       temp = pBestFitness.Get(i);
       temp8=abs(nomFreq-temp);
       temp9=abs(nomFreq-newFitness);
       if (temp9<temp8) {              ! if it is better than former position
          for (j=1;j<=Dimension;j+=1) {
              temp1=pPosition.Get(i,j);
              pBestPosition.Set(i,j,temp1);  ! save new best position/size of BESS
              pBestFitness.Set(i,newFitness);! save new best frequency of MG
              pBestCos.Set(i,newcost);       ! save new best cost of BESS
          }
       }

! Is MG frequency of new particle position better than MG frequency of best global particle position ?
       temp88=abs(nomFreq-bestGlobalFitness);
       if (temp9 > temp88) {                ! if it is better than best global position
          for (j=1;j<=Dimension;j+=1) {
              temp2 = pPosition.Get(i,j);
              bestGlobalPosition.Set(j,temp2); ! save best global position/size of BESS
              bestGlobalFitness = newFitness;  ! save best global frequency of MG
              bestGlobalCos.Set(j,newcost);    ! save best global total cost of BESS
          }
       }
   }
```

Stage 4: Displaying the optimum results

Once the optimization process has been completed (i.e., when the iteration number has been reached), the optimum results of PSO are automatically obtained and deployed. The following code involved in this stage is demonstrated as follows:

```
! Show results of each particle
    printf('Iteration = %d',iteration);
    printf('==========================');
    for (i=1;i<=Dimension;i+=1) {
        temp = pPosition.Get(2,i);        ! show position of each particle
        printf('Position:%d = %f',i,temp);
    }
        temp = pFitness.Get(2);
        printf('Fitness= %f',temp);
    for (i=1;i<=Dimension;i+=1) {
        temp = pVelocity.Get(2,i);        ! show velocity of each particle
        printf('Velocity:%d = %f',i,temp);
    }
    for (i=1;i<=Dimension;i+=1) {
        temp = pBestPosition.Get(2,i);    ! show best position/BESS size of each particle
        printf('Best Position:%d = %f',i,temp);
    }
        temp = pBestFitness.Get(2);       ! show best MG frequency of each particle
        printf('Best Fitness= %f',temp);
    printf('==========================\n');
    printf('Best Global Fitness= %f',bestGlobalFitness);
    pBestGBF.Set(iteration,bestGlobalFitness);  ! show best MG frequency in each iteration


    iteration += 1;
}!End while
```

```
printf('\n\ceProcessing complete');
printf('\chFinal best fitness = %f Hz',bestGlobalFitness);
s = bestGlobalPosition.Size();
for (i=1;i<=s;i+=1) {
      temp = bestGlobalPosition.Get(i);
      printf('\chBest position/solution:%d = %f MW',i,temp);      ! Show optimum power capacity of BESS
      printf('\chBest position/solution:%d = %f MWh',i,temp*5);   ! Show optimum energy capacity of BESS
      C1 = bestGlobalCos.Get(i);
      printf('\chBest total cost of %f MW/%f MWh = %f $/15 years',temp, temp*5,C1);  ! Show optimum total cost of BESS
    }
printf('\ceEnd Particle Swarm Optimization\n');
```

4.2.2.2 Objective Function Script

The main parameters of the objective function script are set via the dialogue window by the user to control the parameters of BESS costs in the DPL command "basic options" as seen in Fig. 4.4.

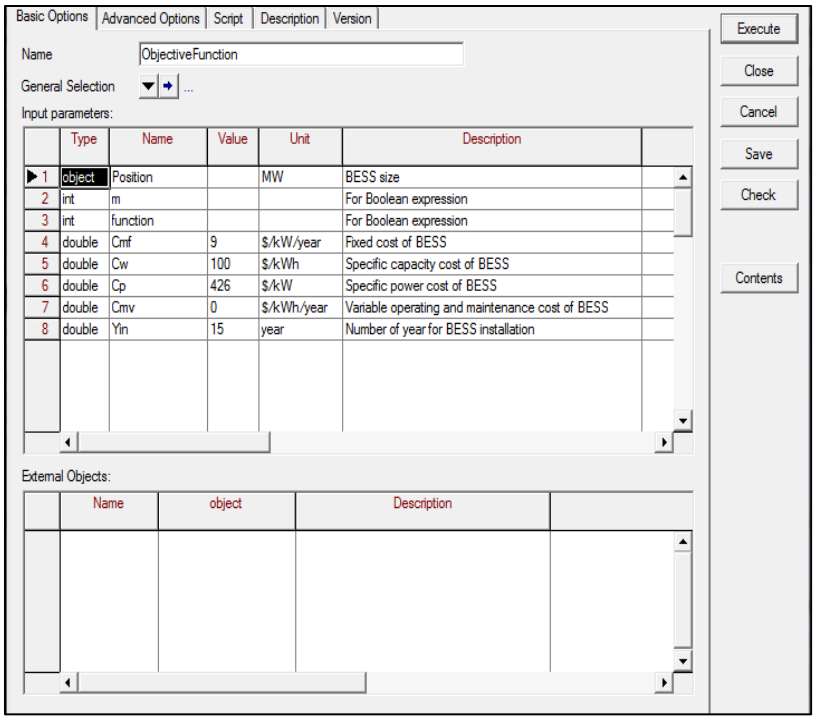

Figure 4.4 The DPL command basic options for the objective function script

The feedback parameters (i.e., system frequency and total cost of BESS) for the PSO script are created in the DPL command "advanced options" as shown in Fig. 4.5.

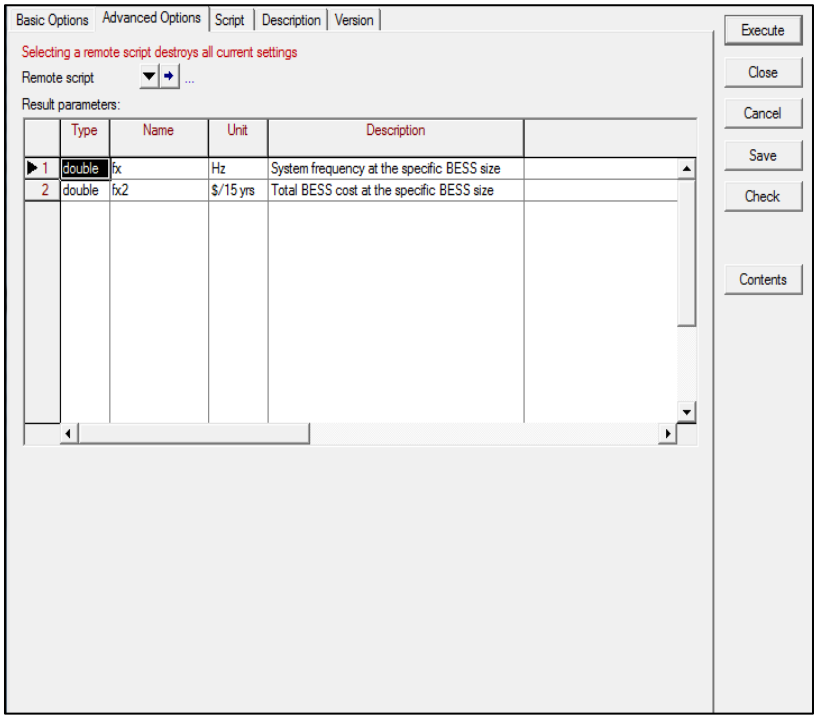

Figure 4.5 The DPL command advanced options for the objective function script

First, all internal variable of the objective function have to be declared as follows:

```
!  Objective function varible declaration
set A,A1;
object O,ldf,ldf1,sim,O1,HY,HM,PV,L1,L2,L3,L4,L5;
double PB,F,i,G1,G2,PV1,L11,L21,L31,L41,L51,sum,Cost,Wannual,cap;
```

Next, the command "ComLdf" is applied in the object "ldf1". Load flow calculation is determined using the "Execute" command. Afterwards, BESS size/particle position is received from the PSO script section and used for determining the total cost of BESS and system frequency of the microgrid. After calculating of the total cost of BESS and system frequency, these feedback values are sent back to the PSO script. The following code involved in this stage is demonstrated as follows:

```
if(function=1){
ldf1 = GetCaseObject('ComLdf');    ! Run load flow calculation
ldf1.Execute();

sum=Position.Get(m,1); ! Receive BESS size/position from PSO and save to the varible 'sum'
A=AllRelevant();       ! Save all elements in set A
O=A.FirstFilt('PWM*.ElmVscmono'); ! Access to BESS element in MG
O.SetVal(sum,'psetp',0);          ! Set BESS size
cap=5*sum;                       ! Determine energy capacity of BESS for 5 hrs usage

Cost=(Cp*1000*sum)+(cap*Cw*1000)+(Yin*Cmf*1000*sum)+(Yin*1000*Cmv*Wannual); ! Calculate total cost of BESS

ldf = GetCaseObject('ComInc');   ! Run initiatial condition
ldf.Execute();

sim = GetCaseObject('ComSim');   ! Run simulation case
sim.Execute();

! Determine the system frequency of the microgrid
A=AllRelevant();
O1=A.FirstFilt('MSR*.ElmTerm');
O1.GetVal(F,'m:fehz');           ! Obtain system frequency of MG at the specific BESS size
printf('Frequency of Microgrid :%f Hz\n',F);

fx=F;      ! Return current frequency at the specific BESS size to PSO
fx2=Cost;  ! Return current total cost of BESS at the specific BESS size to PSO
```

4.3 Results and Discussion

In the performed simulation, the study microgrid performance is tested by implementing the most severe disturbance (i.e., disconnecting of the microgrid from the utility grid) at 10.0 s. The microgrid operation is transited from the grid connected to isolated operation, resulting in the shortage of power supply in the microgrid at that time. It is assumed that the nominal system frequency is 50 Hz and system frequency declines below 49.95 Hz is required the implementation of the optimum size of BESS based on PSO. The power fluctuations of the solar PV farm have been considered in this method and the data are given in Appendix B.

Figs. 4.6, 4.7 and 4.8 display the convergence rate of the optimal size of BESS-based PSO, the total cost of VR BESS-based PSO, and the total cost of PB BESS-based PSO, respectively. Based on these results, it displays that the optimal sizing of BESS-based PSO method is converged to its final state approximately after 15 iterations. It is evident that the attainment is achieved with G_{best} after 15^{th} iterations. The slightly attainment is reached with G_{best} after 20^{th} iterations. However, no difference is observed after 20^{th} iterations. Thus, it can be summarized that the proposed PSO for BESS sizing is symmetrical around the midpoint.

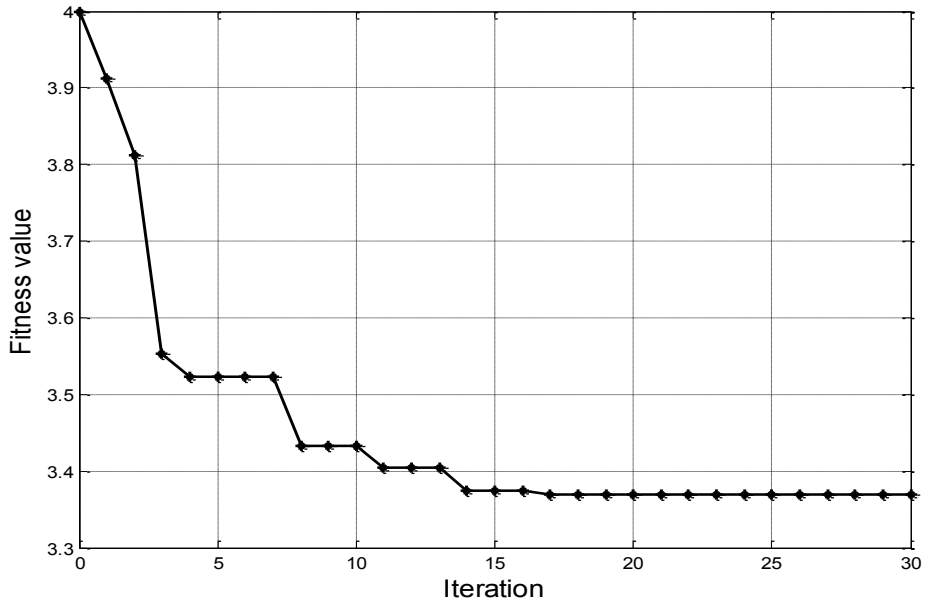

Figure 4.6 The convergence rate for BESS size

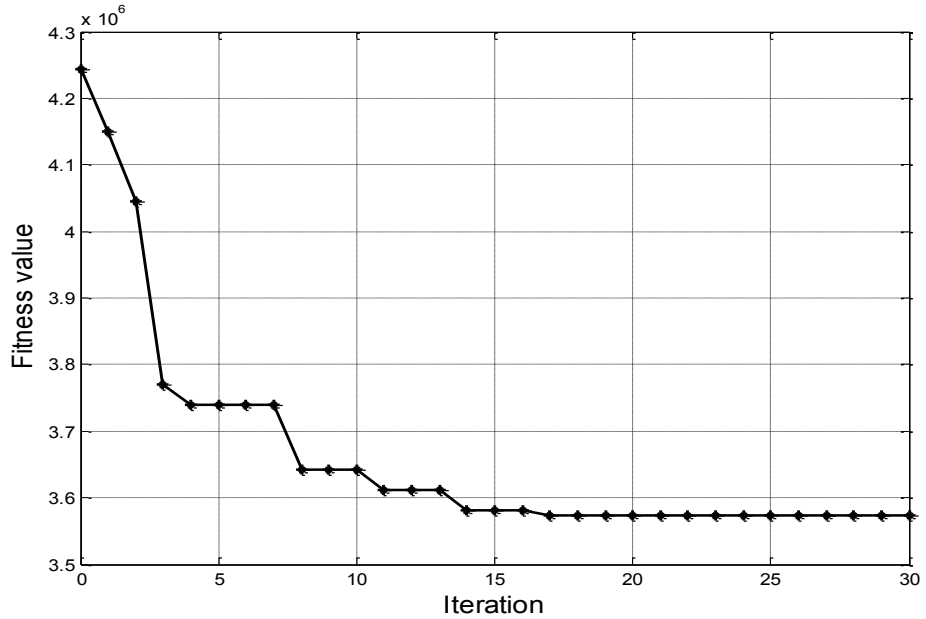

Figure 4.7 The convergence rate for the total cost of VR BESS

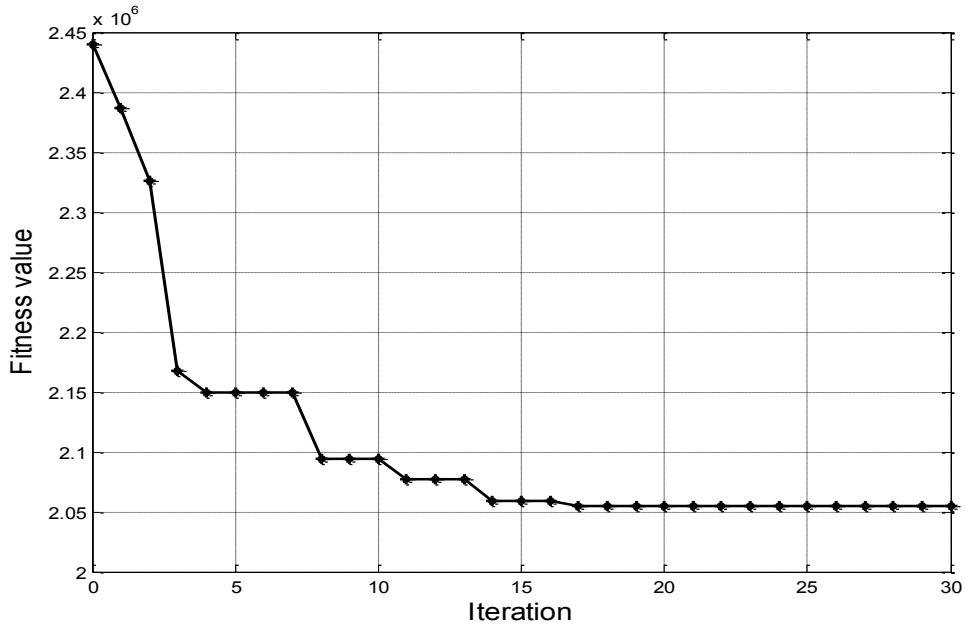

Figure 4.8 The convergence rate for the total cost of PB BESS

As regard to Fig. 4.9, the magnitude of the frequency deviation with the BESS-based conventional size reaches 51 Hz and takes more time to stabilize than the optimal size of BESS-based PSO. Compared with the optimal size of BESS-based analytic method, the optimal size of BESS-based PSO can achieve the finest frequency performance during the severe disturbance. It is obvious that the optimum sizing of BESS-based PSO is able to improve and recover fast, smooth and secure system dynamic stability and performance from the emergency situation to the normal equilibrium state, achieving the best minimum total cost of BESS.

In case of no BESS, the system frequency drops drastically because the power supply cannot meet the load demand, resulting in system collapse.

It is confirmed in Table 4.1 that the performance of system frequency is much better when the optimal size of BESS-based PSO is applied. With applying the optimal size of BESS-based PSO, it can be concluded that there is a significant improvement of the frequency performance of the system in terms of peak deviation and settling time.

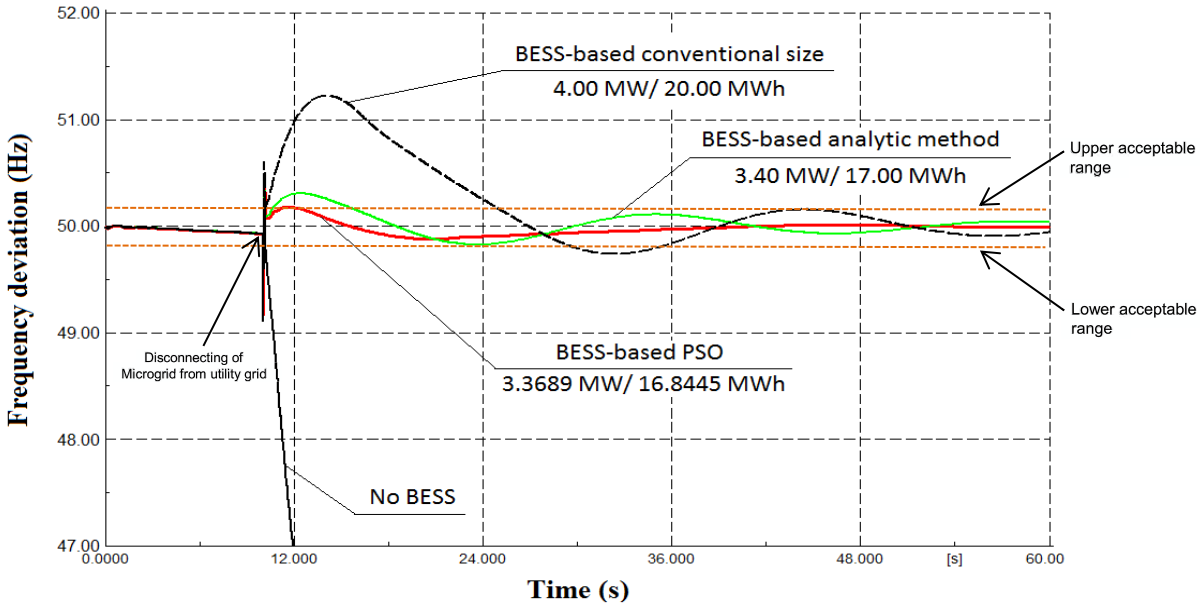

Figure 4.9 Frequency deviation of the microgrid after the severe disturbance

The voltage deviation of the microgrid during the severe disturbance is shown in Fig. 4.10. As regard to the results, the optimal size of BESS-based PSO can remain almost the same voltage deviation as the optimal size of BESS-based analytic method and conventional size of BESS. In case of no BESS, the system voltage decreases drastically because the power supply cannot meet the load demand, causing system collapse.

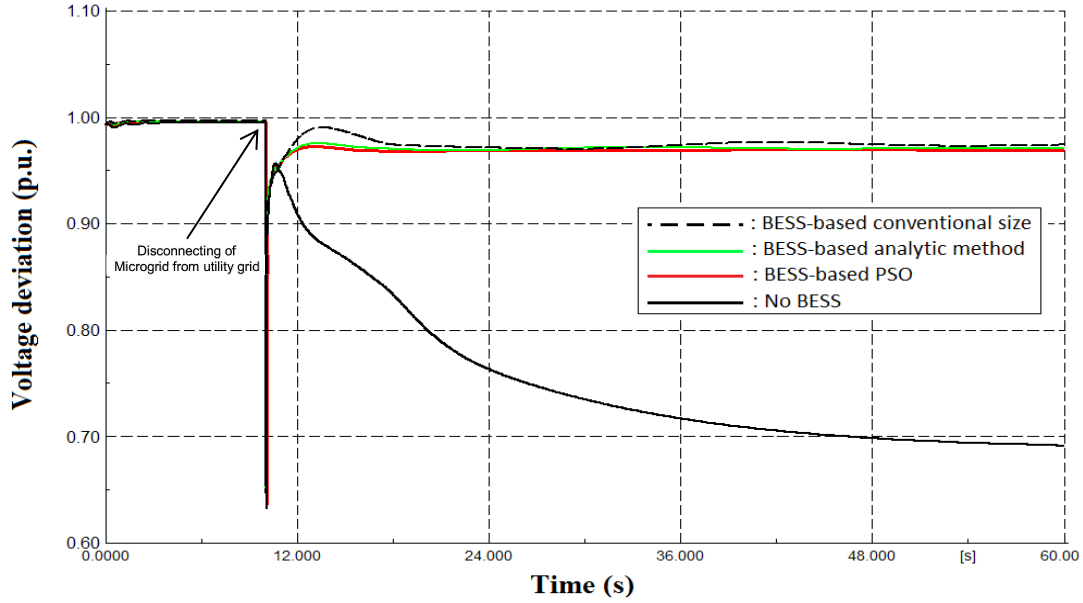

Figure 4.10 Voltage deviation of the microgrid after the severe disturbance

In terms of BESS economical performance, the optimal size of BESS-based PSO evaluates economical performances of BESS installation with different technologies at minimum total cost of BESS for the microgrid. From Table 4.1, the optimal size of BESS-based PSO method gives lower the total cost of BESS than the optimal size of BESS-based analytic method and conventional size. It is obvious that the microgrid system with PB BESS can achieve lower total BESS cost than the microgrid system with VR BESS. Thus, the installation of the polysulfide-bromine BESS is likely to be more cost-effective than the installation of the vanadium redox BESS for 15-years installation in the microgrid system.

Table 4.1 Comparison parameters of different methods

Parameters	BESS-based conventional size	BESS-based analytic method	BESS-based PSO method
Power capacity (MW)	4.000	3.400	3.3689
Energy capacity (MWh)	20.000	17.000	16.8445
Frequency magnitude (Hz), Reference: 50.00	51.223	50.310	50.046
Voltage (p.u.) Reference: 0.990	0.974	0.971	0.970
Total cost of VR BESS ($/15 years)	4,244,000	3,607,400	3,574,403
Total cost of PB BESS ($/15 years)	2,440,000	2,074,000	2,055,029

4.4 Summary

This chapter proposes a novel optimization method to determine an optimum size of BESS at minimum total BESS cost by using PSO-based frequency control for microgrids. The background of PSO is briefly demonstrated. The optimum sizing of BESS-based PSO is designed based on frequency control of the microgrid. Multi-objective functions are considered in this method; that is, the minimization of BESS size and total cost with different storage technologies. The modelling of the proposed

PSO-based frequency control of the microgrid is designed and demonstrated using DIgSILENT PowerFactory/DPL Script. Compared with the analytic method, it is clearly seen that the optimal sizing of BESS-based PSO can improve fast, smooth and secure dynamic stability of the microgrid from the emergency situation to the normal equilibrium state and achieve the best minimum total cost of BESS. Nevertheless, the modern BESS technologies are investigated and compared in terms of the economical performance for microgrids. It is obvious that the optimal size of BESS-based the proposed PSO method can save a huge amount of BESS capacity and investment. For this work, the capacity of BESS is reduced from 4.000 MW/20.000 MWh to 3.3689 MW/16.8445 MWh (i.e., 15.77% of the reduction in the BESS capacity) and the total cost of BESS is reduced from $ 2,440,000 USD to $ 2,055,029 USD (i.e., save $ 384,971 USD) in case of the polysulfide–bromine BESS and from $ 4,244,000 USD to $ 3,574,403 USD (i.e., save $ 669,597 USD) in case of the vanadium redox BESS for 15-years installation. Hence, the installation of polysulfide-bromine BESS is likely to be more cost-effective than the installation of vanadium redox BESS for 15-years installation in a microgrid. Finally, it is concluded that the proposed sizing of BESS by using PSO-based frequency control can help the system operators to guarantee the lowest size of BESS with a reasonable and full use of the microgrid system, so that the microgrid system can operate at the optimum conditions with optimal size of BESS in terms of investment and reliability requirement of the load demand.

Result Evaluation of PSO Method

Based on the PSO method, it shows that the proposed PSO method is not flexible to determine an optimum location of BESS once their output/size change as it is required an operator to manually select and place the BESS location as well as run the PSO script again in DIgSILENT PowerFactory. Thus, a suitable location of BESS in the microgrid has not been considered in this chapter. It can result in the inefficiency in terms of power loss, larger BESS capacity and high cost of BESS. To solve such mentioned problems, a new optimization method, which is capable of simultaneously evaluating an optimum size and location of BESS without enormous uses of programming, is required.

4.5 References

1. J. Kennedy, and R. Eberhart, Particle swarm optimization. In: *Proceeding of IEEE international conference neural networks*, 4 (1): 1942–8, 1995.
2. Z. L. Gaing, A particle swarm optimization approach for optimum design of PID controller in AVR system. *IEEE Trans. Energy Conversion*, 19(2):284–391. 2004.
3. A. A. Esmin, G. Lambert-Torres, and A.C. Zambroni de Souza, A hybrid particle swarm optimization applied to loss power minimization, *IEEE Trans. Power System*., 20(2):859–66, 2005.
4. H. Bevrani, F. Habibi, P. Babahajyani, M. Watanabe, Y. Mitani, Intelligent frequency control in an AC microgrid: on-line PSO-based fuzzy tuning approach. *IEEE Trans. Smart Grids*, 3(4), 1935–1944, 2012.
5. J. Zhu, *Optimization of power system operation*, John Wiley & Sons Inc., New Jesey, 2010.
6. H. Bevrani, *Robust power system frequency control*, 1st edn. Springer, USA, 2009.
7. T. Kerdphol, K. Fuji, Y. Mitani, M. Watanabe, and Y. Qudaih, Optimization of a battery energy storage system using particle swarm optimization for stand-alone microgrids. *International Journal of Electrical Power and Energy Systems*, 81(1), 32–39, 2016.
8. H. Ibrahim, A. Ilinca, J. Perron, Energy storage systems-characteristics and comparisons. *Renew Sustain Energy Rev*, 12(5):1221–50, 2008.
9. S. Chakraborty, T. Senjyu, H. Toyama, A. Saber, T. Funabashi, Determination methodology for optimizing the energy storage size for power system. *IET Gen Trans Distr*, 3(11):987–99, 2009.
10. B. Turker, S. Klein, E. Hammer, B. Lenz, and L. Komsiyska, Modeling a vanadium redox battery system for large scale applications. *Int J Electr Power Energy Syst*, 66:26–32. 2013.
11. C. Lo, and K. Kwan, Economic dispatch and optimal sizing of battery energy storage systems in utility load-leveling operations. *IEEE Trans Energy Convers*, 14 (3):824–9. 1999.
12. F. Chacra, P. Bastard, G. Fleury, R. Clavreul, Impact of energy storage costs on economical performance in a distribution substation. *IEEE Trans Power Syst*. 20(2):684–91. 2005.
13. DIgSILENT GmbH, *PowerFactory user's manual version 14.1*, Gomaringen, Germany, 2012.

Chapter 5

ANN-based BESS Size and Location Optimization

5.1 Introduction of ANN Method

Artificial neural networks (ANN) are computational information systems that mimic the structures of a biological nervous system such as the human brain. The most basic component of the human brain is a specific type of cell, which gives us the capability to estimate, remember, think and implement former experience to our actions. These cells are known as neurons and each of these neurons is able to connect up to 300,000 other neurons. All neurons consist of four basic components: that is, dendrites, soma, axons, and synapses. The processing power of the brain comes from the number of these basic components and multiple connections between them. Looking at the information process of the brain, a biological neuron obtains input from outsources, combines them, performs a nonlinear operation on the result and then gives the final result [1-3].

The ANN structure consists of three main layers as shown in Fig 5.1. First, an input layer, which connects the input signal (X_j) to the neuron via a set of weights (W_{kj}). Next, a hidden layer, which summarizes the bias values (b_k) and the input signals, is weighted by the respective weight values of the neuron. Finally, an output layer is used for limiting the amplitude of the output of the neuron using the

activation transfer function. In addition, a bias is added to the neuron to increase or decrease the net output of the neuron [3-5].

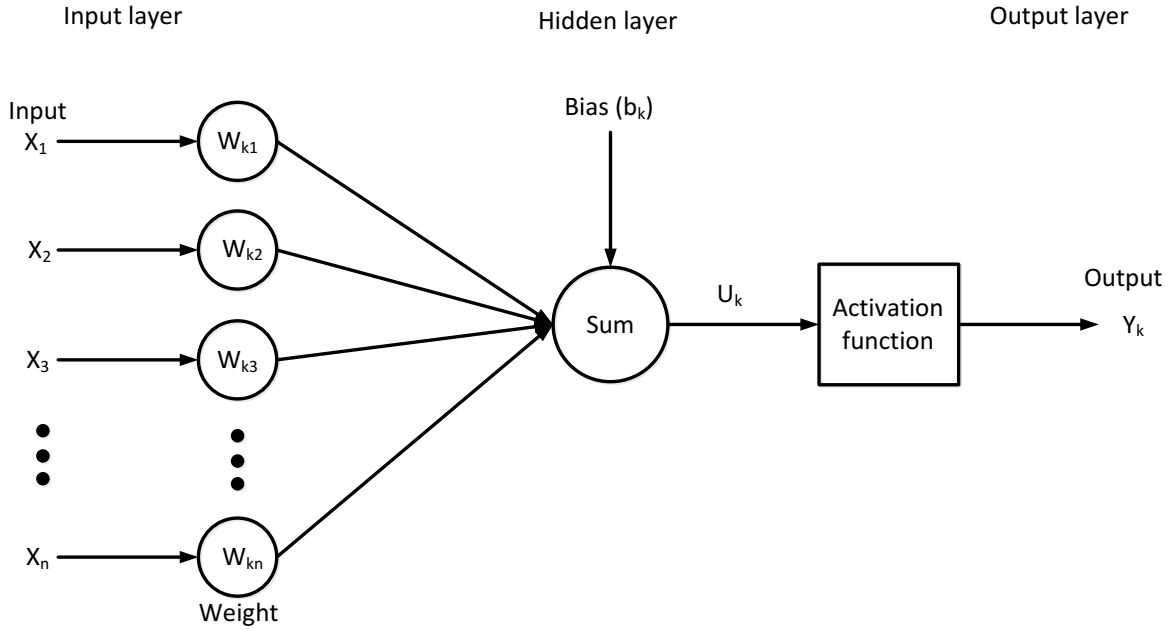

Figure 5.1 ANN structure of a nonlinear model

The mathematical structure of a neuron *k* in ANN is demonstrated as follows [3]:

$$U_k = \sum_{j=1}^{n} (W_{kj} X_j) \tag{5.1}$$

The values for the output nodes can be calculated as follows:

$$Y_k = f(U_k + b_k) \tag{5.2}$$

where

$X_1, X_2, X_3, \ldots, X_n$ are the input signals,
$W_{k1}, W_{k2}, W_{k3}, \ldots, W_{kn}$ are the weights for neuron *k*,
b_k is the bias value,
U_k is the linear combiner,
$f(\,.\,)$ is the activation transfer function,
Y_k is the output signal of the neuron.

The range of ANN outputs depends on the types of the activation transfer function (e.g., hard-limit, log-sigmoid, tan-sigmoid, linear, radial basis) as shown in Fig. 5.2 [3, 5].

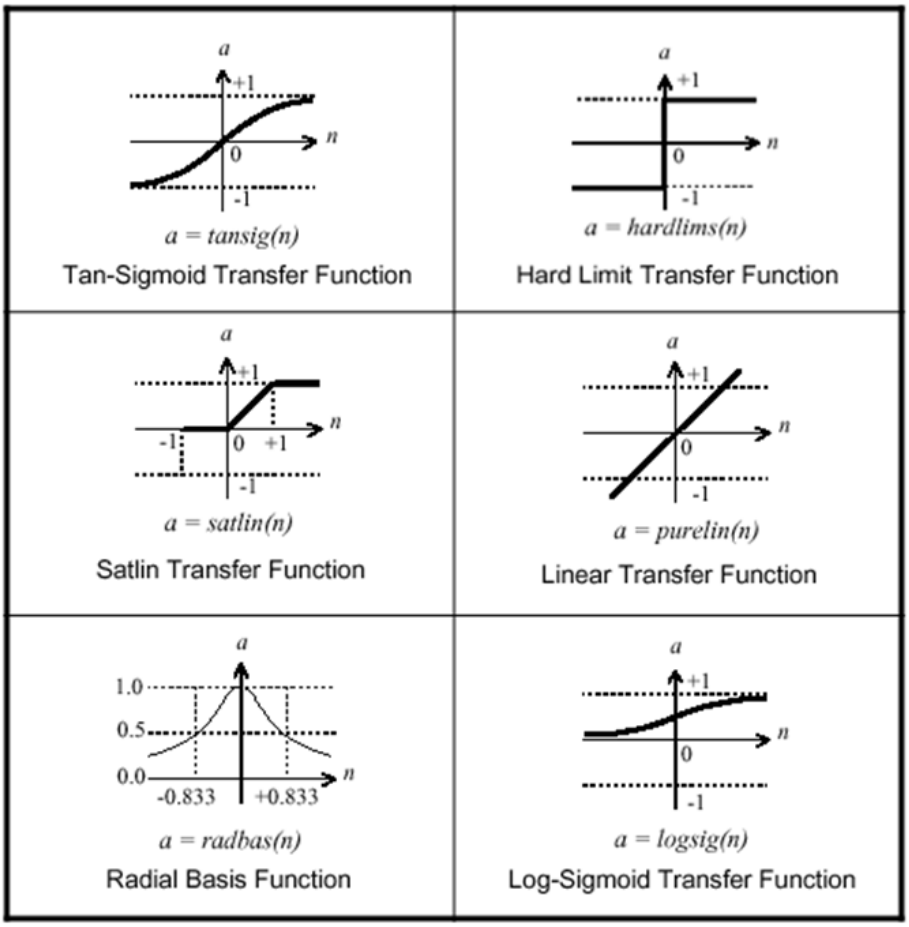

Figure 5.2 Activation transfer functions of ANN

Several researches and studies have proposed and discussed the development and theory of ANN in [6-9]. The development of ANN algorithms is briefly revealed as follows:

The back-propagation neural network (BPNN) is commonly applied to iteratively minimize the cost function with respect to the interconnection weights and neuron thresholds. The BPNN learning rate evaluates what amount of the calculated error sensitivity to weight change for the weight correction. The BPNN training process is stopped either when the mean square error (MSE) or root mean square error (RMSE), between the predictive result of BPNN and the measured experiment result for all elements in the training data, has satisfied a pre-specified threshold or after the completion of a pre-specified number of learning iterations [10].

The modular neural network (MNN) is motivated by the task decomposition. Applying MNN, the task is divided among many local neural networks without communication of each other. The MNN generalization requirement is decreased in comparison with a single MNN that have to learn the whole task. How to choose models and how to build the problem is the main problem of MNN. Thus, MNN is only suitable for a very limited domain of problems [3, 9, 11].

The self-organization feature maps (SOFM) neural network is a clustering method which builds a map of relationships among input patterns. The map is used to give a decreased representation of the original data. SOFM has a single layer of nodes and applies a distance metric to evaluate the output node closet to a given input pattern. The output nodes of SOFM do not related to known classes but to unknown clusters which the network automatically determines in the data [12].

The radial basis function neural network (RBFNN) is a functional approximation network which can be used in identification, memorization and control. It has the capability to learn system behaviors and effectively used for the identification of nonlinear systems. The centers and widths of the activation transfer function are achieved by unsupervised learning. The supervised learning is used to update the connection weights between the hidden and output layers. RBFNN is claimed that these networks learn faster than the feed forward neural networks and requires a smaller number of training data [11, 13].

The recurrent neural network (RNN) is characterized itself from the feed forward neural network by adding at least one feedback loop. RNN may contain a single layer of neurons with each neuron feeding its output signal back to the inputs of all other neurons. The current feedback loops have a deep impact on the learning process of the network and its performance [3, 14].

The following distinguished capabilities of ANN make it an effective tool in power system optimizations.

1. **Nonlinear capability**: ANN have been applied even for nonlinearity problems as the interconnected neurons can implement either linear or nonlinear. The multiple interconnections between neurons can create the system nonlinear. This application is very essential for power system optimization as the parameters or signals from complex structure of power system may be nonlinear [3, 4, 5].

2. **Adaptive capability**: ANN can easily adapt their systems by adjusting the weight values for changes in the environments [3].

3. **Input-output mapping capability**: ANN can correlate a unique input value with a desired response. ANN can modify the weight values using a learning process to achieve the desired response. For training ANN, the network is fed by a set of inputs and the corresponding desired response (i.e., target). Then, the network tries to learn from the examples by creating an input-output mapping. This is the most powerful application of ANN for supervising learning process. Hence, there is no need for enormous uses of programming [3, 4, 5].

4. **Generalization capability**: It makes ANN to solve complex or large-scale tasks that are currently intractable. For solve such tasks, the ANN network must be trained with sufficient signatures and their corresponding physical parameters [3].

5. **Fault tolerance capability**: It can make the potential candidates of ANN for critical tasks with high reliability requirements. Thus, ANN can cope with situations where normal symbolic systems would have difficulty [3].

According to the finite RBFNN performance, the advantages of RBFNN are two major issues: the training processes are substantially faster than the feed forward neural networks and RBFNN does not encounter with the local minima problems, achieving the global solution. Thus, this chapter has chosen the RBFNN as the proposed optimization method to determine an optimum size and location of BESS based on frequency control and power loss minimization for microgrids [15, 16].

5.2 RBFNN Method Structure for Determining BESS Size and Location

The proposed optimization method of BESS contains a two-stage based on an optimum size process and optimum location process. In the first stage, the optimum size of BESS is determined using the RBFNN based on frequency control of the microgrid so that the frequency of the microgrid can recover to a nominal value under

the sudden changes in load/generation or the outage of generation/utility grid. In the second stage, the optimum location of BESS is evaluated using the RBFNN based on power loss minimization of the microgrid so that microgrid can reduce the power loss in the system, improve system stability, and operate at the optimum conditions in terms of investment and reliability requirement of the load demand. The input of the proposed RBFNN method is frequency, voltage and power loss of the microgrid and then the output are an optimum size and location of BESS as shown in Fig. 5.3.

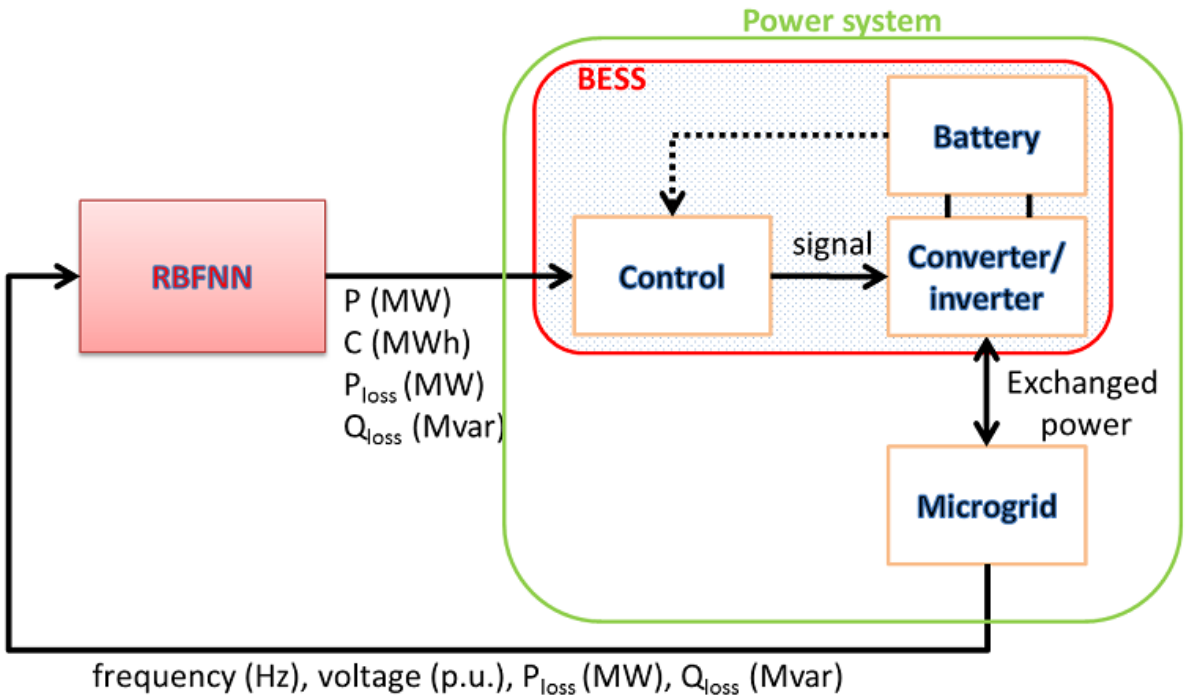

Figure 5.3 The RBFNN method structure for BESS sizing and locating

Looking inside the RBFNN block, it consists of two stages: the optimum size of BESS (Stage 1) and optimum location of BESS (Stage 2). In addition, if a microgrid operator already has a BESS size, the BESS size can be directly fed into the stage 2 so as to evaluate an optimum location of BESS in the microgrid. In each stage, it consists of four blocks that are the historical data based, RBFNN model creation, training RBFNN, and well-trained RBFNN networks as seen in Fig. 5.4.

The design and training of RBFNN models in this book were performed using the neural network toolbox from MATLAB 2013b [17].

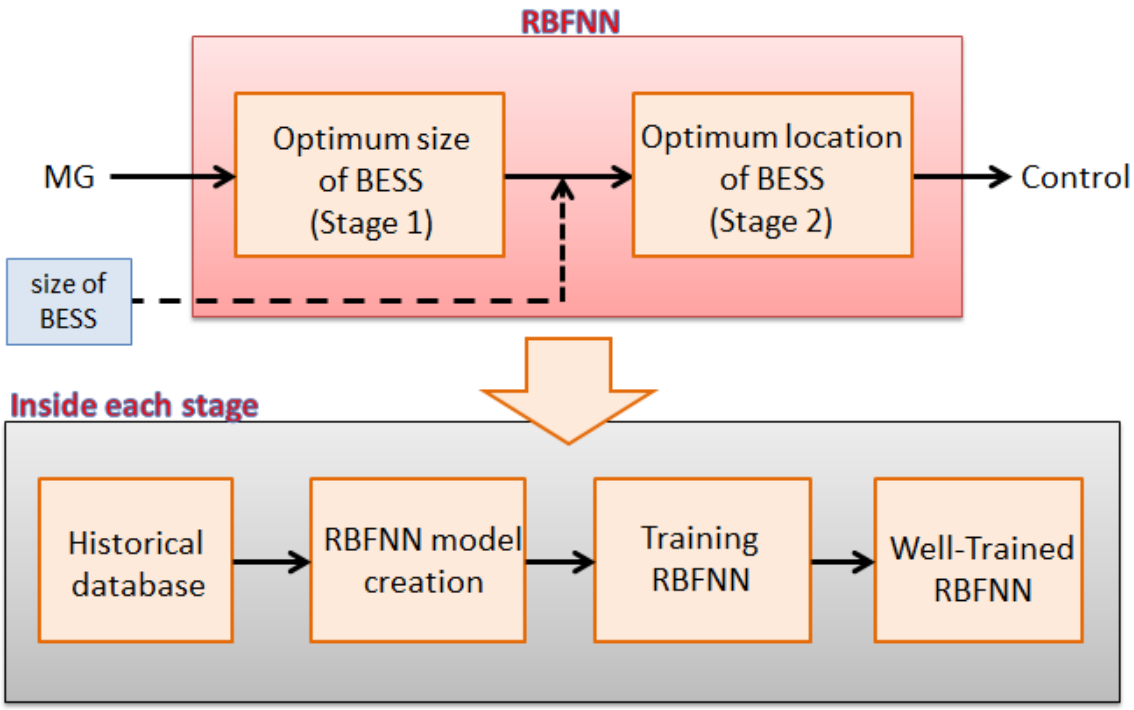

Figure 5.4 The detail inside of the RBFNN block

5.2.1 RBFNN Structure for Determining Size of BESS (Stage 1)

To determine an optimum size of BESS, frequency and voltage control have been considered as the important criteria for the secure system operation. Thus, the input signals of the RBFNN-based Stage 1 are frequency and voltage of the microgrid. The output of the RBFNN-based Stage 1 is an optimum size of BESS. Based on the measured data of the historical frequency and voltage of the microgrid, these data can evaluate an optimum size of BESS in order to recover and stabilize the microgrid from the emergency situation to the normal stage during the sudden changes in load/generation or the loss of generation/utility grid. The proposed RBFNN model based on the optimal BESS size can be demonstrated as a function that maps the input vector $X = [X_1\ X_2]$ to the output vector $Y = [Y_1\ Y_2]$ as shown in Fig. 5.5.

After that, the input vector X is applied to all neurons in the hidden layer. The hidden layer is composed of number q RBFNNs that are connected directly to all the elements in the output layer. A node in the hidden layer will produce a greater output

when the input pattern presented is close to its center. The output of a node will reduce as the distance from the center increase, assuming that a symmetrical basis function is applied. Hence, for an input pattern, only neurons whose centers are close to the input pattern will produce non-zero activation values to the input stimulus.

The radial basis function of BESS size estimation for the j^{th} node in the hidden layer is determined by the Gaussian exponential function as follows [11, 13, 15]:

$$b_j\left(\overline{X}\right) = \exp\left(\frac{-\left(\overline{X} - \mu_j\right)^2}{2\sigma_j^2}\right) \qquad \text{for } j = 1, 2,..., q \tag{5.3}$$

where μ_j is the respective centre, σ_j is the wide of the Gaussian potential function of the j^{th} neuron in the hidden layer.

The network output Y is formed by a linearly weighted sum of the number of radial basis functions in the hidden layer. The values for the output nodes are calculated as follows:

$$Y_k = \sum_{j=1}^{q} W_{kj} b_j\left(\overline{X}\right) \qquad \text{for } k = 1, 2 \tag{5.4}$$

where Y_k is the output of the k^{th} node in the output layer,
$b_j(\overline{X})$ is the output of the j^{th} node in the hidden layer,
W_{kj} is the weight between the j^{th} node in the hidden layer and the k^{th} node in the output layer.

Based on Table 5.1, the parameter details for determining an optimum size of BESS are shown and used in the training and the testing database for Stage 1. The RBFNN-based Stage 1 model was trained with 105 patterns of the data set (i.e., 70 % of data set) and its performance was tested with 45 patterns (i.e., 30 % of data set) randomly selected from the data set. The performance of the RBFNN training was evaluated with the root mean square error (RMSE) reduced to an order of 10^{-4}.

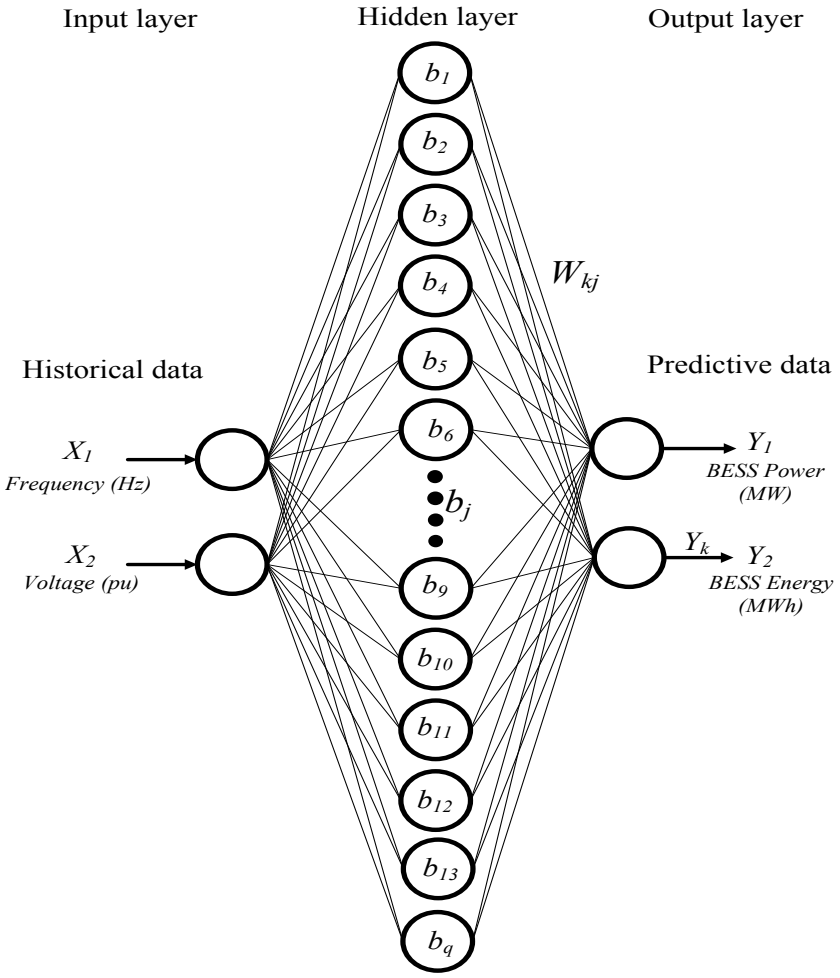

Figure 5.5 The RBFNN structure for determining an optimum size of BESS (Stage 1)

Table 5.1 The proposed RBFNN parameters for Stage 1

Parameters	RBFNN
Goal (RMSE)	0.0001
Inputs	2
Outputs	2
Hidden layer	1
Training data	105
Testing data	45
Hidden layer neurons	40
Output layer neurons	2

5.2.2 RBFNN Structure for Determining Location of BESS (Stage 2)

To evaluate an optimum BESS location, at each bus in the microgrid, the BESS is placed and BESS size is varied from minimum (0 MW) to a higher value and system losses are collected to the database as historical data. Based on historical data of BESS size (MW) and system losses (MW, Mvar), these data can evaluate an optimum location of BESS in the microgrid with the objective of power loss minimization. The proposed RBFNN model-based Stage 2 can be described as a function that maps the input vector Y = [Y_1] to the output vector Loss = [$Loss_1$ $Loss_2$ $Loss_3$ …. $Loss_k$] as shown in Fig. 5.6.

The radial basis function of BESS location prediction for the j^{th} node in the hidden layer is determined by the Gaussian exponential function as follows [11, 13, 15]:

$$b_j\left(\overline{Y}\right) = \exp\left(\frac{-\left(\overline{Y} - \mu_j\right)^2}{2\sigma_j^2}\right) \qquad \text{for } j = 1, 2,..., q \tag{5.5}$$

where μ_j is the respective centre, σ_j is the wide of the Gaussian potential function of the j^{th} neuron in the hidden layer.

The network output *Loss* is formed by a linearly weighted sum of the number of radial basis functions in the hidden layer. The values for the output nodes are calculated as follows:

$$Loss_k = \sum_{j=1}^{q} W_{kj} b_j\left(\overline{Y}\right) \tag{5.6}$$

where $Loss_k$ (k = 1,2,…,m) is the output of the k^{th} node in the output layer which indicates system loss values (MW, Mvar) at the k^{th} bus, W_{kj} is the weight between the j^{th} node in the hidden layer and the k^{th} node in the output layer, $b_j(\overline{Y})$ is the output of the j^{th} node in the hidden layer, m is the number of considered bus in the microgrid.

As regard to Table 5.2, the parameter details for determining an optimum location of BESS are displayed and used in the training and the testing database for Stage 2. The RBFNN-based Stage 2 model was trained with 232 patterns of the data set (i.e., 70 % of data set) and its performance was tested with 88 patterns (i.e., 30 % of data set) randomly selected from the data set. The performance of the RBFNN training was evaluated with the root mean square error (RMSE) reduced to an order of 10^{-4}.

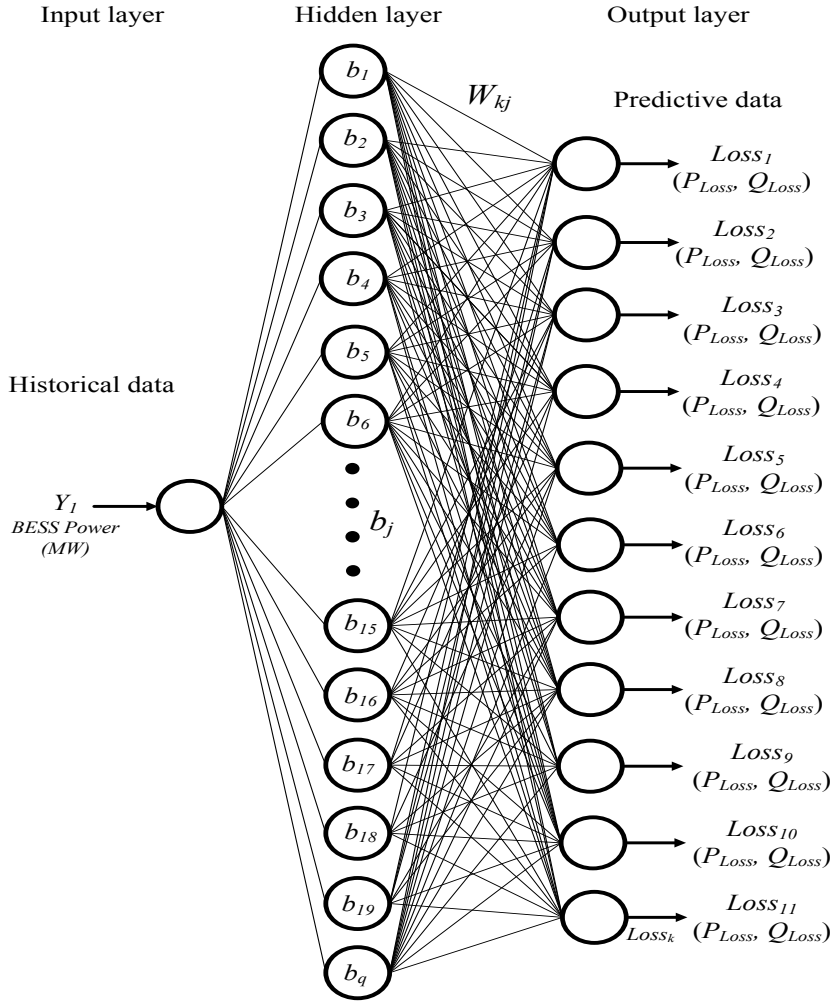

Figure 5.6 The RBFNN structure for determining an optimum location of BESS (Stage 2)

Table 5.2 The proposed RBFNN parameters for Stage 2

Parameters	RBFNN
Goal (RMSE)	0.0001
Inputs	1
Outputs	11
Hidden layer	1
Training data	232
Testing data	88
Hidden layer neurons	40
Output layer neurons	11

As regard to Fig. 5.7, the process of the proposed RBFNN method for determining both optimum size and location of BESS is demonstrated as follows:

Step 1: Input the historical data set for each stage.

Step 2: Specify the target data set for each stage.

Step 3: Divide data set for training and testing process.

Step 4: Train the network for each stage.

Step 5: Obtain the output data for each stage.

Step 6: Check the output performance using regression analysis and RMSE.

Step 7: Obtain the well-trained networks for determining an optimum size and location of BESS which are ready to apply new input data.

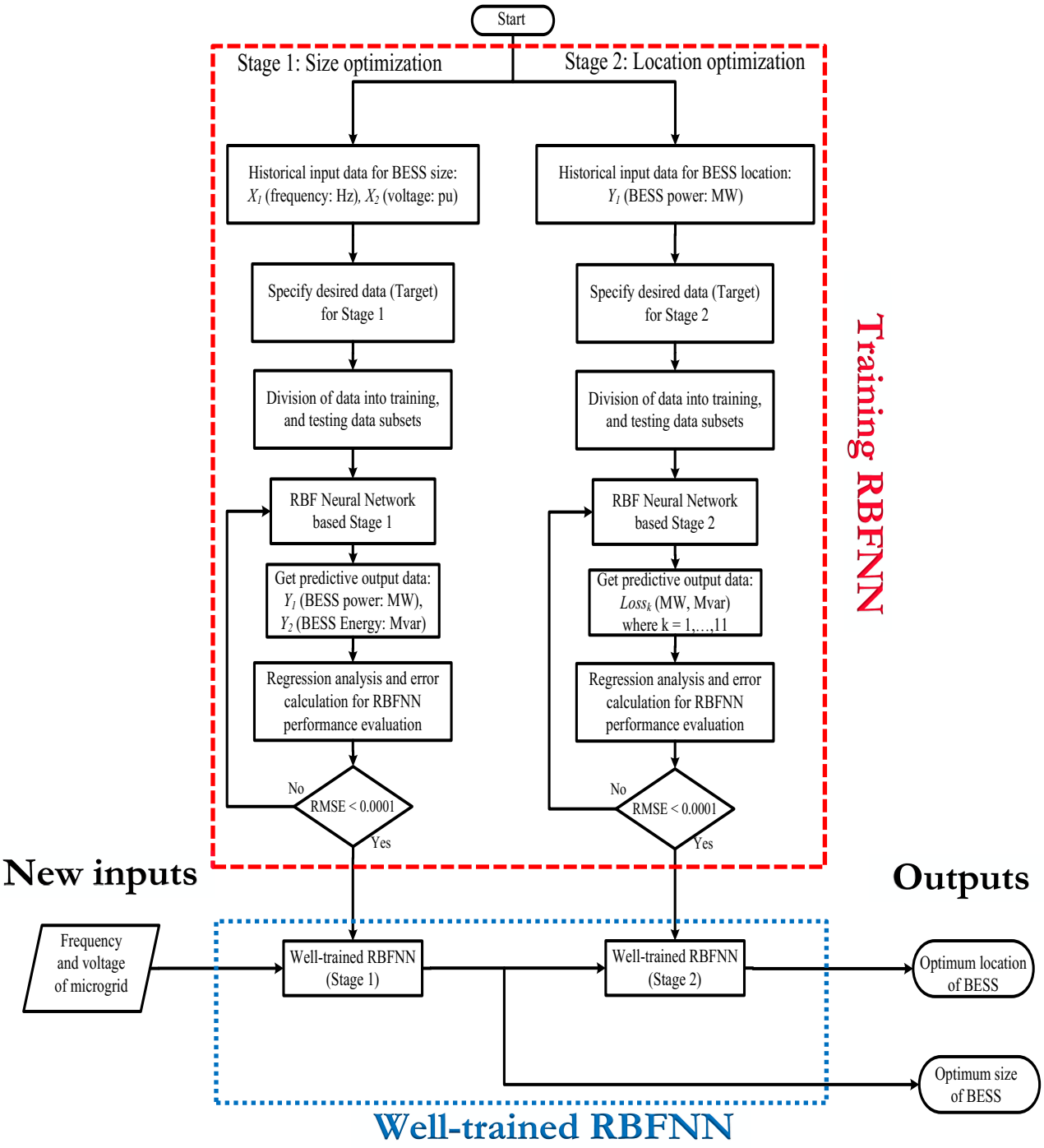

Figure 5.7 The proposed RBFNN method flowchart

5.3 Results and Discussion

This section demonstrates the results of the proposed RBFNN method for estimating an optimum size and location of BESS in order to prevent the microgrid from system instability and collapse in the presence of violent changes of load/generation or the outage of the distributed generation/utility grid. The power fluctuations of the solar PV farm are considered in this method and data are given in Appendix B.

According to Stage 1, two inputs which are frequency and voltage of the microgrid system are fed to the proposed RBFNN model-based Stage 1. The output of the proposed RBFNN can be the predictive result of the optimal size of BESS for the stand-alone microgrid.

In training results of Stage 1 (See Fig. 5.8), the correlation coefficient (R) of the proposed RBFNN model is almost equal to 1 (i.e., 0.99987) which means that the target is equal to the output of the training data. This reason indicates the strong correlation between the target data based on a simulation and the RBFNN output. Hence, it can be confirmed that the proposed RBFNN model-based Stage 1 is high accuracy.

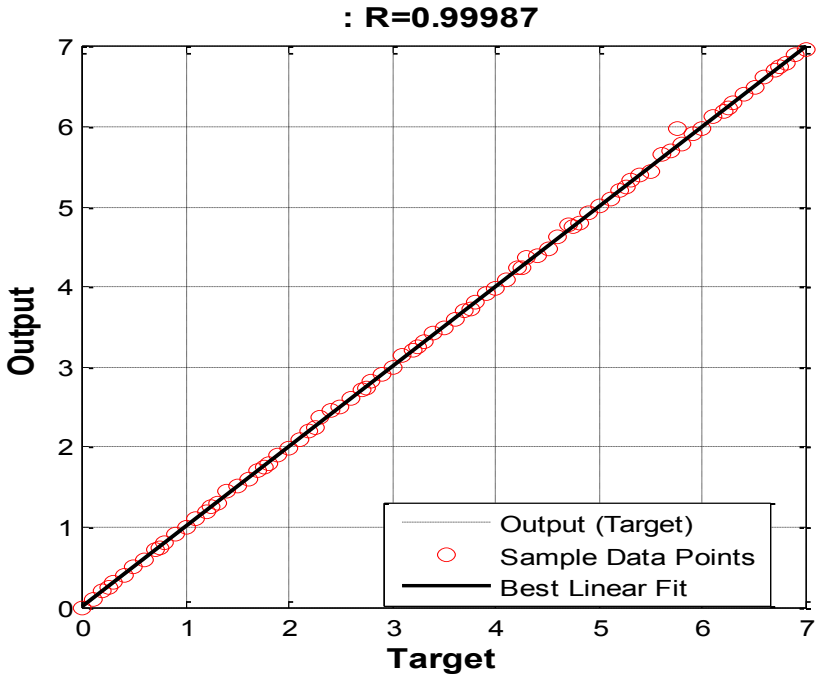

Figure 5.8 A regression analysis between the RBFNN output and target for Stage 1

In the testing results of Stage 1, it shows that the proposed RBFNN model is able to follow the patterns of data (i.e., BESS size based on frequency and voltage of the microgrid) at almost every step mentioned as shown in Fig. 5.9. It is obvious that the proposed RBFNN-based Stage 1 can accurately determine the optimal size of BESS for a microgrid. The predictive outputs of the RBFNN model-based Stage 1 are only slightly different from the target outputs measured from a simulation.

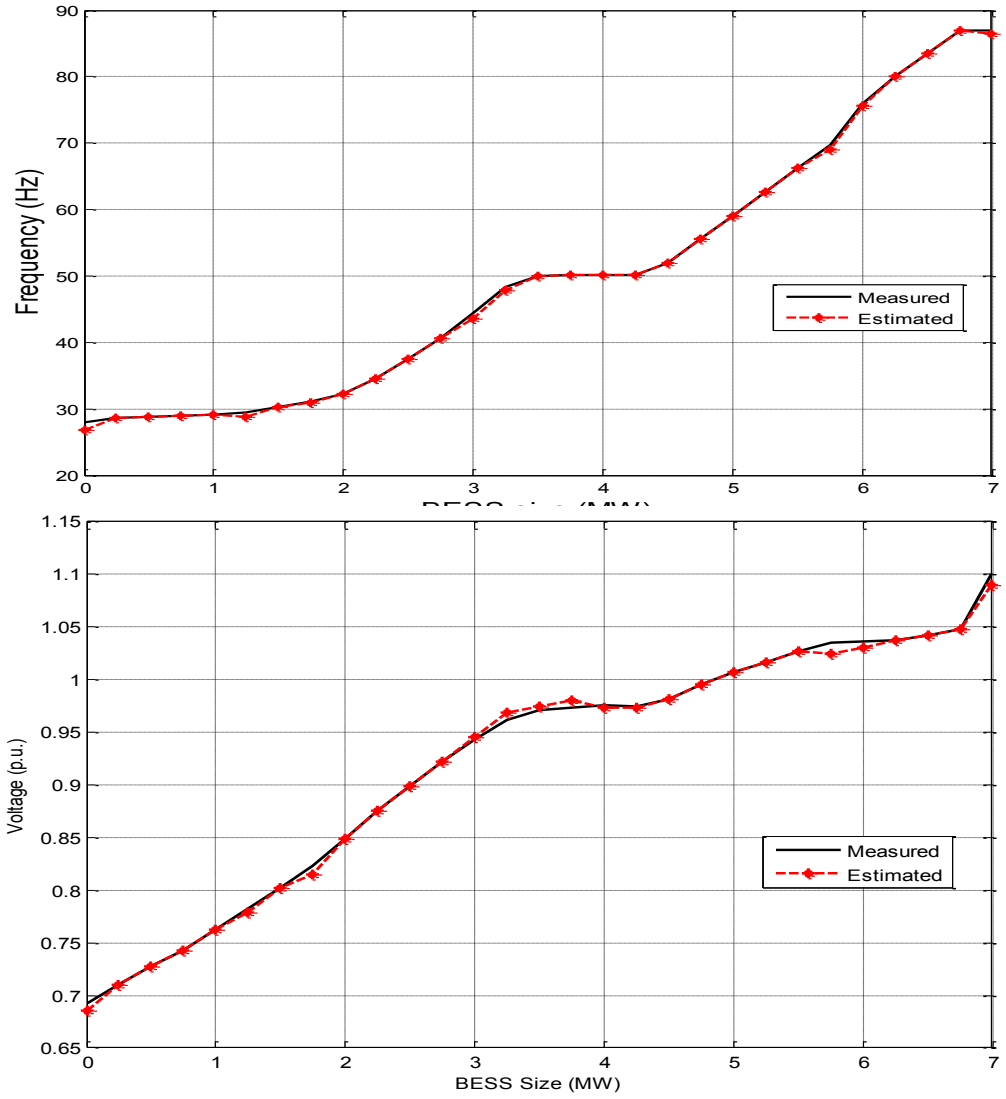

Figure 5.9 A comparison between measured BESS size and estimated BESS size for evaluating an optimum size of BESS

As regard to the training results of Stage 2 (See Fig. 5.10), the correlation coefficient (R) of the proposed RBFNN based Stage 2 is almost equal to 1 (i.e., 0.99981) which means that the target is equal to the output of the training data. This reason specifies the strong correlation between the target outputs based on a simulation and the RBFNN outputs. It can be decided that the proposed RBFNN model-based Stage 2 is also high precision.

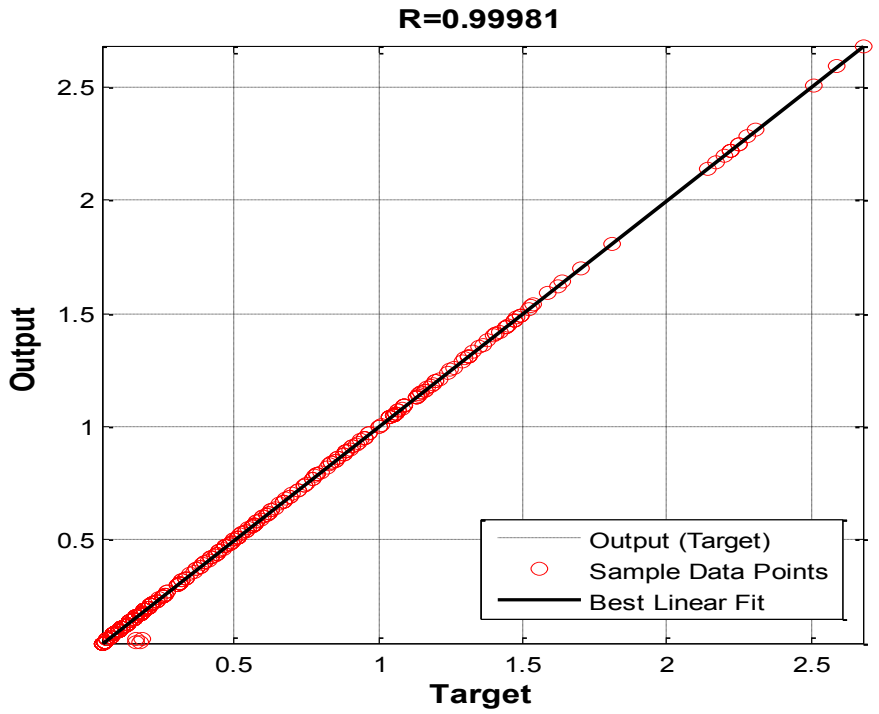

Figure 5.10 A regression analysis between the RBFNN output and target for Stage 2

Looking at the testing results of Stage 2, it shows that the proposed RBFNN-based Stage 2 is able to track the patterns of data (i.e., BESS location based on power losses) at almost every step mentioned as shown in Fig. 5.11. It is proved that the proposed RBFNN-based Stage 2 can precisely determine the optimal location of BESS corresponding to power loss minimization in the microgrid. It can be concluded that the outputs of the proposed RBFNN-based Stage 2 are only slightly different from the targets measured from a simulation. In addition, the 22 kV buses in the typical microgrid are considered for determining an optimal location of BESS as shown in Fig. 5.12.

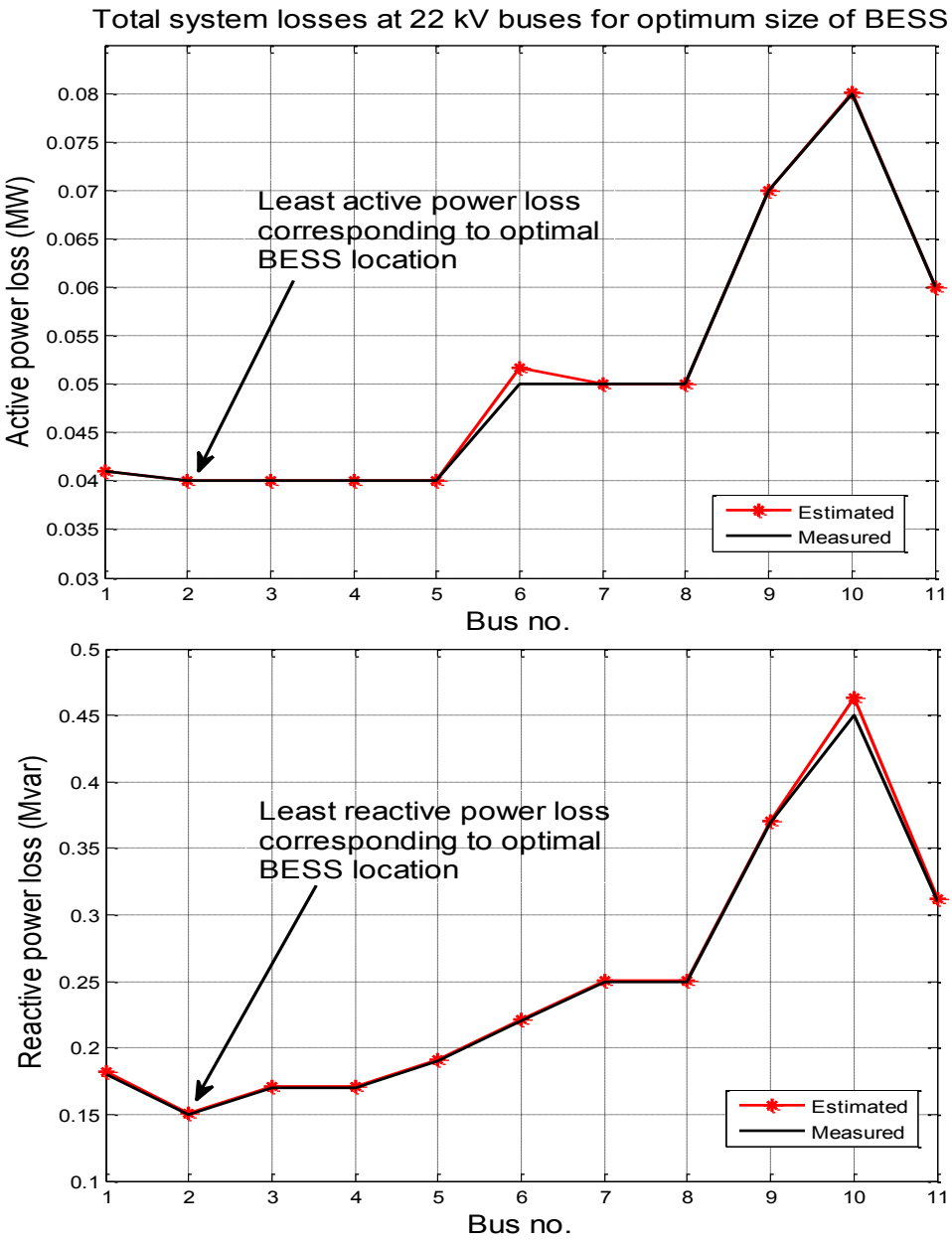

Figure 5.11 A comparison between measured and estimated power loss for determining an optimum location of BESS

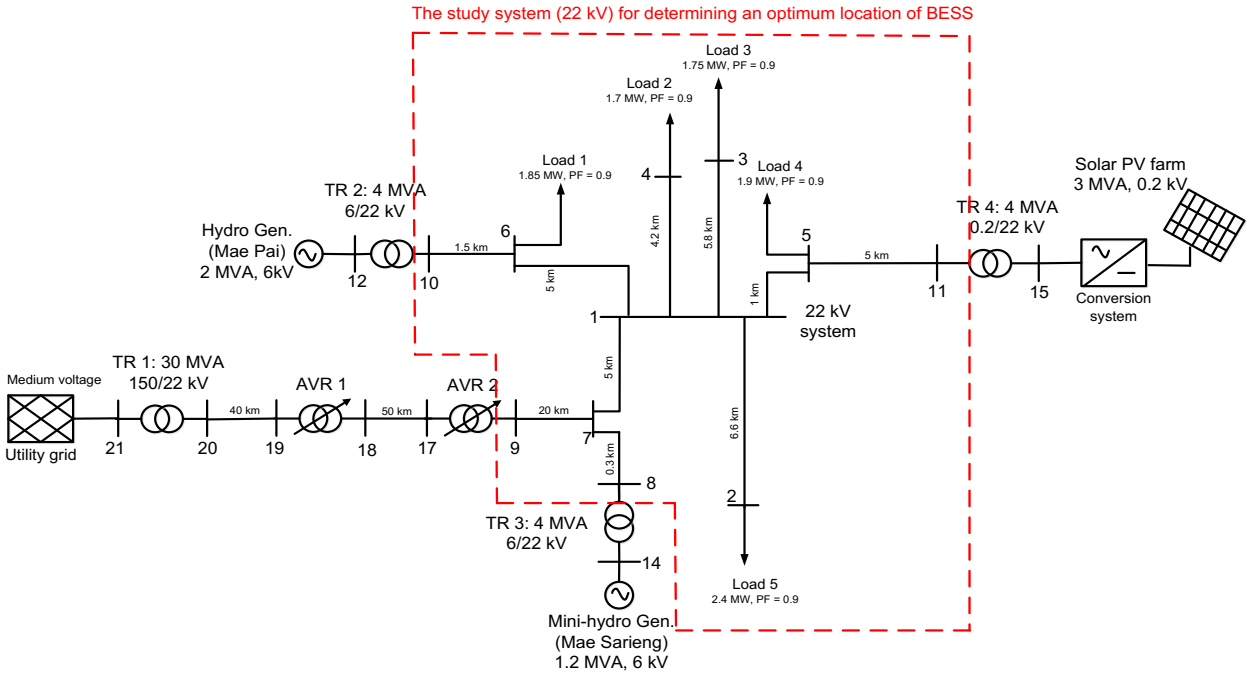

Figure 5.12 The considered buses for determining an optimum location of BESS in the study microgrid

After completing the training and testing processes, the well-trained RBFNN models are obtained which are ready to evaluate an optimum size and location of BESS with a high accuracy. Firstly, normal frequency and voltage referred from the grid-connected operation are fed to the well-trained RBFNN-based Stage 1 as input data in order to determine an optimum size of BESS. The optimum size of BESS is then automatically determined as the predictive output of the well-trained RBFNN-based Stage 1 as seen in Fig. 5.13. The optimum size of BESS is obtained at 3.3796 MW/6.7592 MWh by using the proposed RBFNN method-based Stage 1.

Figure 5.13 The optimum size of BESS for the study microgrid

Afterwards, the optimum size of BESS is fed to the well-trained RBFNN-based Stage 2 as the input data so as to evaluate an optimum location of BESS. The power losses at each bus are then automatically evaluated as the predictive outputs of the well-trained RBFNN-based Stage 2 as shown in Fig. 5.14.

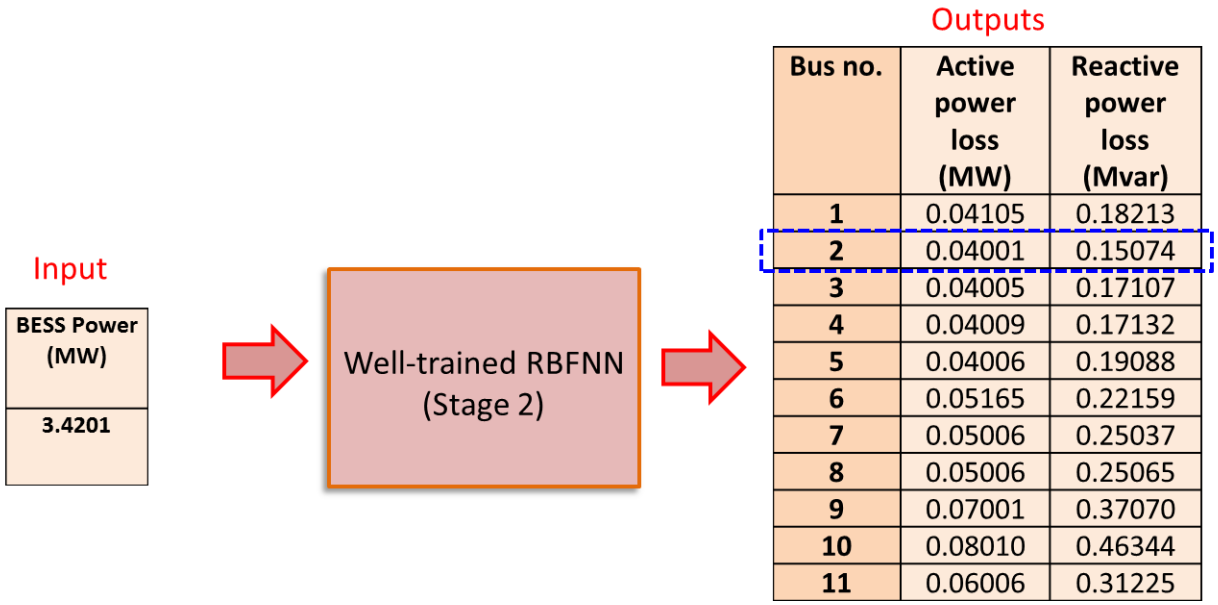

Bus no.	Active power loss (MW)	Reactive power loss (Mvar)
1	0.04105	0.18213
2	0.04001	0.15074
3	0.04005	0.17107
4	0.04009	0.17132
5	0.04006	0.19088
6	0.05165	0.22159
7	0.05006	0.25037
8	0.05006	0.25065
9	0.07001	0.37070
10	0.08010	0.46344
11	0.06006	0.31225

Figure 5.14 The optimum location of BESS for the study microgrid

As regard to Fig. 5.14, it is obvious that the best location of BESS for the study microgrid is at the bus 2 where the total power losses are reduced to 0.04001 MW and 0.15074 Mvar. The second best location of BESS is at the bus 3 where the total power losses are 0.04005 MW and 0.17101 Mvar.

Three adopted error indexes; that is, the mean absolute error (MAE), the mean relative error (MRE) and the root mean square error (RMSE) are used to estimate the proposed RBFNN training performance. These indexes show the learning and generalization errors of the normalized values of the proposed RBFNN models. The computational of these three error indexes can be expressed as:

$$MAE = \frac{1}{n}\sum_{1}^{n}\left|T_i - O_i\right| \tag{5.7}$$

$$MRE = \frac{1}{n}\sum_{1}^{n}\frac{|T_i - O_i|}{T_i} \tag{5.8}$$

$$RMSE = \sqrt{\frac{1}{n-1}\sum_{1}^{n}(T_i - O_i)^2} \tag{5.9}$$

where T_i is the target vector, O_i is the output vector and n is the number of training data or data for each test in the testing data set.

From Table 5.3, three index values revealed that the proposed RBFNN models based Stage 1 and 2 were able to accurately predict the optimum BESS size and location with minimal errors respectively.

Table 5.3 Error indexes for the proposed RBFNN method

Performance predictor	RMSE	MAE	MRE
BESS size optimization (Stage1)	0.0000652	0.0004270	0.0001935
BESS location optimization (Stage 2)	0.0000528	0.0001770	0.0001762

In the performed simulation, the study microgrid performance is tested by implementing the most severe disturbance (i.e., disconnecting of the microgrid from the utility grid) at 10.0 s. The microgrid operation is transited from the grid connected to isolated operation, resulting in the shortage of power supply in the microgrid at that time. It is assumed that the nominal system frequency is 50 Hz and system frequency declines below 49.95 Hz is required the implementation of the optimum size of BESS based on RBFNN connected at the bus 2 in the study microgrid.

Based on Fig. 5.15, the proposed RBFNN method can improve and recover fast, smooth and secure system stability and performance of the microgrid from the emergency situation to the normal equilibrium state. The system frequency-based the proposed RBFNN method is almost the same as the PSO method. It is obvious that the proposed RBFNN method can determine an optimum size of BESS with a high accuracy and low prediction errors.

In case of no BESS, the system frequency drops drastically because the power supply cannot meet the load demand, resulting in system collapse.

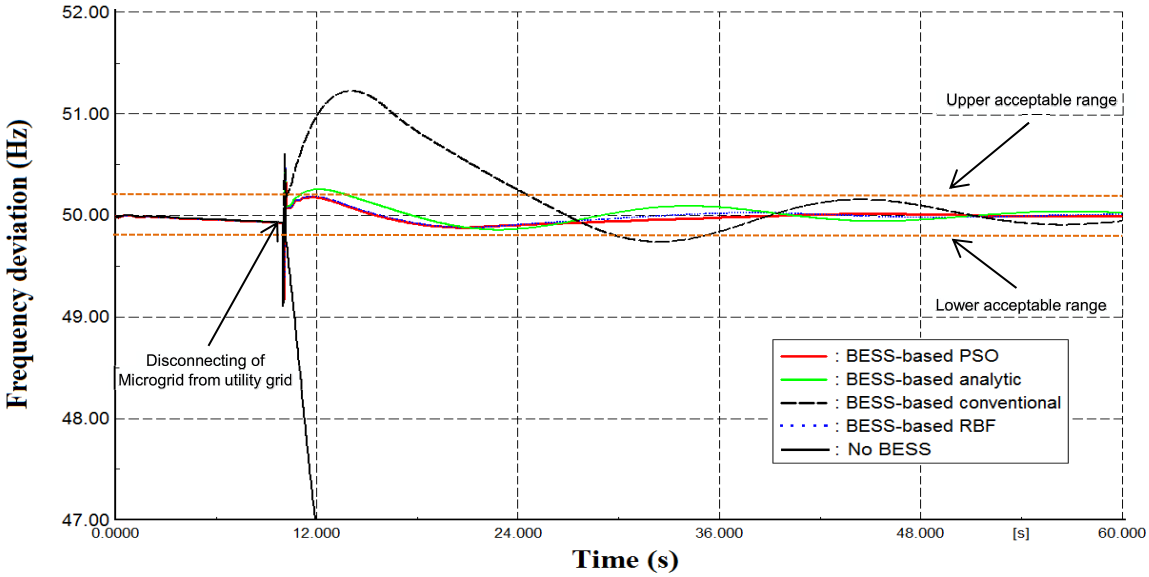

Figure 5.15 Frequency deviation of the microgrid after the severe disturbance

The voltage deviation of the microgrid during the severe disturbance is shown in Fig. 5.16. Based on the result, the proposed RBFNN method can remain nearly the same voltage deviation as the optimum size of BESS-based PSO, analytic method and conventional size of BESS. In case of no BESS, the system voltage decreases drastically because the power supply cannot meet the load demand, causing system collapse.

Therefore, it is confirmed that the proposed RBFNN method can prevent the microgrid from instability and system collapse as well as provide the best reduction in power loss without any violation to frequency and voltage of the microgrid system.

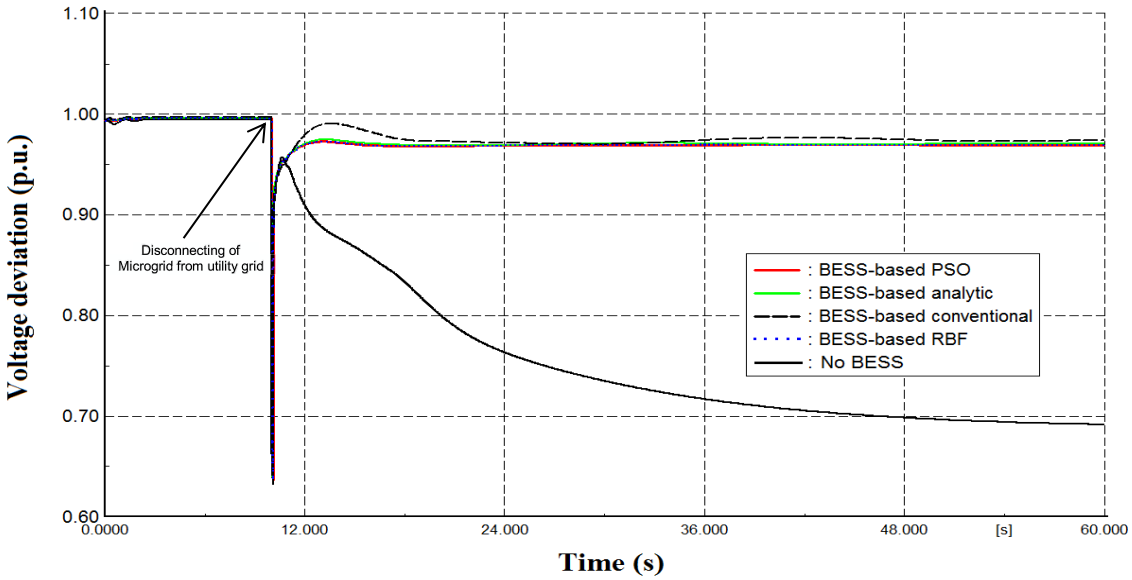

Figure 5.16 Voltage deviation of the microgrid after the severe disturbance

As regard to Table 5.4, the optimum size of BESS-based PSO method can still achieve the best optimum size of BESS compared with the other mentioned methods. However, the PSO consumes longer calculation time with almost 5 minutes. Looking at the proposed RBFNN method, it can achieve nearly the same size of BESS compared with the PSO while it consumes shorter calculation time with only 6 seconds. Hence, it is concluded that the proposed RBFNN method can determine an optimum size and location of the BESS with a high accuracy and shortest calculation time process.

Table 5.4 Comparison parameters of different methods

Case	Power capacity (MW)	Energy capacity (MWh)	Frequency magnitude (Hz)	Voltage (p.u.)	Calculation time (sec.)
BESS-based conventional size	4.000	20.000	51.222	0.974	-
BESS-based analytic method	3.400	17.000	50.310	0.971	372
BESS-based PSO	3.3689	16.8445	50.046	0.970	288
BESS-based RBFNN	3.3796	16.8960	50.049	0.970	6

5.4 Summary

This chapter proposes a new intelligent optimization technique by using radial basis function neural networks (RBFNN) to evaluate an optimum size and location of BESS for microgrids. The proposed RBFNN method consists of a two-stage method: the determination of an optimum BESS size-based frequency control of the microgrid (i.e., Stage 1) and the determination of an optimum BESS location-based power loss minimization of the microgrid (i.e., Stage 2). The design and training of RBFNN models in this chapter are performed using the neural network toolbox from MATLAB 2013b. Based on the results, it is clearly seen that the proposed RBFNN method can determine an optimum size and location of BESS with a high accuracy and low prediction errors. It can achieve the fastest and shortest calculation time

compared with the PSO and analytic methods. The system dynamic and performance of the microgrid based on the RBFNN method are acceptable as they can nearly obtain the same system dynamic and performance with the PSO method. Therefore, it can be summarized that the proposed RBFNN method is appropriate for the intelligent predictive optimum size and location of BESS with only a minor change compared with the measured results based on the simulation and can be used for an online energy storage management in the smart/micro-grid applications.

Result Evaluation of RBFNN Method

As regard to the proposed RBFNN results, it is obvious that the proposed RBFNN method provides the fastest calculation time process and simplistic design method with a high accurate result and finest performance compared with the PSO and analytic methods. There is no need for the enormous uses of programming for the RBFNN method. However, the PSO method can still achieve the best optimum size of BESS compared with other mentioned methods. For these reasons, a brand new optimization idea for combining the advantages of PSO and ANN methods is proposed in the following chapter. Thus, the following chapter is going to design a brand new online optimization method of BESS by exploiting the advantages of both PSO and ANN methods, combining their strengths and applying it as an online effective controller of BESS for smart/micro-grid applications.

5.5 References

1. I. Aleksander and H. Morton, *An introduction to neural computing,* London: Chapman&Hall, 1990.
2. L. V. Fausett, *Fundamental of neural networks,* 1st edition, Englewood Cliffs, New Jersey: Prentice Hall, 1994.
3. S.S. Haykin, *Neural networks: a comprehensive foundation,* 2nd edition, Upper Saddle River, New Jersey: Prentice Hall, 1999.
4. M. T. Hegan, H. B. Demuth, and M. H., *Neural network design,* 1st edition, Boston: PWS

Publications, 1995.

5. The Mathworks, *Neural network toolbox-user's guide,* Mathworks, 1999.
6. C.M. Bishop, *Neural networks for pattern recognition,* New York: Oxford University Press, 1995.
7. S.V. Kartalopoulos, *Understanding neural networks and fuzzy logic: basic concepts and applications,* New York: IEEE Press, 1996.
8. K. Swingler, *Applying neural networks: a practical guide,* London: Academic Press, 1996.
9. R.J. Schalkoff, *Artificial neural networks,* London: McGraw-Hill, 1997.
10. R.M. Pidaparti, and M.J. Palakal, Material model for composites using neural networks, *AIAA Journal,* 31: 1533-1535, 1993.
11. D. Skapura, *Building neural networks,* New York: ACM Press, 1996.
12. T. Kohonen, *Self-organization and associative memory,* Berlin: Springer-Verlag, 1984.
13. M.J.D. Powell, Radial basis function for multi-variable interpolation, *In proceeding of IMA Conference on Algorithm for the Approximation of Function and Data,* 1985.
14. J.L. Elman, "Finding structure in time", *Cognitive Sciences,* 14: 179-211, 1990.
15. T. Kerdphol, Y. Qudaih, K. Hongesombut, M. Watanabe, Y. Mitani, Intelligent Determination of a Battery Energy Storage System Size and Location on RBF Neural Networks for Microgrids. *International Review of Electrical Engineering*, 11(1): 78–87, 2016.
16. T. Kerdphol, K. Fuji, Y. Qudaih, Y. Mitani, Performance Comparison of Artificial Intelligent Approaches for Battery Energy Storage Size optimization in PV-Microgrid. *Journal of Clean Energy Technologies*, 4(6): 389–395, 2016.
17. The Mathworks, *Neural network toolbox-user's guide,* Mathworks, 2013.

Chapter 6

Online Optimization of BESS

6.1 Introduction of Online Optimization Method

Due to the increasing environmental concerns worldwide, the target for integrations in the fraction of electricity supplied by renewable energy resources (RESs) have been set for smart/micro-grids [1, 2]. For example, according to the Kyoto Protocol, Japan promises to reduce its emission by at least 25 % of the 1990 levels by 2020 [3]. Since fossil fuel resources generated electricity are produced more than 40 % of global greenhouse gas (GHG) emissions. Thus, RESs will play an important role in achieving these goals. RESs/DGs, which are located in smart/micro-grids, are gaining more attentions recently and their utilizations are considered for achieving GHG reduction goals [4]. Smart/micro-grids are designed in a way that they can be integrated with the advanced coordinated practices and control technologies for managing DGs or RESs, loads and all devices through the advanced communication technologies. Smart/micro-grids will perform a coordinated control which means the frequency, voltage and active and reactive powers of smart/micro-grids are centrally controlled [5]. Extracting the load/generation changes from time varying and intermittent RESs in smart/micro-grids needs the coordinated control. A conventional coordinated control scheme is typically conducted for 24 hours in advance (e.g., day ahead) due to the idea that the system load can be

predicted a day in advance. Looking at the smart/micro-grids, they are consisted of high integrations of RESs. The conventional coordinated control scheme for a day in advance is not reliable and not accurate enough for managing the smart/micro-grid due to the intermittent and unpredictable the nature of RESs (e.g., wind and solar energy). Especially for wind energy, it can be reliably predicted a few minutes in advance [6]. The quick variation in RESs together with the uncertainty in availability emphasizes the need for an intelligent control technique. Hence, a new intelligent online method is required for the coordinated control of smart/micro-grids. Any changes in loads or generations in smart/micro-grids should be responded optimally by the coordinated control system in the short period of time so as to control the system and operations as efficiency as possible, provide an economically energy use, sustainable and secure power system [7].

Hence, this chapter proposes a brand new online optimization of BESS by using the combination of PSO and ANN methods, and uses it as an online effective controller for the coordinated control system in smart/micro-grids. Any changes in generations/loads will be compensated by the BESS-based online optimization in a short period of time without the necessity of performing the new optimization. To enable the online optimization of the BESS, artificial neural networks (ANN) seem to be most applicable for such an online modeling method in terms of time-varying system modelling, a fast time calculation process and instant responses. ANNs have been widely used to time series prediction [8]. In such a field, the multilayer perceptron neural networks (MLPNN) are widely used as a conventional method in many researches [9-11]. A majority of models are generated based on the MLPNN trained by the gradient descent method. However, their dynamic characteristics are not good enough to make the models suitable for time-varying system modelling, especially for online control systems. In addition, the nature of the MLPNN concerns a gradient-based training, and its slow convergent rate as well as the tendency falling into local minima problems become the main disadvantages [12, 13]. Looking at the characteristic of radial basis function neural networks (RBFNN), they can provide a very significant tool for optimization tasks as they are extremely powerful computational devices with the capability of parallel processing, learning and generalization as well as universal approximation [14]. The advantages of RBFNN are two major issues: the training processes are substantially faster than MLPNN and RBFNN do not encounter with local minima problems [15-17]. Therefore, RBFNN are promoted and introduced as the proposed online optimization model in this chapter. Then, the predictive outputs of the online optimization of BESS-based RBFNN are compared with the online optimization of BESS-based MLPNN (i.e., the most popular/conventional design model for ANN) and the PSO optimization when error efficiency and positional accuracy are concerned.

The outstanding of the online optimization of BESS is that it can be used as an online effective controller of BESS for smart/micro-grids without the necessity of performing the new optimization process at any change in loads/generations or the loss of a generation/utility grid.

6.2 Structure of Online Optimization of BESS

In this chapter, optimum active and reactive powers of BESS are evaluated by using the online optimization of BESS with the objective of frequency control of the microgrid. The goal of the proposed method is to evaluate optimum active and reactive powers of BESS in order to prevent the microgrid from instability and system collapse in the presence of violent changes of generations/loads or the loss of a generation/utility grid [18]. The inputs of the proposed online optimization of BESS are the measured data of generations and loads and the output are optimum active and reactive powers of BESS as shown in Fig. 6.1.

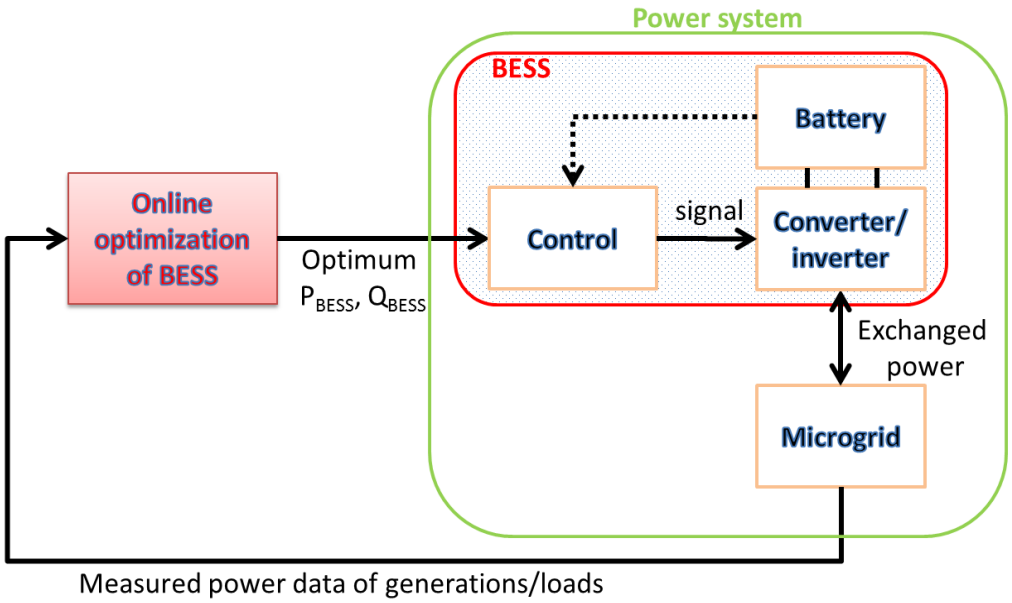

Figure 6.1 The structure of the online optimization of BESS

Looking inside the online optimization of BESS as shown in Fig. 6.2, it is a two-stage process which contains the offline process and online process. As regard to the

offline process, it consists of three parts: PSO optimization (i.e., Chapter 3), database collection and RBFNN training. The online process contains the well-trained RBFNN model which is ready to evaluate online optimum active and reactive powers of BESS so as to prevent the microgrid from instability and system collapse in the presence of violent changes of generations/loads or the loss of a generation/utility grid.

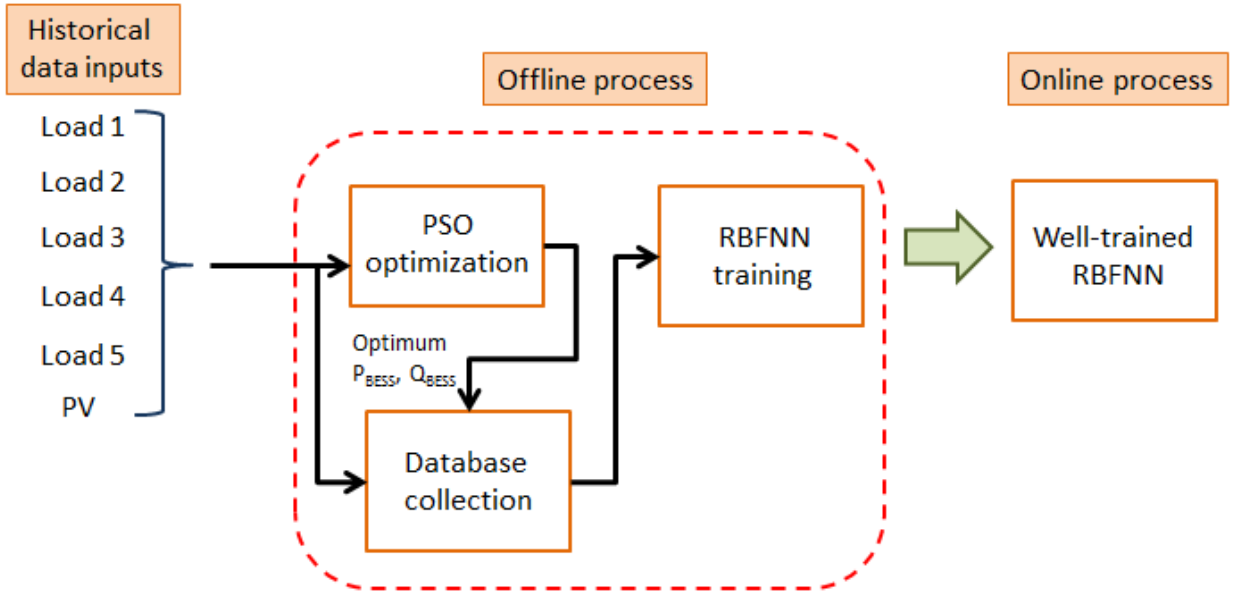

Figure 6.2 Inside of the proposed online optimization of BESS

First of all, the optimum setting powers of BESS are determined by the PSO optimization. The measured power data of generations/loads at every 30 minutes will be the inputs of the PSO optimization in the offline process. The optimum powers of BESS are then evaluated by the PSO and collected in the database collection. These optimum data are applied as target data for the RBFNN generalization and training. With an appropriate RBFNN training, the well-trained RBFNN model is obtained and employed as the online process where the system is using new input data as shown in Fig. 6.3. Afterwards, the optimum active and reactive powers of BESS can be automatically obtained without the necessity of performing the new optimization process at any change in loads/generations. The online optimization of BESS needs to restart the whole process (i.e., offline and online process) again when adding/removing a distributed generation/load to the microgrid system.

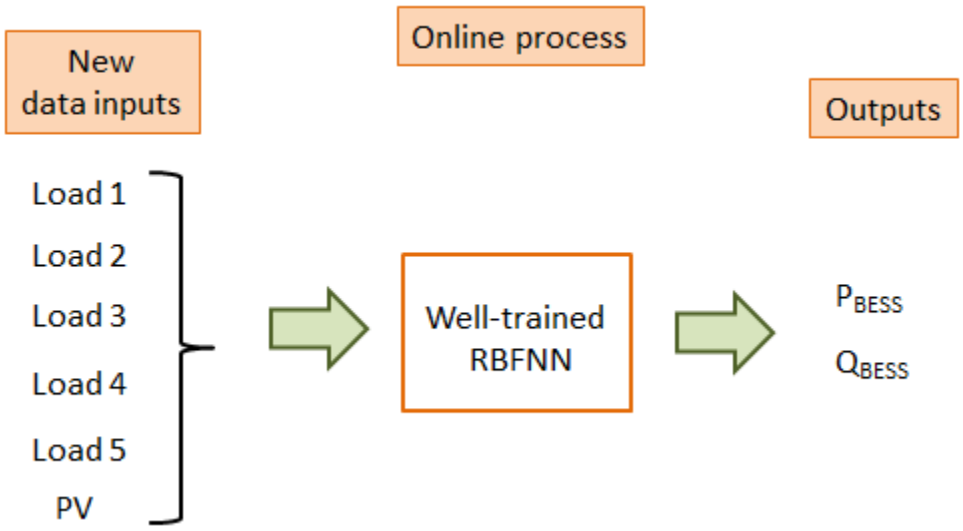

Figure 6.3 The online process structure

The proposed online optimization of BESS is tested through the typical microgrid in Chapter 2 with a 24-hour load/generation profiles. The fluctuations of PV generation due to unpredicted weather conditions are also considered in this study. The PV generation profiles of a sunny and a rainy day are displayed in Fig. 6.4. Three types of loads are involved which are the residential, office, and commercial loads as shown in Fig. 6.5. The load profile depends on peaks and dips due to the various electricity usage situations. As regard to the residential loads, a peak load occurs from 7 pm to 9 pm. For the office and commercial loads, the peak load occurs from 9 am to 5 pm every day due to the electricity usage during the office hours.

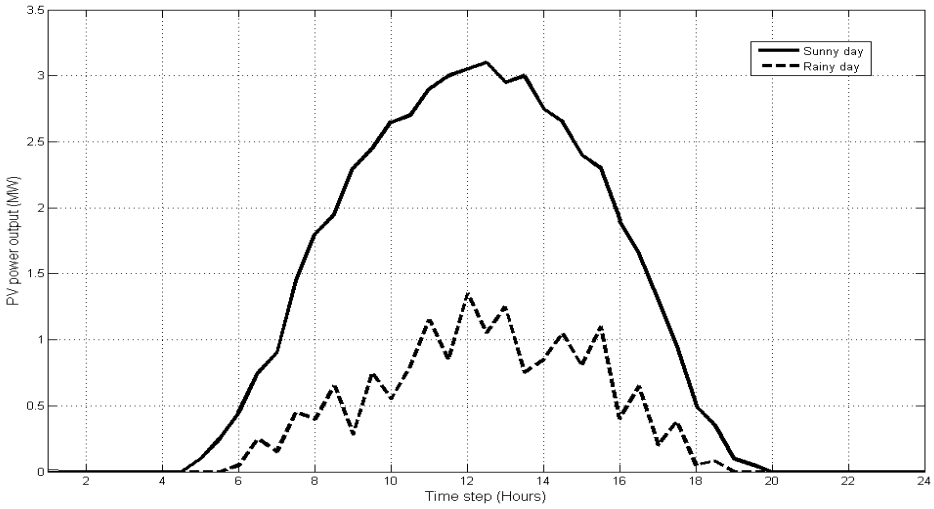

Figure 6.4 PV generation profiles for a sunny and a rainy day

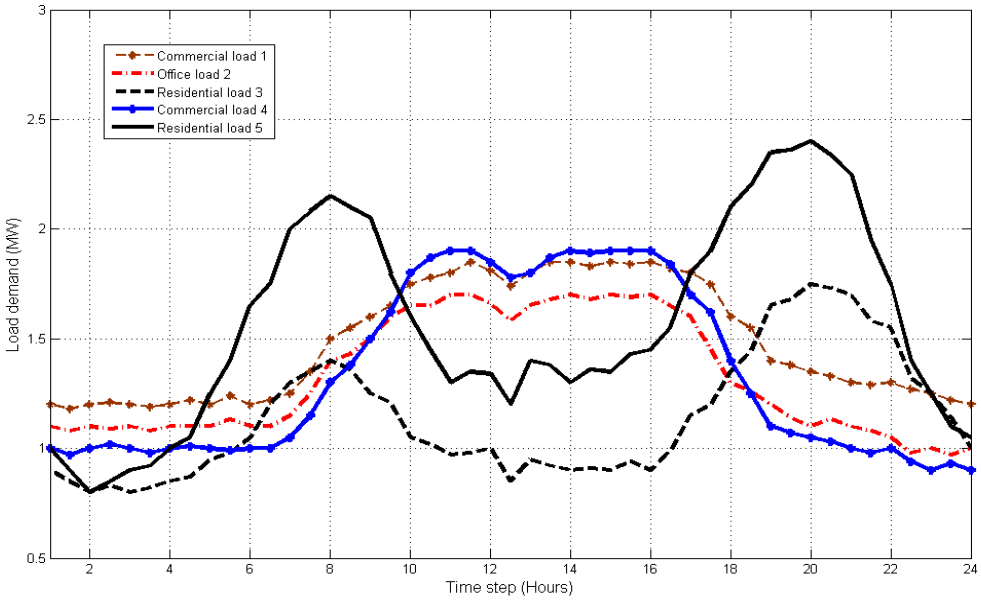

Figure 6.5 Load demand profiles

6.2.1 PSO Optimization

According to the advantage of the PSO method from Chapter 4, it is confirmed that the PSO method provides the best optimum solution compared with other mentioned methods. Hence, in this chapter, the PSO optimization is used to determine optimum powers of BESS in the offline process so as to confirm the finest optimum setting data for the RBFNN generalization and training process. The measured power data of generations/loads at every 30 minutes will be the input of the PSO optimization. Then, the optimum powers of BESS are evaluated by the PSO and collected in the database collection. Afterwards, these optimum data are used as target data for the RBFNN generalization and training.

The objective of the PSO optimization is to evaluate optimum active and reactive powers of BESS in order to avoid the microgrid from instability and system collapse after the loss of the utility grid (e.g., blackouts or disasters). The objective function is represented as follows [19, 20]:

$$\text{Minimize } f_1 = \min (S_{BESS})$$

$$= \min(\lambda_1 P_{BESS} + \lambda_2 Q_{BESS}) \quad (6.1)$$

Subject to:

BESS constraints are imposed on the optimization as follows:

$$P_{BESS}^{\min} \le P_{BESS} \le P_{BESS}^{\max} \quad (6.2)$$

where P_{BESS} is the rated active power of BESS (MW),
P^{BESS}_{min} is the allowed minimum rated active power of BESS,
P^{BESS}_{max} is the allowed maximum rated active power of BESS.

$$Q_{BESS}^{\min} \le Q_{BESS} \le Q_{BESS}^{\max} \quad (6.3)$$

where Q_{BESS} is the rated reactive power of BESS (MWh),
Q^{BESS}_{min} is the allowed minimum rated reactive power of BESS,
Q^{BESS}_{max} is the allowed maximum rated reactive power of BESS.

Microgrid frequency constraint is imposed on the optimization as follows:

$$F_{\min} \le F \le F_{\max} \quad (6.4)$$

where F is the nominal frequency of the isolated microgrid (Hz.),
F_{min} is the allowed minimum nominal frequency of the isolated microgrid,
F_{max} is the allowed maximum nominal frequency of the isolated microgrid.

6.2.2 RBFNN Optimization Method

Due to the advantage of the RBFNN method from Chapter 5, it is confirmed that the RBFNN method provides a fast calculation time with a high accurate result compared with the other mentioned methods. Thus, this chapter proposes the RBFNN method for applying in both offline and online process. In the offline process, the RBFNN method receives the input data from the database collection and then trains these data in the offline process. With an appropriate RBFNN training, the well-trained RBFNN model is obtained with a high accuracy and ready to employ in the online process. In the online process, it contains the well-trained RBFNN model where the system is applying new input data. The optimum active and reactive powers of BESS can be automatically evaluated by the online process without the necessity of performing the new optimization process at any change in loads/generations.

To enable the online optimization of BESS, the proposed RBFNN model is implemented in Fig. 6.6. The input data extracted from the database collection is used as target data in the RBFNN generalization capability. There will be twelve inputs and two outputs. The inputs of the system are the active and reactive powers of the commercial load 1 (X_1, X_2) respectively, the active and reactive powers of the office load 2 (X_3, X_4) respectively, the active and reactive powers of the residential load 3 (X_5, X_6) respectively, the active and reactive powers of the commercial load 4 (X_7, X_8) respectively, the active and reactive powers of the residential load 5 (X_9, X_{10}) respectively and the active and reactive powers of the solar PV system (X_{11}, X_{12}) respectively. The outputs of the system are the active and reactive powers of BESS (Y_1, Y_2) respectively. Then, the proposed RBFNN model-based online optimum active and reactive powers of BESS is demonstrated as a function that maps the input $X = [X_1, X_2, X_3, X_4, X_5, X_6, X_7, X_8, X_9, X_{10}, X_{11}, X_{12}]$ to the output $Y = [Y_1, Y_2]$.

The input vector X is applied to all neurons in the hidden layer. The hidden layer is composed of number q RBFNNs that are connected directly to all the elements in the output layer. A neuron in the hidden layer will produce a greater output when the input pattern presented is close to its center. The output of a node will reduce as the distance from the center increase, assuming that a symmetrical basis function is applied. Hence, for an input pattern, only neurons whose centers are close to the input pattern will produce non-zero activation values to the input stimulus. The basis function for the j^{th} node in the hidden layer is determined by a Gaussian exponential function as follows [15-17]:

$$b_j\left(\overline{X}\right) = \exp\left(\frac{-\left(\overline{X} - \mu_j\right)^2}{2\sigma_j^2}\right), \qquad \text{for } j = 1, 2, ..., q \tag{6.5}$$

where μ_j is the respective centre of the j^{th} neuron in the hidden layer,
σ_j is the wide of the Gaussian potential function of the j^{th} neuron in the hidden layer.

The network output Y is formed by a linearly weighted sum of the number of basis functions in the hidden layer. The values for the output nodes are calculated as follows [18]:

$$Y_k = \sum_{j=1}^{q} W_{kj} b_j\left(\overline{X}\right), \qquad \text{for } k = 1, 2 \tag{6.6}$$

where Y_k is an output of the k^{th} node in the output layer, W_{kj} is a weight value between the j^{th} node in the hidden layer k^{th} node in the output layer, $b_j(\overline{X})$ is an output of the j^{th} node in the hidden layer.

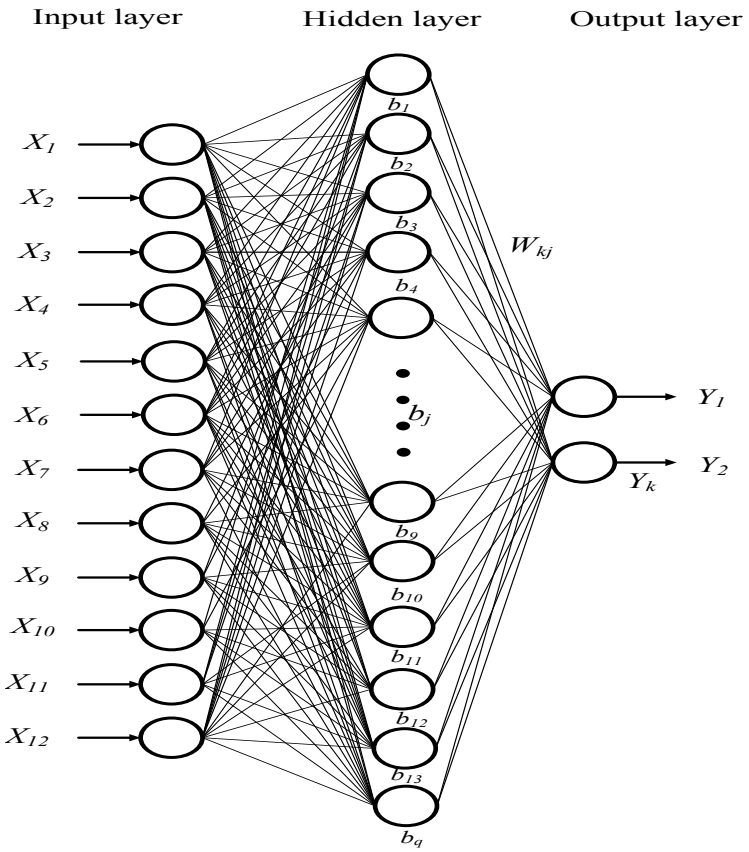

Figure 6.6 The RBFNN structure for determining optimum powers of BESS

As regard to Table 6.1, the parameter details for determining optimum active and reactive powers of BESS are displayed and used in the training and the testing database. The RBFNN model was trained with 940 patterns of the data set (i.e., 70 % of data set) and its performance was tested with 404 patterns (i.e., 30 % of data set) randomly selected from the data set. The performance of the RBFNN training was evaluated with the root mean square error (RMSE) reduced to an order of 10^{-4}. The design and training of the RBFNN model in this chapter were performed using the neural network toolbox from MATLAB 2013b [21].

Table 6.1 RBFNN parameters for determining optimum powers of BESS

Parameters	**RBFNN**
Goal (RMSE)	0.0001
Inputs	12
Outputs	2
Hidden layer	1
Training data	940
Testing and validating data	404
Hidden layer neurons	30
Output layer neurons	2
Activation function	Gaussian exponential

6.2.3 MLPNN Optimization Method (Conventional Method)

Multilayer perceptron neural networks (MLPNN) are known as the most popular model for artificial neural networks (ANN) which are proposed and implemented in many researches [12, 13]. In this chapter, the MLPNN model is considered and selected as the conventional method in order to compare the system performance of the proposed RBFNN model.

The MLPNN model belongs to the class of feed-forward networks. In the MLPNN structure, it is established in a layered feed-forward network and contained by an input layer, hidden layer and output layer. The weight total of the input data and chosen bias are passed through a transfer function to obtain the output data. The number of hidden layers can be changed based on the problem data in the training process. In this chapter, the MLPNN consists of three-layers of neurons which

demonstrate that only one hidden layer is included and one class of activation function is used in the hidden layer and one output layer is contained.

To enable the online optimization of BESS, the proposed MLPNN model is implemented in Fig. 6.7. The input data extracted from the database collection is used as target data in the MLPNN generalization capability. There will be twelve inputs and two outputs. The inputs of the system are the active and reactive powers of the commercial load 1 *(X_1, X_2)* respectively, the active and reactive powers of the office load 2 *(X_3, X_4)* respectively, the active and reactive powers of the residential load 3 *(X_5, X_6)* respectively, the active and reactive powers of the commercial load 4 *(X_7, X_8)* respectively, the active and reactive powers of the residential load 5 *(X_9, X_{10})* respectively and the active and reactive powers of the solar PV system *(X_{11}, X_{12})* respectively. The outputs of the system are the active and reactive powers of BESS *(Y_1, Y_2)* respectively. Then, the MLPNN model-based online optimum active and reactive powers of BESS is demonstrated as a function that maps the input $X = [X_1, X_2, X_3, X_4, X_5, X_6, X_7, X_8, X_9, X_{10}, X_{11}, X_{12}]$ to the output $Y = [Y_1, Y_2]$.

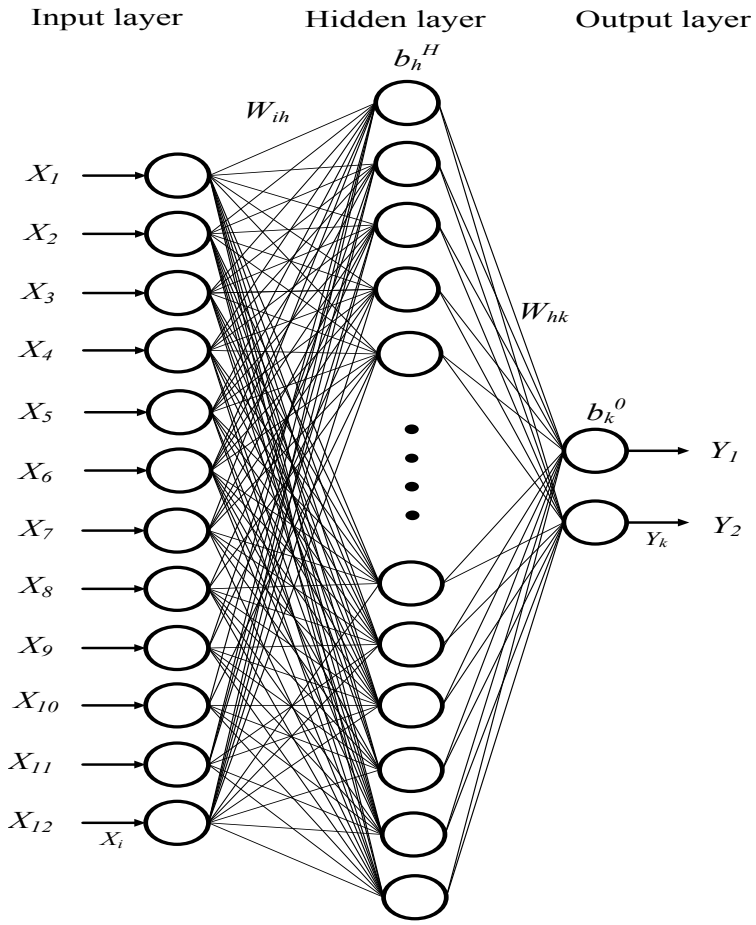

Figure 6.7 The MLPNN structure for determining optimum powers of BESS

Each hidden layer summarizes its weighted inputs which can be expressed as [12]:

$$y_h(n) = \sum_{i=1}^{Ni} W_{ih}(n) X_i(n) + b_h^H \tag{6.7}$$

where W_{ih} (i = 1,2,…,N_i, h = 1,2,…N_h) are the weights of the connections between the input and hidden layers, X_i (i = 1,2,…,N_i) are the input signals, b_h^H (h = 1,2,…, N_h) are the biases at the hidden layer, N_i is the number of the inputs, N_h is the number of neurons in the hidden layer.

The function form of the online optimization of BESS-based MLPNN model (i.e., the outputs from the hidden layers) can be shown as follows:

$$Y_k(n) = \sum_{h=1}^{Nh} W_{hk}(n) \cdot f(y_h(n)) + b_k^0 \tag{6.8}$$

where
$$f(y_h(n)) = f_{sigmoid}(y_h(n)) = \frac{1}{1 + e^{-(y_h(n))}} \tag{6.9}$$

where Y_k (k = 1,2,…,N_k) are the output signals, W_{hk} (h = 1,2,…N_h, k = 1,2,…N_k) are the weight values of the connections between the hidden and output layers, b_k^0 (k = 1,2,…N_k) are the biases at the output layer nodes, f (y_h(n)) is the hidden activation transfer function, N_h is the number of neurons in the hidden layer, N_k is the number of the outputs.

As regard to Table 6.2, the parameter details for determining optimum active and reactive powers of BESS-based MLPNN are displayed and used in the training and the testing database. The MLPNN model was trained with 940 patterns of the data set (i.e., 70 % of data set) and its performance was tested with 404 patterns (i.e., 30 % of data set) randomly selected from the data set. The performance of the MLPNN training was evaluated with the root mean square error (RMSE) reduced to an order of 10^{-4}. The design and training of MLPNN models in this chapter were performed using the neural network toolbox from MATLAB 2013b [21].

Table 6.2 MLPNN parameters for determining optimum powers of BESS

Parameters	MLPNN
Goal (RMSE)	0.0001
Inputs	12
Outputs	2
Hidden layer	1
Training data	940
Testing and validating data	404
Hidden layer neurons	30
Output layer neurons	2
Activation function	Sigmoid

6.3 Results and Discussion

This section describes the results of the proposed online optimization of BESS with the objective of frequency control of the microgrid. Thus, the online optimization of BESS-based RBFNN will automatically determine online optimum powers of BESS in order to avoid the isolated microgrid from instability and collapse in the presence of violent changes of loads or the outage of a distributed generation. The validity of the online optimization of BESS-based RBFNN is verified by comparing to the optimum results-based PSO (i.e., target data). Then, the predictive results and performance of the online optimization of BESS-based RBFNN method are compared with the online optimization of BESS-based MLPNN method when error efficiency and positional accuracy are considered.

In the training results of the online optimization of BESS method, the correlation coefficient (R) is used to measure the fitness where, a value closer to 1 indicates a better fit. From Figs. 6.8 and 6.9, it shows that the correlation coefficient of the proposed online optimization of BESS-based RBFNN model is higher than the correlation coefficient (R) of the online optimization of BESS-based MLPNN model and almost equal to 1 (i.e., 0.9999) which means that the targets are equal to the outputs of the training data. This reason indicates the strong correlation between the optimization data and the neural network output. Hence, it is obvious that the proposed online optimization of BESS-based RBFNN approach achieves the best high-accuracy compared with the online optimization of BESS-based MLPNN approach.

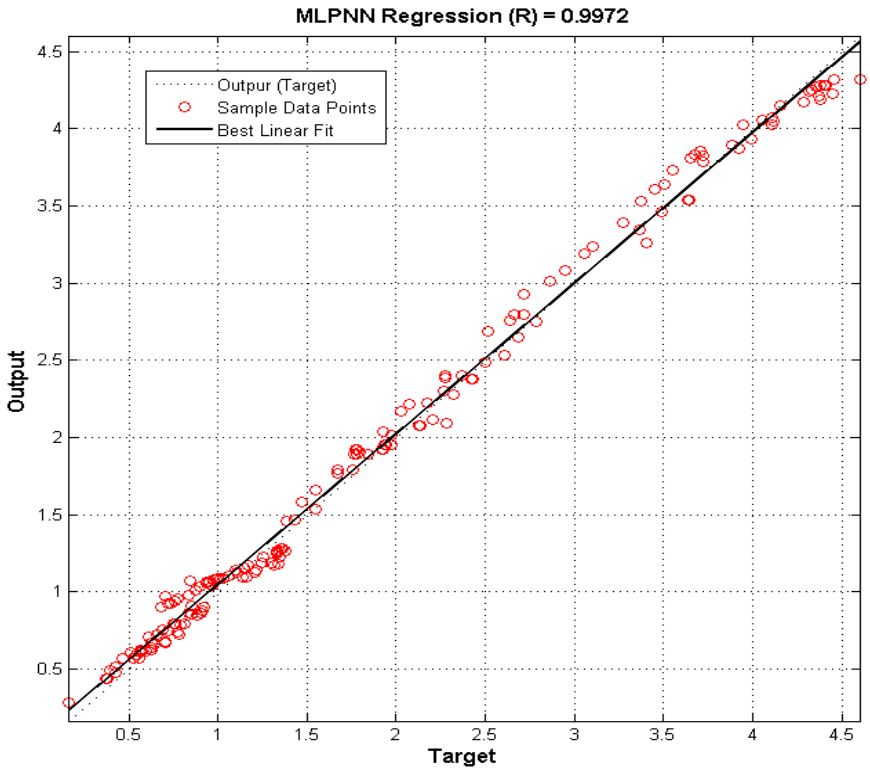

Figure 6.8 A regression analysis between the network outputs and the optimization targets based on MLPNN

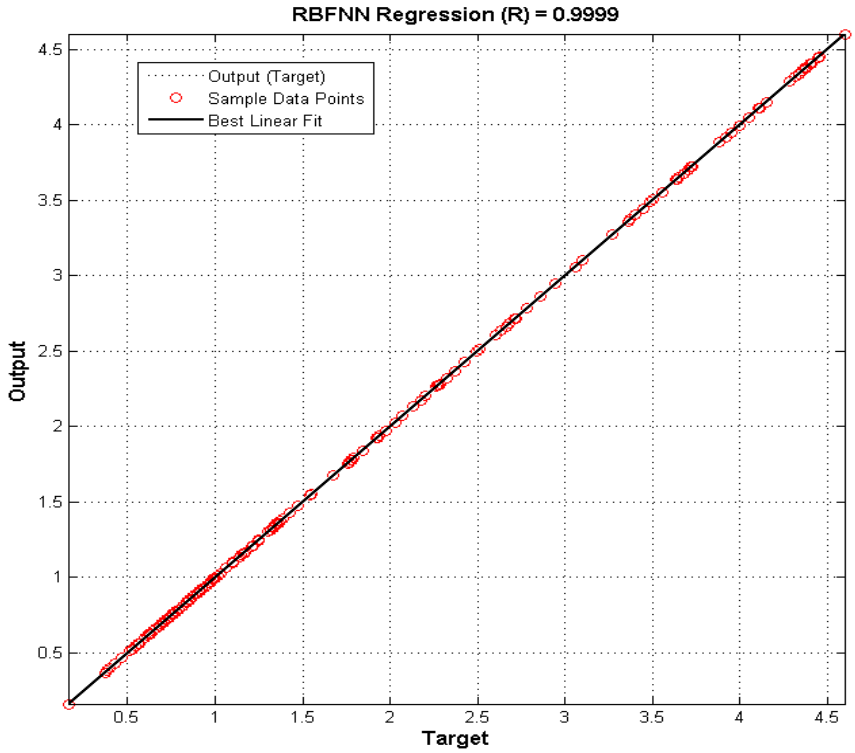

Figure 6.9 A regression analysis between the network outputs and the optimization targets based on RBFNN

Three adopted error indexes; that is, the mean absolute error (MAE), the mean relative error (MRE) and the root mean square error (RMSE) are used to estimate the RBFNN/MLPNN training performance. These error indexes show the learning and generalization error of the normalized values of the online optimization of BESS-based RBFNN/MLPNN model. The computational of the three error indexes can be expressed as [18]:

$$MAE = \frac{1}{n}\sum_{1}^{n}\left|T_i - O_i\right| \tag{6.10}$$

$$MRE = \frac{1}{n}\sum_{1}^{n}\frac{\left|T_i - O_i\right|}{T_i} \tag{6.11}$$

$$RMSE = \sqrt{\frac{1}{n-1}\sum_{1}^{n}(T_i - O_i)^2} \tag{6.12}$$

where T_i is the target vector, O_i is the output vector and n is the number of training data or data for each test in the testing data set.

Compared with the online optimization of BESS-based MLPNN model, Table 6.3 shows that the proposed online optimization of BESS-based RBFNN model has the minimum statistic error in terms of MAE, MRE and RMSE. It is concluded that the proposed online optimization of BESS-based RBFNN is the effective way to improve the prediction accuracy. In addition, the proposed online optimization of BESS-based RBFNN is able to accurately predict the optimum active and reactive powers of BESS with minimal errors.

Table 6.3 Error indexes for the online optimization of BESS

Output	MAE	MRE	RMSE
Y_1-based RBFNN (Active power)	0.0004270	0.0001935	9.947×10^{-7}
Y_2 – based RBFNN (Reactive power)	0.0001770	0.0001762	7.821×10^{-7}
Y_1-based MLPNN (Active power)	0.01485	0.00636	0.000067
Y_2 – based MLPNN (Reactive power)	0.01696	0.02231	0.000064

Looking at the testing results of the online optimization of BESS method, the online optimization of BESS-based RBFNN/MLPNN has been trained and tested using the typical microgrid, load demand and generation profiles under the environments of a sunny and rainy day without the support of the utility grid (i.e., isolated mode). The predictive results of the online optimization of BESS-based RBFNN/MLPNN method are verified with the optimum data obtained from the PSO optimization conducted offline as shown in Figs. 6.10-6.13.

Figs. 6.10-6.11 show the predictive results of the online optimization of BESS under the typical load and generation profiles with the environment of a sunny day for a 24-hour, respectively. Figs. 6.12-6.13 show the predictive results of the online optimization of BESS under the typical load and generation profiles with the environment of a rainy day for a 24-hour, respectively. As regard to these figures, the proposed online optimization of BESS-based RBFNN method is better than the online optimization of BESS-based MLPNN method when the accuracy and efficiency are concerned. The capability of the online optimization of BESS-based MLPNN is poor compared to the proposed online optimization of BESS-based RBFNN. It is obvious that the proposed online optimization of BESS-based RBFNN is able to follow the target patterns-based PSO at almost every time step mentioned. Compared with the online optimization of BESS-based MLPNN model, the outputs of the proposed online optimization of BESS-based RBFNN model are only slightly different from the optimization targets-based PSO.

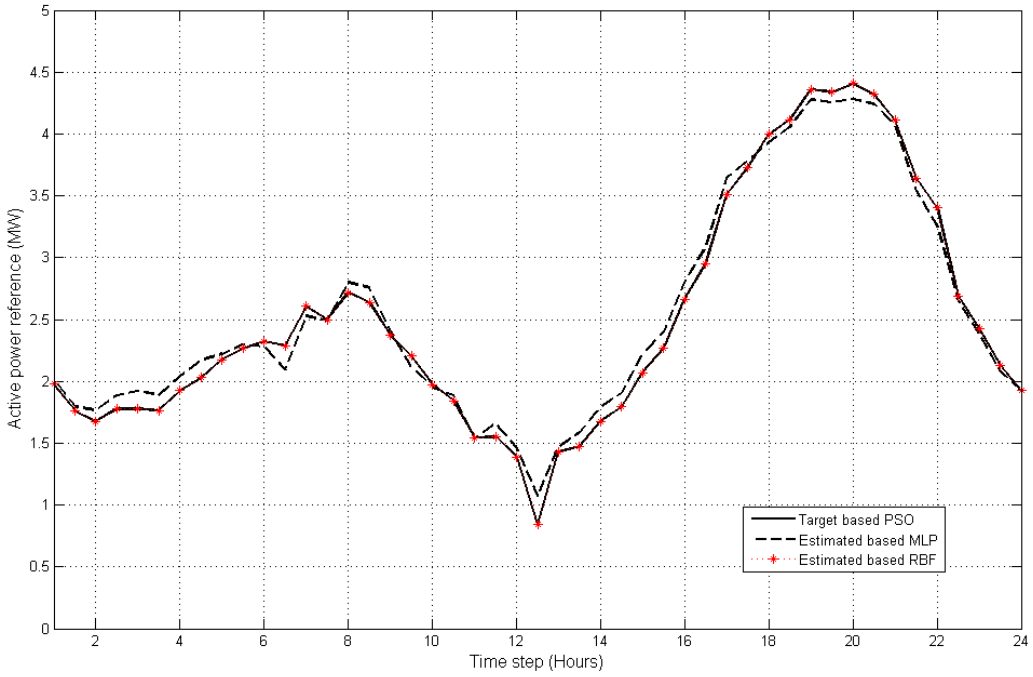

Figure 6.10 The active power of BESS under the environment of a sunny day

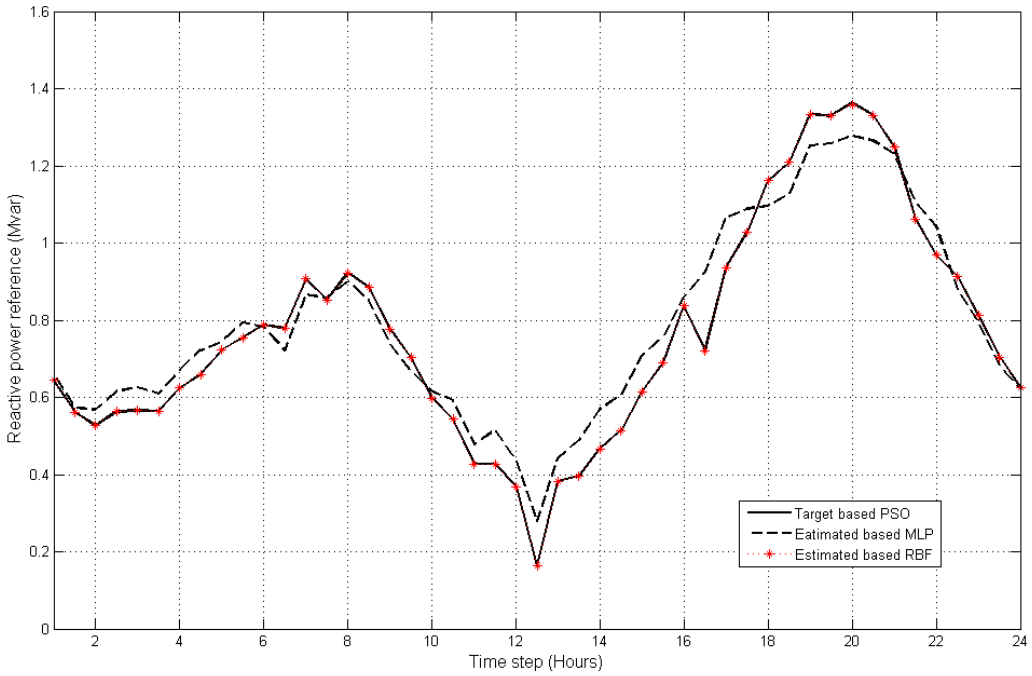

Figure 6.11 The reactive power of BESS under the environment of a sunny day

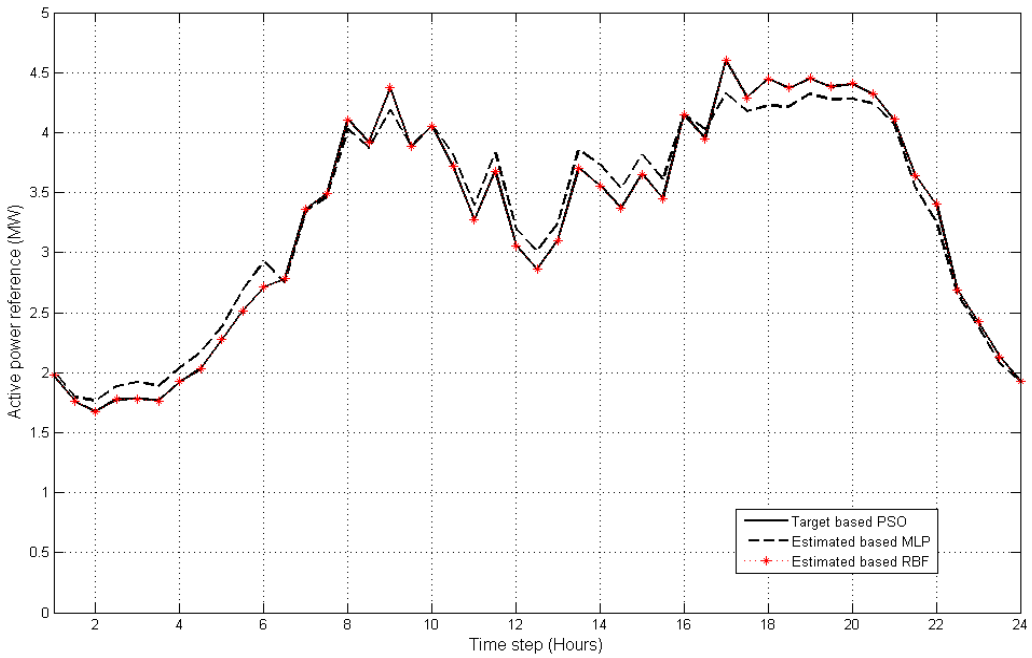

Figure 6.12 The active power of BESS under the environment of a rainy day

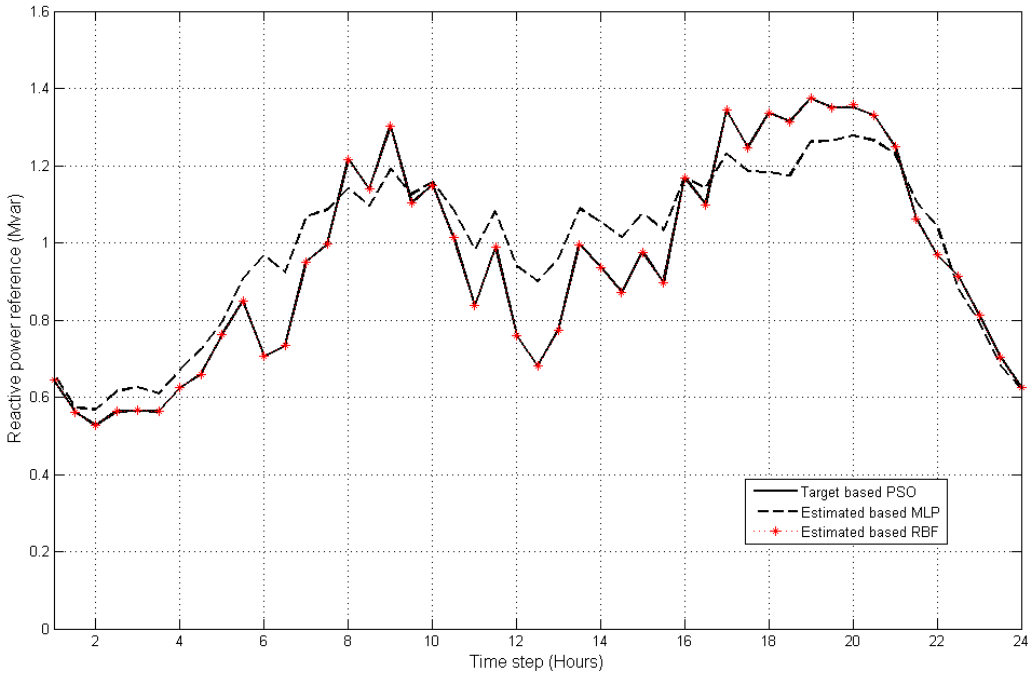

Figure 6.13 The reactive power of BESS under the environment of a rainy day

Looking at the frequency and voltage profiles of the stand-alone microgrid for a 24-hour, frequency and voltage profiles are an important criterion which have to be monitored to ensure that the frequency and voltage of the stand-alone microgrid are satisfied within the require limit in order to prevent the stand-alone microgrid from instability and collapse in the presence of violent changes of loads or the outage of distributed generation. Figs 6.14 and 6.15 show the frequency and voltage profiles of the microgrid under the environment of a sunny day, respectively. Based on these figures, it can be seen that frequency and voltage variations of the proposed online optimization of BESS-based RBFNN are within the acceptable ranges which are between 49.95 Hz and 50.05 Hz for frequency regulation, and between 0.99 p.u. and 1 p.u. for voltage regulation. On the contrary, frequency variations of the online optimization of BESS-based MLPNN exceed the acceptable range of frequency regulation in some parts of the duration.

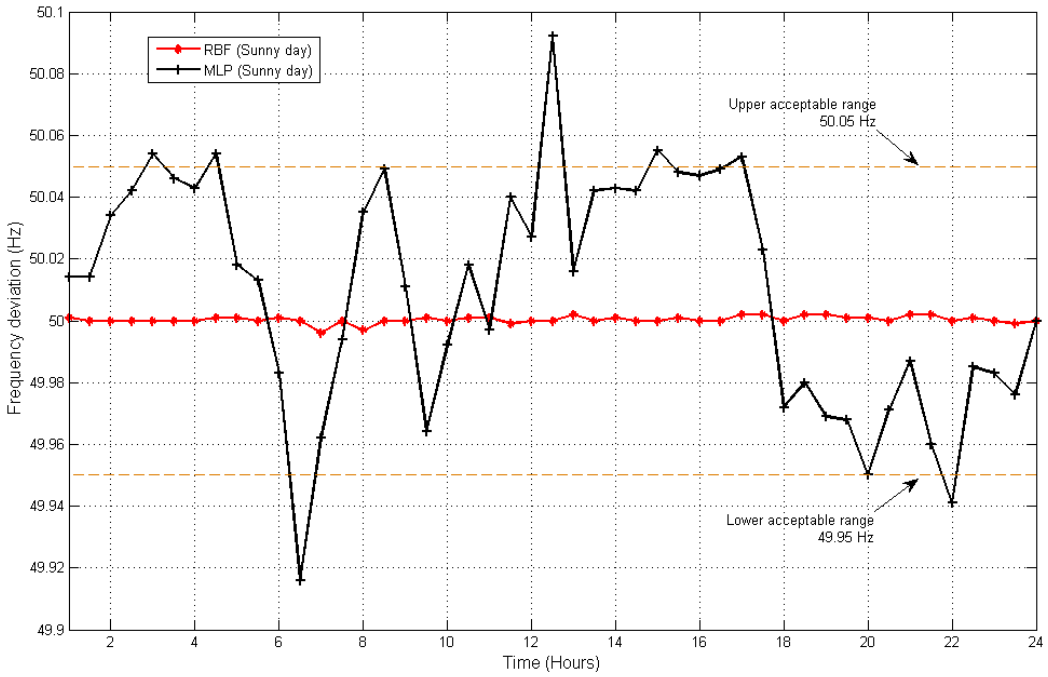

Figure 6.14 Frequency deviations of the isolated microgrid under the environment of a sunny day

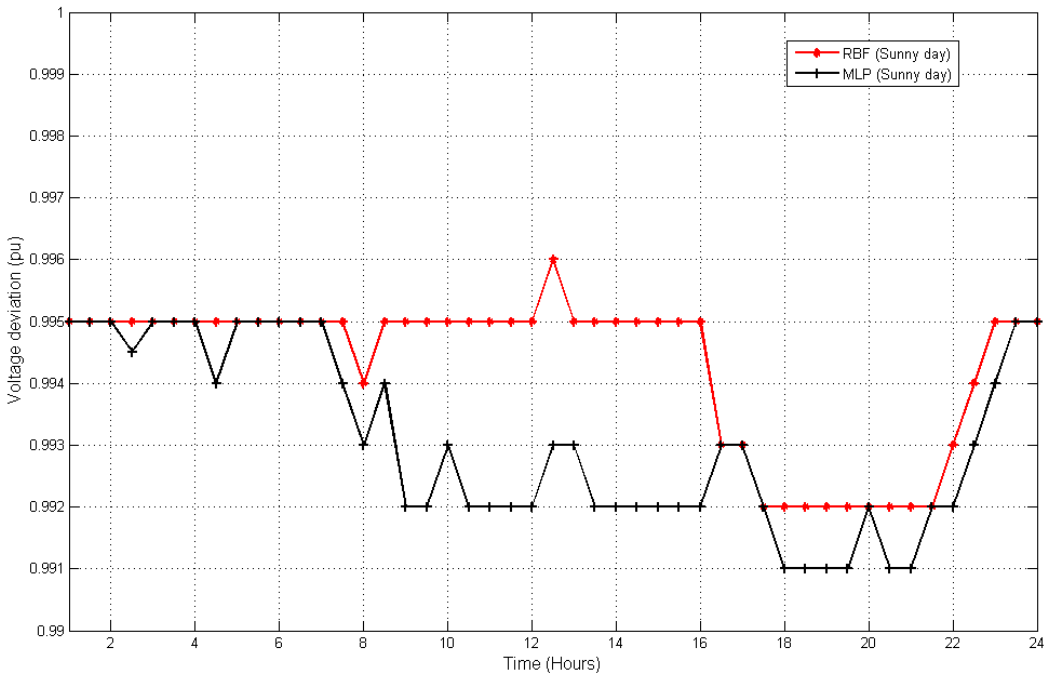

Figure 6.15 Voltage deviations of the isolated microgrid under the environment of a sunny day

Figs 6.16 and 6.17 show the frequency and voltage profiles of the isolated microgrid under the environment of a rainy day, respectively. As regard to these figures, it is obvious that frequency and voltage variations of the proposed online optimization of BESS-based RBFNN are still maintain within the acceptable ranges under the fluctuations of PV profile due to the bad weather condition which are between 49.95 Hz and 50.05 Hz for frequency regulation, and between 0.99 p.u. and 1 p.u. for voltage regulation. On the contrary, frequency variations of the online optimization of BESS-based MLPNN cannot hold within the acceptable range and exceed the acceptable range of frequency regulation in various durations of time.

Thus, it can be concluded that the proposed online optimization of BESS-based RBFNN method can accurately determine the online optimum active and reactive powers of BESS so as to prevent the microgrid from instability and system collapse in the presence of violent changes of generations/loads or the loss of a generation/utility grid. Thus, the proposed online optimization of BESS-based RBFNN can be used as an online effective controller of BESS for smart/micro-grids without the necessity of performing the new optimization process at any change in loads/generations.

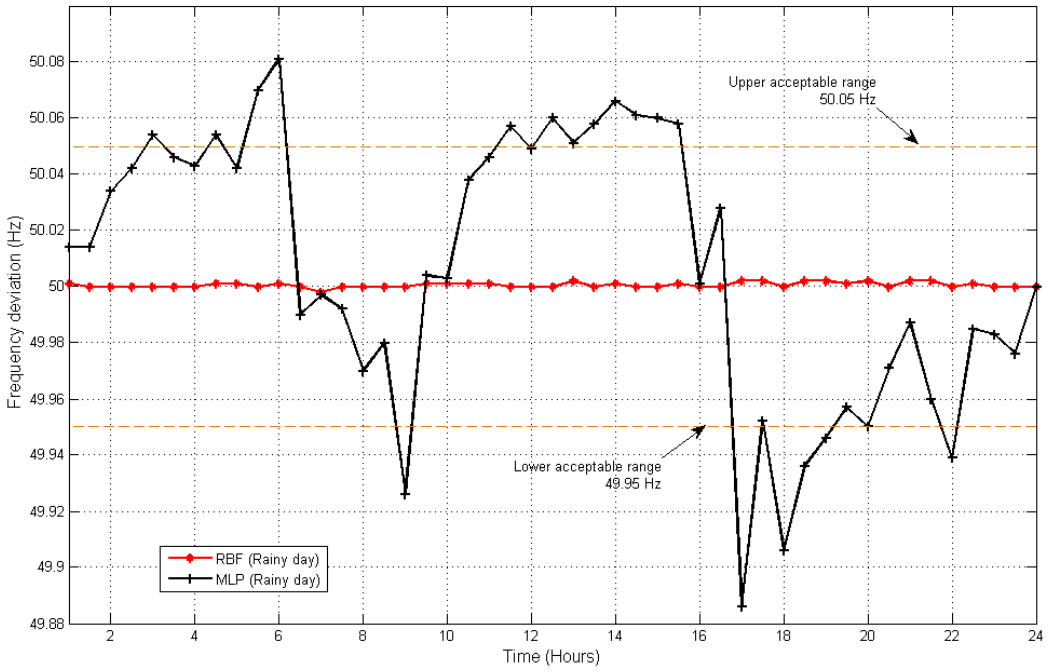

Figure 6.16 Frequency deviations of the isolated microgrid under the environment of a rainy day

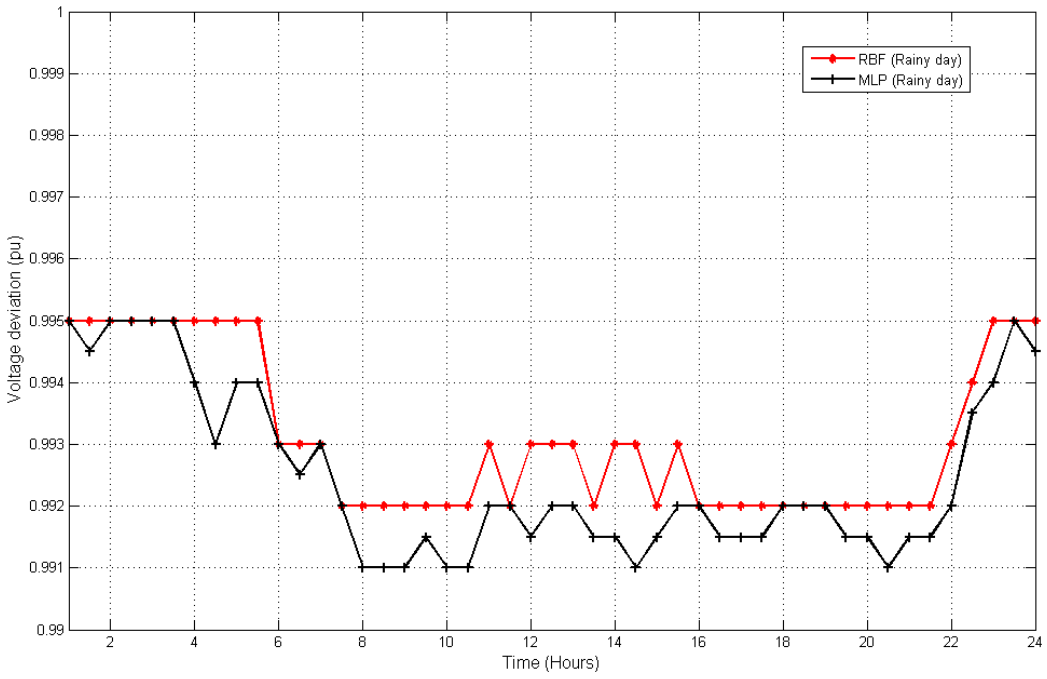

Figure 6.17 Voltage deviations of the isolated microgrid under the environment of a rainy day

6.4 Summary

This chapter proposes a brand new online optimization method, known as the online optimization of BESS by using the combination of both PSO and RBFNN methods for determining online optimum active and reactive powers of BESS for microgrids. The BESS is centrally managed and controlled by an effective controller developed using the proposed online optimization of BESS. Any changes in generations/loads in the microgrid will be compensated by the effective controller in a short period of time without the necessity of performing the new optimization process. Based on the results, it is obvious that the proposed online optimization of BESS-based RBFNN method can accurately determine online optimum active and reactive powers of BESS based on the frequency control of the microgrid under the circumstances of a sunny and rainy day including the PV fluctuations and typical load changes. Compared with the conventional ANN method known as the MLPNN model, it is clearly seen that the proposed online optimization of BESS-based RBFNN model provides the superior and finest performance when the error

efficiency and positional accuracy are concerned. The validity of the proposed online optimization of BESS-based RBFNN is verified by comparing to the optimum results-based PSO. As it has been demonstrated, the results of online optimization of BESS-RBFNN method is about the same with the optimum results-based PSO which means the proposed online optimization of BESS-based RBFNN is feasible and accurate enough to evaluate online optimum active and reactive powers of BESS for microgrids. The outstanding of the online optimization of BESS is that it can be used as an online effective controller of BESS for smart/micro-grids without the necessity of performing the new optimization process at any change in loads/generations or the loss of a generation/utility grid.

6.5 References

1. R. Wiser, and G. Barbose, Renewables portfolio standards in the United States as a status report with data through, Technical report, *Lawrence Berkeley National Laboratory*, 2007.
2. T. Ackermann, G. Andersson, and L. Soder, Distributed generation: a definition, *Electrical Power Systems Research*, 57(3): 195-204, 2001.
3. Government of Japan, *Kyoto Protocol Target Achievement Plan (Provision Translation)*, Tokyo, Japan: Ministry of the Environment, Government of Japan, pp. 81-82, 2008.
4. G. Pepermans, J. Driesen, D. Haeseldonckx, R. Belmans, and W. D'haeseleer, Distributed generation: definition, benefits and issues, *Energy Policy,* 33(6): 787-798, 2005.
5. J.M. Guerrero, F. Blaabjerg, T. Zhelev, K. Hemmes, E. Monmasson, S. Jemei, et al., Distributed generation: toward a new energy paradigm, *IEEE industrial electronics magazine,* pp.52-64, 2010.
6. C. Monteiro, R. Bessa, V. Miranda, A. Botterud, J. Wang, and G. Conzelmann, Wind power forecasting: State-of-the-art, Technical report, *Argonne National Laboratory, Decision and Information Sciences Division*, 2009.
7. K. Rahbar, J. Xu, and R. Zhang, Real-time energy storage management for renewable integration in microgrid: an off-line optimization approach, *IEEE Trans. On Smart Grid*, 6(1):124–134, 2015.
8. K. Swingler, *Applying neural networks: a practical guide,* London: Academic Press, 1996.
9. R.J. Schalkoff, *Artificial neural networks,* London: McGraw-Hill, 1997.

10. G. Li, J. Na, D. Stoten, and X. Ren, Adaptive neural network feedforward control for dynamically substructured systems, *IEEE Trans., Control System Technology*, 22(3):944–954, 2014.
11. H. Karami, M.F. Mousavi, M. Shamsipur, and S. Riahi, New dry and wet Zn-polyaniline bipolar batteries and prediction of voltage and capacity by ANN, *Journal of Power Sources*, 154(1):298–307, 2006.
12. F. Sereno, J.P. Marques de Sa, A. Matos, J. Bernades, A comparative study of MLP and RBF neural nets in the estimation of the foetal weight and length, *Proceeding of RECPAD*, pp. 1-9. 2000.
13. H. Memarian, S.K. Balasundram, Comparison between multi-layer perceptron and radial basis function networks for sediment load estimation in a tropical watershed, *Journal of Water Resource and Protection*, 1:870-876, 2012.
14. J. Park, and I. W. Sandberg, Universal approximation using radial basis functions network, *Neural Computation,* 3(2):246–257, 1991.
15. M. Bianchini, P. Frasconi, and M. Gori, Learning without local minima in radial basis function networks*, IEEE Trans. Neural Networks*, 6(1):749–756, 1995.
16. Y. Tang, and W.K. Wong, Distributed synchronization of coupled neural networks via randomly occurring control*, IEEE Trans. On Neural Networks and Learning Systems*, 24(3):435-447, 2015.
17. H. Zyandehroodi, A. Mohamed, H. Shareef, M. Mohammadjafari, Performance comparison of MLP and RBF neural networks for fault location in distribution networks with DGs, *Proceeding of IEEE Conference on Power Energy*, pp. 342-345, 2010.
18. M.J.D. Powell, Radial basis function for multi-variable interpolation, *In proceeding of IMA Conference on Algorithm for the Approximation of Function and Data,* 1985.
19. T. Kerdphol, Y. Qudaih, M. Watanabe, Y. Mitani, RBF neural network-based online intelligent management of a battery energy storage system for stand-alone microgrids, Energy, sustainability and society, 6(5):1-16, 2016.
20. J. Kennedy, and R. Eberhart, Particle swarm optimization. In: *Proceeding of IEEE international conference neural networks*, 4 (1): 1942–8, 1995.
21. The Mathworks, *Neural network toolbox-user's guide,* Mathworks, 2013.

Chapter 7

Conclusions

This research have solved the optimization problems about energy system and contributed in the future online control and management of energy system.

Firstly, the optimization-based analytic method is designed as a reference method to compare with the proposed optimization methods.

Secondly, the proposed optimization based on the PSO method provides the finest optimum solution for determining an optimum size of BESS for microgrids. This method will be useful to help the operators to guarantee a lowest size and total cost of BESS with a constraint of frequency control and the full use of the microgrid.

Afterwards, the proposed optimization based on the RBFNN offers the fastest calculation time and accurate results with a low prediction error for determining both optimum size and location of BESS for microgrids. This method will be beneficial to help the operators to evaluate an optimum size of BESS with a constraint of frequency control and determine an optimum location of BESS with a constraint of power loss minimization, guaranteeing the full use of microgrids.

Finally, the proposed combined optimization technique of both PSO and RBFNN methods produces a novel online optimization method to evaluate online optimum active and reactive powers of BESS in order to prevent the microgrid from instability and system collapse in the presence of violent changes of generations/loads or the outage of generations/utility grid without the necessity to performing the new

optimization process. This method produces a fast time calculation and accurate result for evaluating online optimum active and reactive powers of BESS as well as it can be used as an online effective controller for microgrids.

The proposed optimization methods in this book are verified and tested through the typical micogrid including whole system parameters, actual domestic loads/customers and generations which is available at the promoting renewable energy in Mae Hong Son province, Thailand. This is a first microgrid pilot project in Thailand which is initiated and funded by UNDP and GEF incorporating the Ministry of Energy of Thailand aimed for promoting DGs/RESs, learning and sharing knowledge and supporting the environmental agreements.

The outstanding of this research is that the optimization problems have been solved by using artificial intelligent techniques which are accurate, secure and simple for control and management of energy system.

Appendix A: Microgrid System Parameters

Table A.1 Busbar Parameters

Name	Nominal voltage (kV)	Type	System type	Phase Technology
1	22	Busbar type22kV	AC	ABC
2	22	Busbar type22kV	AC	ABC
3	22	Busbar type22kV	AC	ABC
4	22	Busbar type22kV	AC	ABC
5	22	Busbar type22kV	AC	ABC
6	22	Busbar type22kV	AC	ABC
7	22	Busbar type22kV	AC	ABC
8	22	Busbar type22kV	AC	ABC
9	22	Busbar type22kV	AC	ABC
10	22	Busbar type22kV	AC	ABC
11	22	Busbar type22kV	AC	ABC
12	6	Busbar type6kV	AC	ABC
13	22	Busbar type22kV	AC	ABC
14	6	Busbar type6kV	AC	ABC
15	0.2	Busbar type0.2kV	AC	ABC
16	0.4	Busbar type0.4kV	AC	ABC
17	22	Busbar type22kV	AC	ABC
18	22	Busbar type22kV	AC	ABC
19	22	Busbar type22kV	AC	ABC
20	22	Busbar type22kV	AC	ABC
21	150	Busbar type150kV	AC	ABC

Table A.2 Line Parameters

Line	Type	Length (km)	I_{rated} (kA)	Z_1 (ohm)	$Phiz_1$ (deg)	R_1 (Ohm)	X_1 (Ohm)	R_0 (Ohm)	X_0 (Ohm)	$Phiz_0$ (deg)
1-7	SCDC1	5	1	1.771	81.605	0.258	1.752	0.633	4.994	1.803
7-9	SCDC1	20	1	7.087	81.605	1.034	7.011	2.532	19.977	1.803
7-8	SCDC1	0.3	1	0.106	81.605	0.015	0.105	0.037	0.299	1.803
17-18	SCDC1	50	1	17.718	81.605	2.586	17.528	6.331	49.942	1.803
19-20	SCDC1	40	1	14.174	81.605	2.069	14.022	5.065	39.954	1.803
1-6	SCDC1	5	1	1.771	81.605	0.258	1.752	0.633	4.994	1.803
6-10	SCDC1	1.5	1	0.531	81.605	0.077	0.525	0.189	1.498	1.803
5-11	SCDC1	5	1	1.771	81.605	0.258	1.752	0.633	4.994	1.803
1-5	SCDC1	1	1	0.354	81.605	0.051	0.350	0.126	0.998	1.803
1-4	SCDC1	4.2	1	1.488	81.605	0.217	1.472	0.531	4.195	1.803
1-3	SCDC1	5.8	1	2.055	81.605	0.300	2.033	0.734	5.793	1.803
1-2	SCDC1	1	1	0.354	81.605	0.051	0.350	0.126	0.998	1.803
1-13	SCDC1	1	1	0.354	81.605	0.051	0.350	0.126	0.998	1.803

Table A.3 Transformer Parameters

Name	Technology	Rated power (MVA)	Rated Voltage (kV)		Vector Group		Nominal Frequency (Hz)
			HV-side	LV-side	HV-side	LV-side	
TR1	3-phase	30	150	22	YN	YN	50
TR2	3-phase	4	22	6	YN	YN	50
TR3	3-phase	4	22	6	YN	YN	50
TR4	3-phase	4	22	0.2	YN	YN	50
TR5	3-phase	5	22	0.4	YN	YN	50

Table A.4 Automatic Voltage Regulator (AVR) Parameters

Name	Technology	Rated power (MVA)	Rated Voltage (kV)		Vector Group		Nominal Frequency (Hz)
			HV-side	LV-side	HV-side	LV-side	
AVR1	3-phase	30	22	22	YN	YN	50
AVR2	3-phase	30	22	22	YN	YN	50

Table A.5 Utility Grid Parameters

Name	Bus type	Input mode	Setpoint	Angle (deg)	Voltage setpoint (p.u.)
Utility grid	SL (Slack bus)	P, Q	Local	0	1

Table A.6 Domestic Load Parameters

Name	Technology	System Type	Type (TypLod)	Peak Power (MW)	Power Factor	Voltage (p.u.)
Load 1	3PH PH-E	AC	Lod-1	1.85	0.9, ind	1
Load 2	3PH PH-E	AC	Lod-1	1.70	0.9, ind	1
Load 3	3PH PH-E	AC	Lod-1	1.75	0.9, ind	1
Load 4	3PH PH-E	AC	Lod-1	1.90	0.9, ind	1
Load 5	3PH PH-E	AC	Lod-1	2.40	0.9, ind	1

Appendix B: Control Parameters for Solar PV Model

Table B.1 Active Power Reduction Parameters

Parameter	Value
Start of Active power reduction (Hz)	50.2
End of Active power reduction (Hz)	50.05
Gradient of active power reduction (%Hz)	40
Filter time constant (s)	0.01

Table B.2 Controller Parameters

Parameter	Value
Kp Gain, Active power PI-controller	0.005
Tip Integration time constant, active power PI-controller	0.03
Tmpp Time delay MPP-Tracking (s)	5
Tr Measurement delay (s)	0.001
Deadband for AC voltage support (p.u.)	0.1
Droop static for AC voltage support	2
id_min, Active current limit (p.u.)	0
U_min, Minimum allowed DC voltage (V)	330
iq_min, Minimum reactive current limit (p.u.)	-1
iq_max, Maximum reactive current limit (p.u.)	1
id_max, Maximum active current limit (p.u.)	1
Allowed absolute current (p.u.)	1
Absolute reactive current in normal operation (p.u.)	1

Table B.3 DC Busbar and Capacitor Parameters

Parameter	Value
Capacitor capacity on DC busbar (s)	0.0172
Initial DC voltage (V)	700
Nominal DC voltage (kV)	0.2
Rated power (MW)	0.5

Table B.4 PV Array Parameters

Parameter	Value
Open circuit voltage (STC) of module (V)	43.8
MPPT voltage of module (V)	35
MPPT current of module (A)	4.58
Short circuit current of module	5
Temperature correction factor (voltage)	-0.0039
Temperature correction factor (current)	0.0004
Serial modules number	20
Parallel modules number	140
Time constant of module (s)	0

Table B.5 Solar PV Power Generation Data

Time (sec)	Solar PV Power (MW)
0	2.80
1	2.81
2	2.80
3	2.82
4	2.83
5	2.84
6	2.82
7	2.83
8	2.83
9	2.84
10	2.85
11	2.86
12	2.87
13	2.87
14	2.87
15	2.86
16	2.86
17	2.86
18	2.87
19	2.88
20	2.89
21	2.90
22	2.90
23	2.93
24	2.94
25	2.94
26	2.96
27	2.97
28	2.96
29	2.99
30	3.00
31	3.01
32	3.01
33	3.00
34	3.00
35	3.01

Time (sec)	Solar PV Power (MW)
36	3.00
37	3.01
38	3.00
39	3.00
40	2.98
41	2.96
42	2.96
43	2.95
44	2.97
45	2.98
46	2.98
47	2.98
48	2.96
49	2.96
50	2.96
51	2.95
52	2.95
53	2.95
54	2.94
55	2.94
56	2.94
57	2.93
58	2.93
59	2.92
60	2.92
61	2.92
62	2.92
63	2.92
64	2.91

Appendix C: Control Parameters for BESS Model

Table C.1 Calibration of Parameters for BESS Model

Parameter	Value
State of charge (SOC) at initialization	0.9
Capacity per battery cell (Ah)	480
Voltage of empty battery cell (V)	12
Voltage of full battery cell (V)	14
Number of parallel battery cells	65
Number of series battery cells	70
Nominal voltage of source (kV)	0.4
Internal resistance per battery cell (ohm)	0.001

List of Publications by the Author

Technical Journals and Transactions

1. Kerdphol T, Qudaih Y, Mitani Y, Optimum Battery Energy Storage System using PSO considering Dynamic Demand Response for Microgrids, *International Journal of Electrical Power & Energy Systems*, Elsevier, United Kingdom, vol. 83, No. 1, pp.58–66, 2016
(Impact factor 2015: 2.587)

2. Kerdphol T, Fuji K, Qudaih Y, Watanabe M, Mitani Y, Optimization of Battery Energy Storage System using Particle Swarm Optimization for Stand-alone Microgrids, *International Journal of Electrical Power & Energy Systems*, Elsevier, United Kingdom, vol. 81, No. 1, pp.32–39, 2016
(Impact factor 2015: 2.587)

3. Kerdphol T, Qudaih Y, Watanabe M, Mitani Y, RBF Neural Network-based Online Intelligent Management of a Battery Energy Storage System for Stand-alone Microgrids, *Energy, Sustainability and Society*, Springer–Verlag, Germany, vol. 6, No. 5, pp.1–16, 2016
(SCImargo Journal Rank 2015: Q2)

4. Kerdphol T, Qudaih Y, Hongesombut K, Watanabe M, Mitani Y, Intelligent Determination of a Battery Energy Storage System Size and Location based on RBF Neural Networks for Microgrids, *International Review of Electrical Engineering*, University of Naples Federico II, Italy, vol. 11, No. 1, pp.78–86, 2016
(SCImargo Journal Rank 2015: Q2, Impact factor: 1.364)

5. Kerdphol T, Qudaih Y, Mitani Y, Optimal Battery Energy Storage System using Particle Swarm Optimization for Microgrid System, *International Review of Electrical Engineering*, University of Naples Federico II, Italy, vol. 10, No. 2, pp.125–130, 2015
(SCImargo Journal Rank 2015: Q2, Impact factor: 1.364)

6. Kerdphol T, Fuji K, Qudaih Y, Mitani Y, Performance Comparison of Artificial Intelligence Approaches for Energy Storage Size Optimization in PV-Microgrids, *Journal of Clean Energy Technologies*, United States, vol. 4, No. 6, pp.389–395, 2015

7. Kerdphol T, Qudaih Y, Garasi P, Mitani Y, Optimal Sizing of Battery Energy Storage System in Microgrid considering Load Shedding Scheme, *International Journal of Smart Grid and Clean Energy*, United States, vol. 4, No. 1, pp.22–29, 2015

*Also presented at *International Conference on Smart Grid and Clean Energy Technologies* (IEEE ICSGCE 2014), Dubai, United Arab Emirates, 2014

8. Kerdphol T, Qudaih Y, Mitani Y, Robust Hydro-Thermal Power System Controller considering Energy Capacitor System and Wind Power Source, *International Journal of Process System Engineering*, Switzerland, vol. 3 No. 1/2/3, pp.90–109, 2015
*Also presented at *International Conference on Smart Energy Grid Engineering Conference* (IEEE SEGE 2014), Ontario, Canada, 2014

Conference Proceedings (Reviewed)

1. Kerdphol T, Tripathi R, Hanamoto T, Qudaih Y, Mitani Y, ANN based Optimized Battery Energy Storage System Size and Loss Analysis for Distributed Energy Storage Location in PV-Microgrid. *IEEE PES Innovative Smart Grid Technology Conference* (IEEE PES ISGT Asia 2015), Bangkok, Thailand, 2015.

2. Koyamatsu K, Shiyota A, Mitani Y, Kerdphol T, Qudaih Y, Construction of PV Simulator by using Geographic Information System and Digital Surface Model. *IEEE PES Asia-Pacific Power and Energy Engineering Conference*, Brisbane, Australia, 2015

3. Kerdphol T, Qudaih Y, Mitani Y, PSO based Optimal Size and Allocation of Battery Energy Storage System for Micro-grid System. *International Conference of Electrical Engineering* (ICEE 2015), Hong Kong, 2015

4. Qudaih Y, Kerdphol T, Mitani Y, Different Optimization Schemes for Community based Energy Storage Systems. *4th International Conference on Electric Power and Energy Systems Conference* (IEEE EPECS 2015), Sharjah, United Arab Emirates, 2015

5. Kerdphol T, Qudaih Y, Mitani Y, Battery Energy Storage System Size Optimization in Microgrid using Particle Swarm Optimization. *IEEE PES Innovative Smart Grid Technology Europe Conference* (IEEE PES ISGT Europe 2014), Istanbul, Turkey, 2014

6. Kerdphol T, Qudaih Y, Mitani Y, Watanabe M, Size Optimization of Battery Energy Storage System using Particle Swarm Optimization for a Stand-alone Microgrid System. *Conference of Symposium on Applied Engineering & Sciences* (SASE 2014), Kitakyushu, Japan, 2014

7. Khairudin, Qudaih Y, Mitani Y, Kerdphol T, Wavelet Demodulation Method Based Out of Step Detection and Damping Estimation in Japan Campus Wams. *18th Power System Computation Conference* (PSCC 2014), Warsaw, Poland, 2014

Biography of the Author

Thongchart Kerdphol was born on November 13, 1988, at Chachoengsao Hospital in Chachoengsao province, Thailand. He is the son of Police Captain Chartchai Kerdphol and Mrs. Pranee Payayam. He studied in Chacheongsao until high school. After high school, Kerdphol passed a national entrance examination for entering national university and moved to Bangkok in 2007 to attend an engineering school at Kasetsart University, Bangkok, Thailand. He decided to study electrical engineering for the bachelor degree. After graduating the bachelor degree, Kerdphol decided to attend a master degree at electrical engineering department, Kasetsart University in 2011. During that time, he was hired as a teaching assistant/lab leader at electrical engineering department, Kasetsart University. He taught on an electrical and electronics circuit practice class including electrical measurements such as periodic wave forms, analysis of networks such as nodal and mesh analysis, first order RLC circuits. His master thesis was focused on the robust controller designs of interline power flow controller by using H-infinity loop shaping and fuzzy logic control methods. After graduating the master degree, Kerdphol was awarded the 2013 academic excellence honours by Kasetsart University for his excellence in classes and master thesis. He decided to move to Japan in the middle of 2013 as a research student at Mitani laboratory, Kyushu Institute of Technology. In the fall semester of 2013, he entered the doctoral course of electrical and electronics engineering at Mitani laboratory, Kyushu Institute of Technology. During that time, he was hired to work as a research assistant at Mitani laboratory until the doctoral graduation. His work and thesis were involved the intelligent optimization techniques for evaluating an optimum size and location of BESS for microgrids. In the fall of 2015, Kerdphol was awarded the PhD support grant from the Institute of Electrical and Electronics Engineers, Power and Energy Society (IEEE PES). His research area includes power system analysis, dynamics and controls, impacts of renewable energy resources on power system dynamics and performance, automatic generation control and frequency regulation, emergency control, smart/micro-grids. He is the members of the Council of Engineers of Thailand (COE) and the Institute of Electrical and Electronics Engineers (IEEE).